Sensor and Simulation Notes

Note 123

February 1971

Low-Frequency Magnetic Field Distribution of a Half Toroid Simulator Joined to a Finitely Conducting Ground: Modified Ground Connections

M. I. Sancer and A. D. Varvatsis
Northrop Corporate Laboratories
Pasadena, California

Abstract

In this note the low-frequency magnetic field distribution of a half toroid simulator joined to the ground through modified ground connections is considered. These ground connections, as distinguished from the simple ground connections that were examined in a previous note, are such that at the center of the toroid the field is the same as in the case of a perfectly conducting ground. Plots are given of the field components at points on, above, and below the ground. Plots are also presented that are related to the difference between the actual field and the low frequency component of the EMP magnetic field. Specifically we consider the magnitude of the difference between these vector fields normalized to the magnitude of the EMP field. In the symmetry plane that bisects the toroid, we plot contours that correspond to constant values of this ratio. Finally, we find the maximum value of this ratio on the perimeter of a circle lying in the ground plane and centered at the origin or on the surface of a hemisphere resting on the ground and centered at the origin. Plots are given of these maxima versus the appropriate radius normalized to the radius of the toroid.

I. Introduction

In a previous note[1] the low-frequency magnetic field of a half toroid simulator directly connected to a finitely conducting ground was studied. It was found that the ground currents produce no vertical magnetic field. Thus, for an inclination angle of the half toroid $\xi_1 \neq 0$ (Fig. 1) the static magnetic field at the origin of the coordinate system has a non-zero vertical component due to the current flowing in the half toroid. This is an undesirable feature since an ideal simulator should not allow a vertical magnetic field component in the static limit. The situation to be simulated is the interaction of the low-frequency content of the electromagnetic pulse due to a nuclear explosion, with a finitely conducting ground. We know that in the limit of zero frequency the ground behaves as perfectly conducting and consequently the total magnetic field has no vertical component. It has been shown in reference 2 that if the ground were perfectly conducting the half toroid simulator is capable of matching, at the origin of our coordinate system, the low frequency magnetic field of the EMP. In the case of a finitely conducting ground we would like, in addition to securing a vanishing vertical component of the low-frequency magnetic field at the origin, to make the tangential component at the origin independent of the conductivity of the ground and equal to the one corresponding to infinite conductivity. In reference 1 we found that if the ends of the half toroid are directly connected to the ground the matching of the tangential component is not accomplished. In the present note we use different ground connections which redirect the currents flowing in the ground connections and through the ground, in a way that tends to imitate the half toroid image. These alternate ground connections are such that the static magnetic field at the origin of our coordinate system is equal to the field at the same point as in the case of a perfectly conducting ground[3]. This feature can be achieved by a variety of ground connections. The ones we use in this note were chosen primarily because of their simplicity from both the computational and the implementation point of view. Thus, instead of directly connecting the end points of the half toroid to the ground we symmetrically stretch two wires from the end points to the feed points on the same side as the projection of the inclined half toroid onto the ground (Fig. 2). The length of these extra wires and the angle they

make with the line connecting the end points of the toroid depend on the inclination angle of the half toroid ξ_1. For each ξ_1 they are such that the total magnetic field at the origin of our coordinate system is the same as for the case of a half toroid directly joined to a perfectly conducting ground.

To be able to see how the field calculated at points other than the origin differs from the field for the perfectly conducting ground situation, and also from the EMP field that is to be simulated, we present plots of field quantities for the same range of parameters as in reference 3. Thus, for points on or above the ground, we plot the total magnetic field components, normalized to $(I/2a)\cos \xi_1$, versus z/a with parameters x/a, y/a and ξ_1. $(I/2a)\cos \xi_1 \hat{a}_z$ is the EMP field to be simulated, I is the current in the half toroid, a the radius of the half toroid and ξ_1 the inclination angle with respect to the x axis. We denote the magnetic field normalized to I/2a by $\underline{h}$ i.e., $\underline{h} = (2a/I)\underline{H}$. We also exhibit contour plots of the quantity $|\Delta \underline{h}|/\cos \xi_1$ where $\Delta \underline{h} = \underline{h} - \cos \xi_1 \hat{a}_z$. This quantity is zero only at the origin for both the finite conductivity case examined in this note and also the infinite conductivity case. We present the plots in the y = 0 plane with ξ_1 as a parameter. To further compare the present situation with that of a perfectly conducting ground we compute $|\Delta \underline{h}|/\cos \xi_1$ on the circumference of a circle situated on the ground and the surface of a mathematical hemisphere resting on the ground. The centers of both the circle and the hemisphere coincide with the origin of our coordinate system. We find the maximum deviations for the two cases and we plot them versus the radius of the circle or the radius of the hemisphere, both normalized to the radius of the toroid, with ξ_1 as a parameter. For points in the ground we only plot the total magnetic field components normalized to $(I/2a)\cos \xi_1$, versus z/a with x/a, y/a and ξ_1 as parameters.

II. Formulation

Consider the situation depicted in Fig. 2. For a given inclination angle ξ_1 we want to determine the length L and the angle α so that the total magnetic field at the origin of the coordinate system is equal to $\underline{H} = H_z \hat{a}_z$ where $H_z = (I/2a)\cos \xi_1$. This latter field has the same value as the magnetic field due to a half toroid directly connected to a perfectly conducting ground.

As we found in a previous note[1] the magnetic field due to the ground currents is obtained by replacing the ground currents with two semi-infinite current elements oriented downward from the feed points to infinity. Thus, they produce no vertical magnetic field at any point. The wire connections, from the end points of the half toroid to the feed points, however, do produce a vertical magnetic field at the origin of the coordinate system which is directed opposite to the vertical component of the field due to the half toroid. To calculate the field of the wire segments we should find the field due to a current element of finite length. If reference 1 we have found the magnetic field due to a semi-infinite current element.(eq. 9). The same procedure applies to the present case except that to preserve current continuity we have to apply charges ± It at both ends. Referring to Fig. 3 the field at the origin due to the wire segment $1G_1$ is then given by

$$\underline{H}_1 = \hat{a}_x H_{1x} \quad , \quad H_{1x} = \frac{I}{4\pi\rho} (\cos \alpha + \cos \beta) \tag{1}$$

We can easily see that

$$\rho = a \sin \alpha \quad , \tag{2}$$

$$\cos \beta = \frac{L - a \cos \alpha}{\sqrt{L^2 + a^2 - 2La \cos \alpha}} \quad .$$

Thus, to make the total vertical component equal to zero we demand

$$- \frac{2I}{4\pi a \sin \alpha} \left(\cos \alpha + \frac{L - a \cos \alpha}{\sqrt{L^2 + a^2 - 2La \cos \alpha}}\right) + \frac{I}{4a} \sin \xi_1 = 0 \quad . \tag{3}$$

where $(I/4a)\sin \xi_1$ is the x-component of the field produced by the half-toroid at the origin of our coordinate system. Equation (3) can be rewritten as

$$\frac{L - a\cos\alpha}{\sqrt{L^2 + a^2 - 2La\cos\alpha}} = (\frac{\pi}{2}\sin\xi_1 - \cot\alpha)\sin\alpha \quad . \tag{4}$$

Defining

$$(\frac{\pi}{2}\sin\xi_1 - \cot\alpha)\sin\alpha = m \quad , \tag{5}$$

we understand that

$$L - a\cos\alpha \gtreqless 0$$

if $$\tag{6}$$

$$m \gtreqless 0 \quad .$$

Solving (4) with respect to L we obtain

$$L = a\cos\alpha \pm \frac{|m|a\sin\alpha}{\sqrt{1 - m^2}} \quad . \tag{7}$$

In view of the restrictions imposed by (6), (7) can be rewritten as

$$\frac{L}{a} = \cos\alpha + \frac{[(\pi/2)\sin\xi_1 - \cot\alpha]\sin\alpha}{\sqrt{1 - (\pi^2/4)\sin^2\xi_1 + \pi\cot\alpha\sin\xi_1}} \quad . \tag{8}$$

Next we calculate the field due to the two semi-infinite currents which represent the ground currents. The field due to a semi-infinite current I has been calculated in reference 1 (eq. 9); it is given by

$$H = \frac{I}{4\pi\rho}(1 + \cos\gamma) \quad , \tag{9}$$

where γ is the angle between the vectorial current element and the vector joining the finite end with the observation point, and ρ is the shortest distance from the observation point to the current element. Referring to Fig. 4 we see that the contribution from both semi-infinite currents at the origin of our coordinate system is directed along the z-axis and is given by ($\gamma = \pi/2$)

$$\underline{H}_G = \hat{a}_z H_G = \hat{a}_z \frac{2I}{4\pi R}\sin\psi \quad . \tag{10}$$

where

$$R = \sqrt{L^2 + a^2 - 2La\cos\alpha} \quad ,$$

$$\sin\psi = \frac{a - L\cos\alpha}{\sqrt{L^2 + a^2 - 2La\cos\alpha}} \quad . \tag{11}$$

Thus, we demand

$$\frac{I}{2\pi}\frac{a - L\cos\alpha}{L^2 + a^2 - 2La\cos\alpha} = \frac{I}{4a}\cos\xi_1 \quad , \tag{12}$$

or

$$\cos\alpha = \frac{1 - (\pi/2)\cos\xi_1(r^2 + 1)}{(1 - \pi\cos\xi_1)r} \quad ,$$

$$r = L/a \quad . \tag{13}$$

Combining (8) and (12) we can solve for L/a and α, provided a meaningful solution exists. Few special cases are easy to see. For example from (8) we find

$$L/a = \cos\alpha$$

$$\text{for} \qquad \cot\alpha = \frac{\pi}{2}\sin\xi_1 \quad . \tag{14}$$

For $L/a = \cos\alpha$, (12) gives $(\pi/2)\cos\xi_1 = 1$, and

$$\left.\begin{aligned} \cos\xi_1 = \frac{2}{\pi}\ (\xi_1 = .2803\pi) \ , \ \cot\alpha = \frac{1}{2}\sqrt{\pi^2 - 4}\ \ (\alpha = .2197\pi) \\ \frac{L}{a} = \frac{1}{\pi}\sqrt{\pi^2 - 4} = .7712 \end{aligned}\right\} \tag{15}$$

Another special case can be obtained from (12) by setting $\cos\xi_1 = 1/\pi$. We find $L/a = 1$ and from (8) we can solve for α.

$$\cos \xi_1 = 1/\pi \quad (\xi_1 = .3969\pi)$$
$$L/a = 1 \quad . \tag{16}$$

By studying (13) we can easily see that the following inequalities hold

$$\cos \xi_1 \leq 1/\pi$$
$$L/a \geq 1 \tag{17}$$

and

$$\cos \xi_1 \geq 1/\pi$$
$$\frac{(\pi/2)\cos \xi_1 - 1}{(\pi/2)\cos \xi_1} < L/a \leq 1 \quad . \tag{18}$$

Thus, the minimum value for L/a is $1 - 2/\pi$ which corresponds to $\xi_1 = 0$ and $\alpha = 0$.

$$\xi_1 = 0 \quad , \quad \alpha = 0$$
$$L/a = 1 - 2/\pi = .3634 \quad . \tag{19}$$

Notice that (1) is not directly applicable for $\alpha = 0$, but if we carefully go to the limit ($\alpha = 0$, $\beta = \pi$) we find $H_{1x} = 0$ as we should.

We have solved for L/a and α and we have also computed the cartesian coordinates of the feed points G_1 and G_2 as functions of the inclination angle ξ_1. The results are presented in table 1.

III. Total Magnetic Field at a Given Observation Point

The total magnetic field at a given point on or above the ground is the superposition of the field due to the half toroid and the field due to the currents flowing in the wire connections and the ground. The field due to the half-toroid has been calculated in reference 3.

Referring to Fig. 5, P is the observation point characterized by the three cartesian coordinates x, y, z with $x \geq 0$. First we calculate the field due to the current flowing in the wire segment $1G_1$. The magnitude of the field at P is given by

$$H_1 = \frac{I}{4\pi\rho_1} (\cos \alpha_2 + \cos \alpha_1) \tag{20}$$

where

$$\begin{aligned} \rho_1 &= R_1 \sin \alpha_1 \quad , \\ \cos \alpha_1 &= - \frac{\hat{S}_1 \cdot \underline{R}_1}{R_1} \quad , \\ \cos \alpha_2 &= \frac{\hat{S}_1 \cdot \underline{R}_2}{R_2} \quad . \end{aligned} \tag{21}$$

and $\hat{S}$ is a unit vector parallel to $(1G_1)$. The field is directed parallel to the unit vector $(\underline{R}_1 \times \hat{S}_1)/R_1 \sin \alpha_1$. Simple algebraic calculations yield the following results

$$\begin{aligned} H_{1x} &= \frac{I}{4\pi(R_1 \sin \alpha_1)^2} (\cos \alpha_1 + \cos \alpha_2)\{(y + a - L \cos \alpha) \sin \alpha \\ &\qquad - (z - L \sin \alpha) \cos \alpha\} \\ H_{1y} &= \frac{- xI \sin \alpha}{4\pi(R_1 \sin \alpha_1)^2} (\cos \alpha_1 + \cos \alpha_2) \quad , \\ H_{1z} &= \frac{xI \cos \alpha}{4\pi(R_1 \sin \alpha_1)^2} (\cos \alpha_1 + \cos \alpha_2) \quad , \end{aligned} \tag{22}$$

where

$$\cos\alpha_1 = -\frac{\cos\alpha(y + a - L\cos\alpha) + (z - L\sin\alpha)\sin\alpha}{R_1} \quad ,$$

$$\cos\alpha_2 = \frac{(y + a)\cos\alpha + z\sin\alpha}{R_2} \quad ,$$

$$R_1 = [x^2 + (y + a - L\cos\alpha)^2 + (z - L\sin\alpha)^2]^{\frac{1}{2}} \quad , \tag{23}$$

$$R_2 = [x^2 + (y + a)^2 + z^2]^{\frac{1}{2}} \quad .$$

Similar calculations for the field due to wire segment $(2G_2)$ yield

$$H_{2x} = \frac{I}{4\pi(R_1' \sin\beta_1)^2}(\cos\beta_1 + \cos\beta_2)\{-\cos\alpha(z - L\sin\alpha) - \sin\alpha(y - a + L\cos\alpha)\} \quad ,$$

$$H_{2y} = \frac{xI\sin\alpha}{4\pi(R_1' \sin\beta_1)^2}(\cos\beta_1 + \cos\beta_2) \quad , \tag{24}$$

$$H_{2z} = \frac{xI\cos\alpha}{4\pi(R_1' \sin\beta_1)^2}(\cos\beta_1 + \cos\beta_2) \quad ,$$

where

$$\cos\beta_1 = -\frac{-\cos\alpha(y - a + L\cos\alpha) + \sin\alpha(z - L\sin\alpha)}{R_1'}$$

$$\cos\beta_2 = \frac{-\cos\alpha(y - a) + z\sin\alpha}{R_2'}$$

$$R_1' = [x^2 + (y - a + L\cos\alpha)^2 + (z - L\sin\alpha)^2]^{\frac{1}{2}}$$

$$R_2' = [x^2 + (y - a)^2 + z^2]^{\frac{1}{2}} \quad .$$

Next we calculate the field due to the ground currents. As we mentioned earlier for observation points on or above the ground, the ground currents can be replaced by two semi-infinite current elements oriented downward to

infinity. Referring again to Fig. 4 we calculate the field due to the semi-infinite current at G_1. The magnetude of the field at P is equal to

$$H_{G_1} = \frac{I}{4\pi\rho_3}(1 + \cos\gamma_1) \quad . \tag{26}$$

where $\rho_3 = R_1 \sin\gamma_1$ and γ_1 is the angle between $\underline{R}_1$ and $-\hat{a}_x$. Thus,

$$\cos\gamma_1 = -\frac{R_{1x}}{R_1} \quad . \tag{27}$$

Noticing that $\underline{H}_{G_1}$ is parallel to the unit vector $-(\underline{R}_1 \times \hat{a}_x)/R_1 \sin\gamma_1$ we can perform simple algebraic calculations to find

$$\begin{aligned} H_{G_1x} &= 0 \\ H_{G_1y} &= -\frac{IR_{1z}}{4\pi R_1^2(1 - \cos\gamma_1)} \quad , \\ H_{G_1z} &= \frac{IR_{1y}}{4\pi R_1^2(1 - \cos\gamma_1)} \quad , \end{aligned} \tag{28}$$

where

$$\begin{aligned} \cos\gamma_1 &= \frac{-x}{R_1} \quad , \\ R_{1y} &= y + a - L\cos\alpha \quad , \\ R_{1z} &= z - L\sin\alpha \quad , \end{aligned} \tag{29}$$

and R_1 is given by (23).

Similar calculations for the field due to the semi-infinite current at G_2 yield

$$H_{G_2x} = 0$$

$$H_{G_2y} = \frac{IR'_{1z}}{4\pi R_1'^2(1 - \cos \gamma_2)} \tag{30}$$

$$H_{G_2z} = \frac{-IR'_{1y}}{4\pi R_1'^2(1 - \cos \gamma_2)} \quad ,$$

where

$$\cos \gamma_2 = -\frac{x}{R'_1}$$

$$R'_{1z} = z - L \sin \alpha \tag{31}$$

$$R'_{1y} = y - a + L \cos \alpha \quad ,$$

and R'_1 is given by (25).

Next we consider the magnetic field in the ground due to the currents flowing in the wire connections and the ground. The contribution due to the half toroid can be calculated with the aid of reference 3. Formulas (22) and (24) apply equally well for points above, on or in the ground. Thus, we can use (22) and (24) to calculate the field in the ground ($x < 0$) due to the two wire segments ($1G_1$) and ($2G_2$).

Consider now the contribution due to the ground currents. For calculation of the field at points in the ground it has been shown in reference 1 that the ground currents can be replaced by two semi-infinite currents oriented upward from the feed points to infinity. In the present case $x < 0$. Consequently for points with $x < 0$ we can use (28) and (30). Notice that the corresponding angles γ_1 and γ_2 are again larger than $\pi/2$, therefore, for $x < 0$ (29) and (31) should read

$$\cos \gamma_1 = \frac{x}{R_1} \quad ,$$

$$\tag{32}$$

$$\cos \gamma_2 = \frac{x}{R'_1} \quad .$$

Finally we present the formulas for the magnetic field due to the half toroid. They are valid for any observation point above, on or below the ground and their derivation is given in reference 3.

$$H_{tx} = (H_\lambda \sin\beta + H_\beta \cos\beta)\cos\xi_1 - H_3 \sin\xi_1$$

$$H_{ty} = H_\beta \sin\beta - H_\lambda \cos\beta$$

$$H_{tz} = H_3 \sin\xi_1 - (H_\lambda \sin\beta + H_\beta \cos\beta)\cos\xi_1$$

where the subscript t indicates the toroid field, and

$$H_\lambda = \frac{I}{16\pi a}\frac{B}{A}\left(\frac{m}{A}\right)^{\frac{1}{2}}\left\{\frac{2-m}{1-m}\left[E\left(\frac{\pi+\beta}{2}\middle|m\right)-E\left(\frac{\beta}{2}\middle|m\right)\right]-2\left[F\left(\frac{\pi+\beta}{2}\middle|m\right)-F\left(\frac{\beta}{2}\middle|m\right)\right]\right.$$
$$\left.+\frac{m(2-m)}{1-m}\sin\frac{\beta}{2}\cos\frac{\beta}{2}\left\{\left[1-m\sin^2\left(\frac{\beta}{2}\right)\right]^{-\frac{1}{2}}+\left[1-m\cos^2\left(\frac{\beta}{2}\right)\right]^{-\frac{1}{2}}\right\}\right\}$$

$$H_\beta = \frac{I}{8\pi a}\frac{B}{A}\left(\frac{m}{A}\right)^{\frac{1}{2}}\left\{\left[1-m\cos^2\left(\frac{\beta}{2}\right)\right]^{-\frac{1}{2}}-\left[1-m\sin^2\left(\frac{\beta}{2}\right)\right]^{-\frac{1}{2}}\right\}$$

$$H_3 = \frac{I}{4\pi a}A^{-3/2}m^{\frac{1}{2}}\left\{\frac{1}{4(1-m)}\left[(1+A)m-2A\right]\left[E\left(\frac{\pi+\beta}{2}\middle|m\right)-E\left(\frac{\beta}{2}\middle|m\right)\right]+\frac{A}{2}\left[F\left(\frac{\pi+\beta}{2}\middle|m\right)-F\left(\frac{\beta}{2}\middle|m\right)\right]\right.$$
$$\left.+\frac{m}{4(1-m)}\left[(1+A)m-2A\right]\sin\frac{\beta}{2}\cos\frac{\beta}{2}\left\{\left[1-m\sin^2\left(\frac{\beta}{2}\right)\right]^{-\frac{1}{2}}+\left[1-m\cos^2\left(\frac{\beta}{2}\right)\right]^{-\frac{1}{2}}\right\}\right\}$$

$$A = \left\{x^2\cos^2\xi_1 + y^2 + z^2\sin^2\xi_1 + xz\sin 2\xi_1\right\}^{\frac{1}{2}}/a$$

$$B = \frac{-x\sin\xi_1 + z\cos\xi_1}{a}$$

$$m = \frac{4A}{(1+A)^2 + B^2}$$

$$\beta = \arctan \frac{x \cos \xi_1 + z \sin \xi_1}{-y}$$

$$E(p + s|q) - E(p|q) = \int_p^{p+s} (1 - q \sin^2 t)^{\frac{1}{2}} dt$$

$$F(p + s|q) - F(p|q) = \int_p^{p+s} (1 - q \sin^2 t)^{-\frac{1}{2}} dt \quad .$$

Summary and Discussion of Results

The purpose of this note is to alleviate some of the difficulties encountered in the situation examined in reference 1 with respect to the simulation of the EMP. In reference 1 the half toroid is directly joined at its ends to a finitely conducting ground and the pattern of the resulting ground currents is independent of the inclination angle of the toroid with respect to the ground. As a result a vertical component of the low frequency magnetic field exists at the origin and in a region close to the origin. This feature makes the simulation of the low frequency content of the EMP around the origin less satisfactory than when the ground is considered perfectly conducting. In fact when the ground is considered perfectly conducting the simulation at the origin is exact and remains good in a region near the origin.

The main undesirable features discussed in reference 1 are the following. a) The magnetic field in the symmetry plane xz and especially close to the origin deviates considerably from the magnetic field that would exist if the ground were perfectly conducting. b) Increasing the inclination angle ξ_1 of the toroid increases the field distortion relative to the perfectly conducting ground case. c) The maximum normalized field deviation $|\underline{\Delta h}|/\cos \xi_1$ over the surface of a hemisphere centered at the origin or on the perimeter of a circle with center at the origin assumes large values close to the origin, thus deteriorating the simulation.

To alleviate these shortcomings we modified the ground connections. Our basic motivation was to approximately create the image toroid which exists for a perfectly conducting ground. This image approaches the ground surface as the inclination angle ξ_1 increases. To satisfy this requirement we ground the toroid not directly as in reference 1 but through two wire segments that lie in the ground plane and form an angle α with respect to the line joining the ends of the half toroid (Fig. 2). The length L of each segment and the angle α are functions of ξ_1 and they become progressively larger as ξ_1 increases. In that fashion the current path from one end of the toroid to the other through the ground is a function of ξ_1 and tends to imitate the perfectly conducting ground image of the toroid. The field at the origin is chosen to coincide with that corresponding to a perfectly conducting ground and consequently it

also coincides with the desired EMP signal. To see how successful the modified connections are in imitating a perfectly conducting ground we present plots of field quantities for the same range of parameters as in reference 3. For points on or above the ground we plot the total magnetic field components, normalized to $(I/2a)\cos \xi_1$ versus z/a with parameters x/a, y/z and ξ_1. Due to symmetry we choose $y \geq 0$. For $\xi_1 = 0$ and a perfectly conducting ground ($\sigma = \infty$) any plane through the z axis is equivalent for the calculation of the field components. Consequently, in reference 3 the z and ψ magnetic field components are plotted versus z/a with ψ/a as a parameter (the azimuthal component is zero). ψ is the polar radius in the xy plane. Contour plots are also given for constant $|\Delta \underline{h}|/\cos \xi_1$ in a typical $z\psi$ plane. Only positive z's are considered because of the symmetry about the xy plane for a vertical toroid. In the modified ground connections case and $\xi_1 = 0$ only the $y = 0$ plane corresponds to the $z\psi$ planes considered in the $\sigma = \infty$ situation. Plots of the x and z field components are given versus z/a with x/a as a parameter. (The y-component is zero.) Also contour plots for constant $|\Delta \underline{h}|/\cos \xi_1$ are presented in the $y = 0$ plane.

In the perfectly conducting case for any inclination angle ξ_1, the y component of the field is zero in the xz ($y = 0$) plane. This is also the case in this plane for $\sigma \neq \infty$. The x component is zero in the $x = 0$ ground plane for $\sigma = \infty$. This is not the case for the modified connections case except at the origin. Thus, we give plots of $h_x/\cos \xi_1$ ($h_x = (2a/I)H_x$) versus z/a with y/a and ξ_1 as parameters. As ξ_1 increases the y coordinate of the ground contact G_2 decreases and for observation points with $y \geq y_{G_2}$, h_x turns out to be infinite when z is large enough to hit the wire segment. This shortcoming, however, is not of importance since from the geometry we can show that as long as the maximum distance of an observation point from the origin is less than .6a we never hit the wire; on the other hand the simulation region is closer to the origin where our h_x stays small. Even for a perfectly conducting ground the simulation has deteriorated for points with $r > .6a$. As a result we only plot a finite x-component of the field in the $x = 0$ plane. The y and z components of the field are finite in the entire $x = 0$ plane. The reason is that the field produced by the wire segment in its immediate vicinity, in the $x = 0$ plane, has zero y and z components. We present plots for $h_y/\cos \xi_1$ and $h_z/\cos \xi_1$ versus z/a with y/a and ξ_1 as parameters. Similar

plots are also given in reference 3.

We present contour plots of constant $|\Delta\underline{h}|/\cos\xi_1$ only for y = 0, i.e., along the symmetry plane. In reference 3 contour plots are also given in the planes y = .5a and .8a. In these planes the modified connections do not imitate the perfectly conducting ground well when we get close to the wire segments. In the contour plots a star * is used to indicate the position of the intersection of the toroid with the plane under consideration.

Finally we maximize $|\Delta\underline{h}|/\cos\xi_1$ on the circumference of a circle in the x = 0 plane and over the surface of a hemisphere resting on the ground. The centers of the circle and the hemisphere coincide with the origin. Studying the plots of the present note and comparing them to the ones in reference 1 (simple ground connections) and in reference 3 (perfectly conducting ground) we can draw the following general conclusions. a) The main undesirable features present in the simple ground connections case and discussed earlier have been reduced through our modified ground connections. b) Away from the origin (r > .3a) the simple connections tend to represent the $\sigma = \infty$ case better than our modified connections except for ξ_1 large ($2\xi_1/\pi \geq .7$). Thus, for $2\xi_1/\pi = .7$ the inequality becomes r > .4a and for $2\xi_1/\pi = .9$, r > .6a. c) For large x ($x \geq .8a$) all three cases seem equivalent; the reason is that the observation points are much closer to the half toroid than to the rest of the currents and consequently the field is not sensitive to the current path that closes the half toroid. If the comparison is restricted to the modified connections versus $\sigma = \infty$ we can make the following observations. a) The magnetic field for the perfectly conducting ground is best approximated in the xz symmetry plane of the toroid. b) For observation points in the x = 0 plane, the x-component of the field gets rapidly distorted in the vicinity of the wire segments. The distortion of the y and z components is significantly less. The reason is that in the x = 0 plane either wire segment can only produce a vertical field. c) Comparison of the maximum field deviation curves for the two cases exhibits a variety of features. Close to the origin (i.e. small r/a) the fit is best for $\xi_1 = 0$. For larger r/a the $\xi_1 = 0$ and $2\xi_1/\pi = .2$ curves for the mofified connections start to rapidly deviate from the $\sigma = \infty$ curves. For ξ_1 large i.e., $2\xi_1/\pi = .5$, .7 and .9 the deviation is considerably less.

Specifically for $2\xi_1/\pi = .9$ the two curves exhibit the same trend and their percentage deviation varies slowly with r/a. These features can be understood if we take into account that both the $\sigma = \infty$ and the modified connections cases are expected to best simulate the EMP for small r/a and small ξ_1 and that the modified connections best approximate the $\sigma = \infty$ case for large ξ_1.

For points below the ground the field calculated with the modified connections exhibits the following features. a) The rate of decay for all three components increases with ξ_1. b) The x-component has the most sensitive ξ_1 dependence. c) The decay rate for all three components increases with increasing y for ξ_1 fixed. These features can be explained by referring to the geometry of the currents flowing through the toroid, the wire segments, and the ground. To draw a comparison between the simple connections studied in reference 1 and the modified connections, we first make the following observations. a) For the simple connections the x-component is due to the toroid only but for the modified connections the wire segments can significantly contribute. b) The y-component is not affected by the wire segments. Therefore, any difference between the two cases should be attributed to the variable location of the equivalent current elements in the modified connections case. c) Currents in all the possible paths produce a z component for both cases. Proper interpretation of the plots and consideration of the above observations can provide an adequate explanation for the following features pertaining to the comparison between the simple and modified connections. a) For fixed ξ_1 and y all three components for the modified connections decay faster than for the simple connections. This difference is enhanced by increasing ξ_1 and is mostly pronounced for the x-component. b) For fixed ξ_1 and increasing y the decay rate for all three components in both cases increases. This increase is slower for the modified connections and especially for the x component.

In this note we have attempted to design the ground connections in a way that would imitate a perfectly conducting ground for the calculation of the low frequency magnetic field. Our ultimate goal is of course the simulation of the EMP. We have compared our results to the $\sigma = \infty$ case only because a perfectly conducting ground appears to provide an upper bound for the EMP simulation (at least in a small region around the origin). From the practical

point of view the value of our modified connections can be judged by a direct comparison of the field distribution to the real EMP situation and all of our curves have been appropriately normalized to facilitate such a comparison.

Table 1*

$2\xi_1/\pi$	L/a	$2\alpha/\pi$	z_{G_2}/a	y_{G_2}/a
0	.363	0	0	.636
1/90	.364	.024	.014	.636
1/45	.365	.047	.027	.636
1/30	.367	.071	.041	.635
2/45	.370	.093	.054	.634
1/18	.374	.115	.067	.632
1/15	.379	.136	.081	.630
7/90	.384	.157	.094	.627
4/45	.390	.176	.107	.625
1/10	.397	.195	.120	.622
1/9	.404	.212	.132	.618
11/90	.412	.229	.145	.615
2/15	.420	.244	.157	.610
13/90	.428	.258	.169	.606
7/45	.437	.271	.180	.602
1/6	.446	.283	.192	.597
8/45	.455	.295	.203	.593
17/90	.465	.305	.214	.588
.2	.474	.314	.225	.582
19/90	.484	.323	.236	.577
2/9	.494	.332	.246	.572
7/30	.504	.339	.256	.566
11/45	.514	.346	.266	.560
23/90	.524	.353	.276	.555
4/15	.534	.359	.285	.549
5/18	.543	.364	.294	.543
13/45	.553	.369	.303	.537
3/10	.563	.374	.312	.531
14/45	.573	.378	.321	.525
29/90	.582	.383	.329	.520
1/3	.592	.386	.337	.514
31/90	.601	.390	.345	.508
16/45	.611	.393	.353	.502
11/30	.620	.396	.361	.496
17/45	.629	.399	.369	.490
7/18	.638	.402	.376	.485
2/5	.647	.404	.384	.479
37/90	.656	.407	.391	.474
19/45	.665	.409	.399	.468
13/30	.674	.412	.406	.463
4/9	.682	.414	.413	.457
41/90	.691	.417	.421	.452
7/15	.699	.419	.428	.447
43/90	.708	.421	.435	.442
22/45	.716	.424	.442	.436
.5	.725	.426	.450	.431
23/45	.733	.428	.457	.426
47/90	.742	.431	.465	.422
8/15	.750	.433	.472	.417
49/90	.759	.435	.480	.412

Table 1 (Continued)

$2\xi_1/\pi$	L/a	$2\alpha/\pi$	z_{G_2}/a	y_{G_2}/a
5/9	.767	.438	.487	.407
17/30	.776	.441	.495	.403
26/45	.784	.443	.503	.398
53/90	.793	.446	.511	.394
3/5	.802	.449	.520	.389
11/18	.811	.452	.528	.385
28/45	.820	.455	.537	.381
19/30	.829	.458	.546	.376
29/45	.838	.461	.556	.372
59/90	.848	.465	.565	.368
2/3	.858	.468	.575	.364
61/90	.868	.472	.586	.359
31/45	.878	.475	.596	.355
.7	.889	.479	.607	.351
32/45	.900	.483	.619	.347
13/18	.912	.487	.631	.343
11/15	.924	.491	.644	.338
67/90	.936	.496	.658	.334
34/45	.949	.500	.672	.329
23/30	.963	.505	.687	.325
7/9	.978	.511	.703	.320
71/90	.993	.516	.719	.315
4/5	1.009	.521	.737	.310
73/90	1.027	.527	.756	.305
37/45	1.045	.533	.776	.300
5/6	1.066	.539	.798	.294
38/45	1.087	.545	.821	.288
77/90	1.111	.552	.847	.281
13/15	1.136	.559	.874	.274
79/90	1.164	.566	.904	.266
8/9	1.196	.574	.937	.257
.9	1.230	.581	.973	.248
41/45	1.269	.589	1.013	.237
83/90	1.313	.598	1.059	.224
14/15	1.363	.606	1.111	.210
17/18	1.422	.616	1.170	.192
43/45	1.491	.625	1.240	.172
87/90	1.576	.635	1.324	.146
44/45	1.681	.643	1.428	.112
89/90	1.821	.656	1.563	.067

*In this table we give the location of the wire segments as a function of the inclination angle ξ_1 (Fig. 2). The increments of ξ_1 are 1° ($= \pi/180$). We also give the basic angles that were used in the plots, i.e. $2\xi_1/\pi = 0, .2, .5, .7$ and .9. The cartesian coordinates of G_1 are $z_{G_1} = z_{G_2}$, $y_{G_1} = -y_{G_2}$.

Table of Plots

	$h_x/\cos\xi_1$ vs. z/a					$h_y/\cos\xi_1$ vs. z/a					$h_z/\cos\xi_1$ vs. z/a				
$2\xi_1/\pi$	0	.2	.5	.7	.9	0	.2	.5	.7	.9	0	.2	.5	.7	.9
Fixed Parameter															
y/a = 0	6A	14A	22A	30A	38A						6C	14C	22C	30C	38C
y/a = .5	7A	15A	23A	31A	39A	7B	15B	23B	31B	39B	7C	15C	23C	31C	39C
y/a = .8	8A	16A	24A	32A	40A	8B	16B	24B	32B	40B	8C	16C	24C	32C	40C
x/a = 0	9A	17A	25A	33A	41A	9B	17B	25B	33B	41B	9C	17C	25C	33C	41C
x/a = -.2	10A	18A	26A	34A	42A	10B	18B	26B	34B	42B	10C	18C	26C	34C	42C
x/a = -.5	11A	19A	27A	35A	43A	11B	19B	27B	35B	43B	11C	19C	27C	35C	43C
x/a = -.8	12A	20A	28A	36A	44A	12B	20B	28B	36B	44B	12C	20C	28C	36C	44C
x/a = -1	13A	21A	29A	37A	45A	13B	21B	29B	37B	45B	13C	21C	29C	37C	45C

Contour Plots

$\frac{x}{a}$ versus $\frac{z}{a}$ for constant values of $\frac{|\underline{h} - \hat{a}_z \cos\xi_1|}{\cos\xi_1}$ and $\frac{y}{a} = 0$

$2\xi_1/\pi$	0	.2	.5	.7	.9
Figure No.	46	47	48	49	50

Maximum Deviation Plots

$\frac{|\underline{h} - \hat{a}_z \cos\xi_1|}{\cos\xi_1}$ maximized over a circle versus $\frac{r}{a}$, Figure No. 51

$\frac{|\underline{h} - \hat{a}_z \cos\xi_1|}{\cos\xi_1}$ maximized over a hemisphere versus $\frac{r}{a}$, Figure No. 52

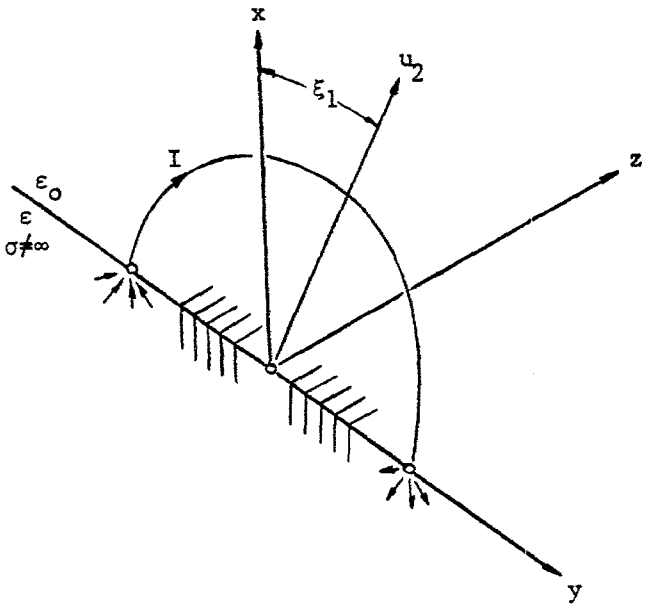

Fig. 1. Geometry of a half toroid directly connected to a finitely conducting ground. The u_2 axis lies in the plane of the toroid which has a radius a.

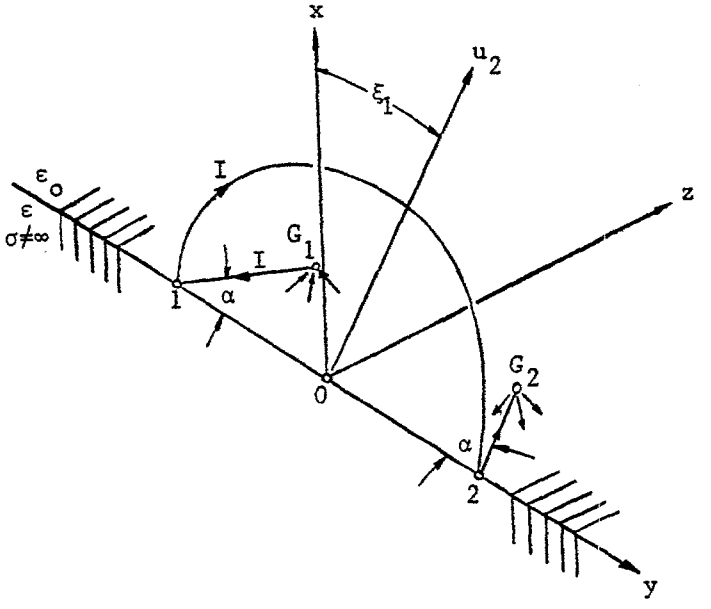

Fig. 2. Geometry of a half toroid connected to a finitely conducting ground by modified connections. $(1G_1)$ and $(2G_2)$ are wire segments lying in the yz plane.

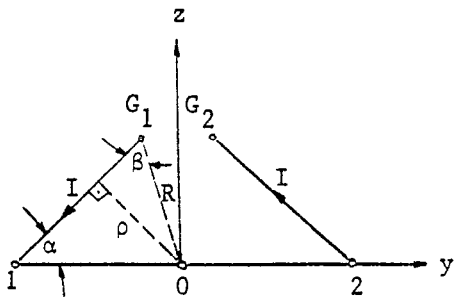

Fig. 3. Geometry for the calculation of the magnetic field at the origin due to the currents flowing in the wire segments ($1G_1$) and ($2G_2$). The length of each segment is L.

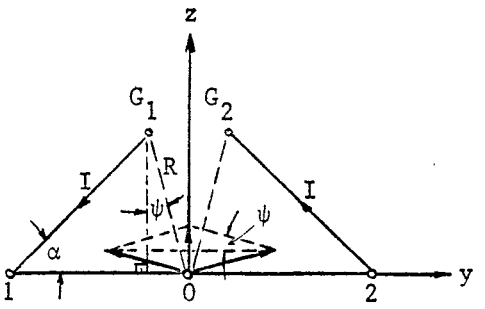

Fig. 4. Geometry for the calculation of the magnetic field at the origin due to the ground currents. For this calculation the ground currents can be replaced by two semi-infinite current elements oriented downward from the field points G_1, G_2 to infinity.

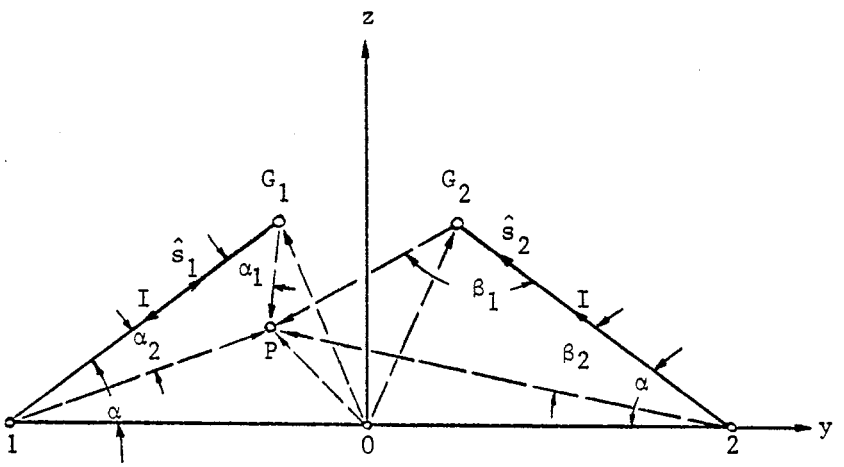

Fig. 5. Geometry for the calculation of the magnetic field at an observation point P(x,y,z) with $x \geq 0$, due to currents flowing in the wire segments ($1G_1$), ($2G_2$) and in the ground. (0P) = $\underline{r}$, (G_1P) = $\underline{R}_1$, (1P) = $\underline{R}_2$, (0G_1) = $\underline{r}_{G_1}$, (0G_2) = $\underline{r}_{G_2}$, (G_2P) = $\underline{R}_1'$, (2P) = $\underline{R}_2'$ and (10) = (02) = $a\hat{a}_y$.

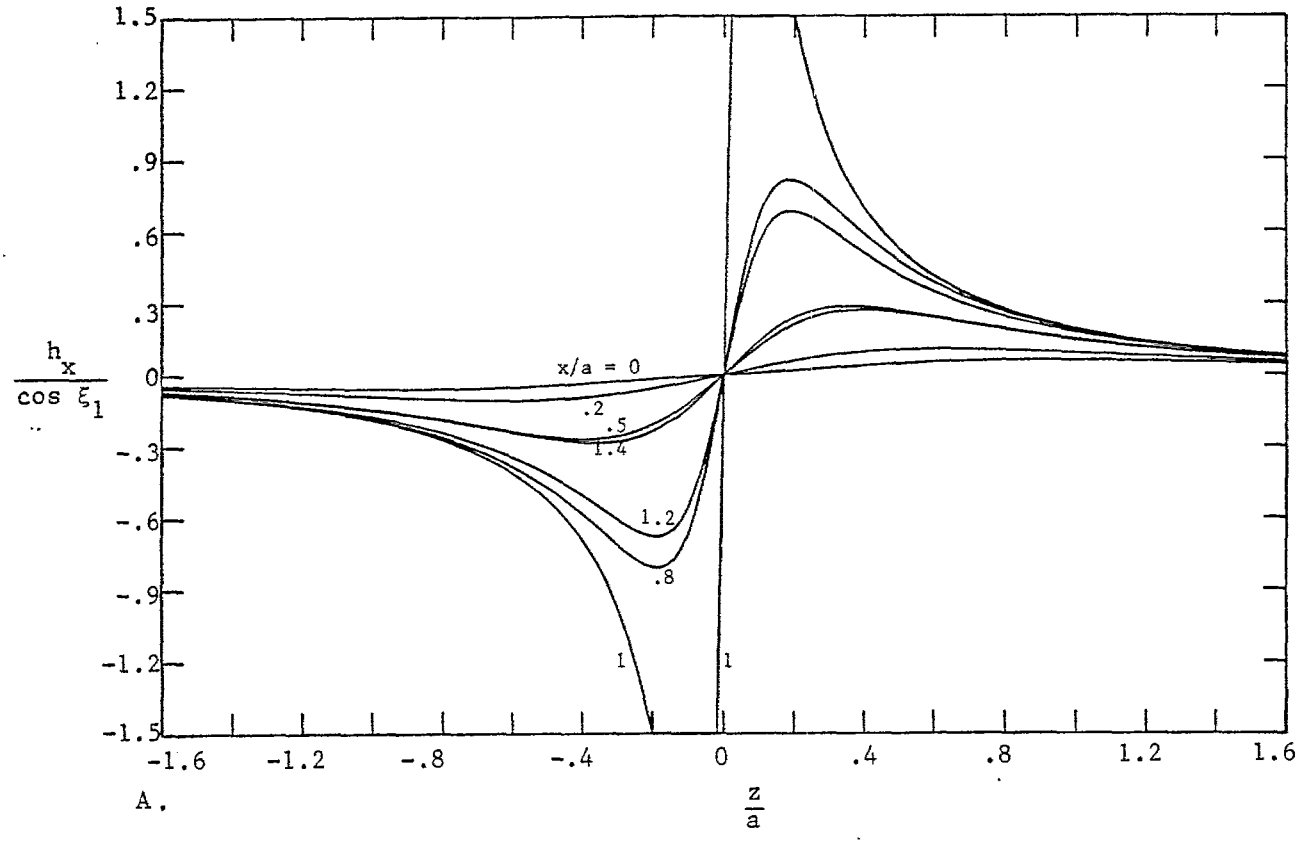

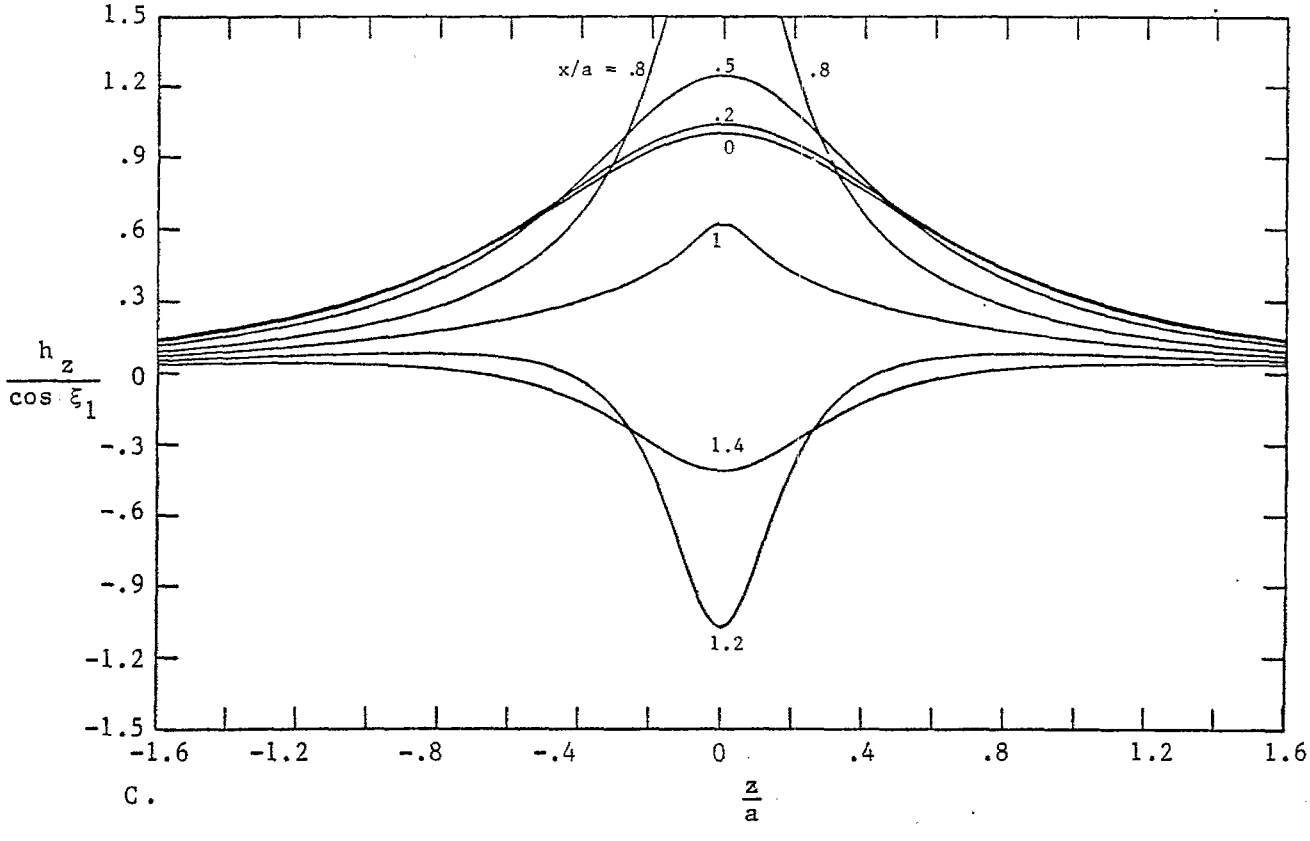

Figure 6. Magnetic Field Components as a Function of z: $\frac{2\xi_1}{\pi} = 0$; $\frac{y}{a} = 0$.

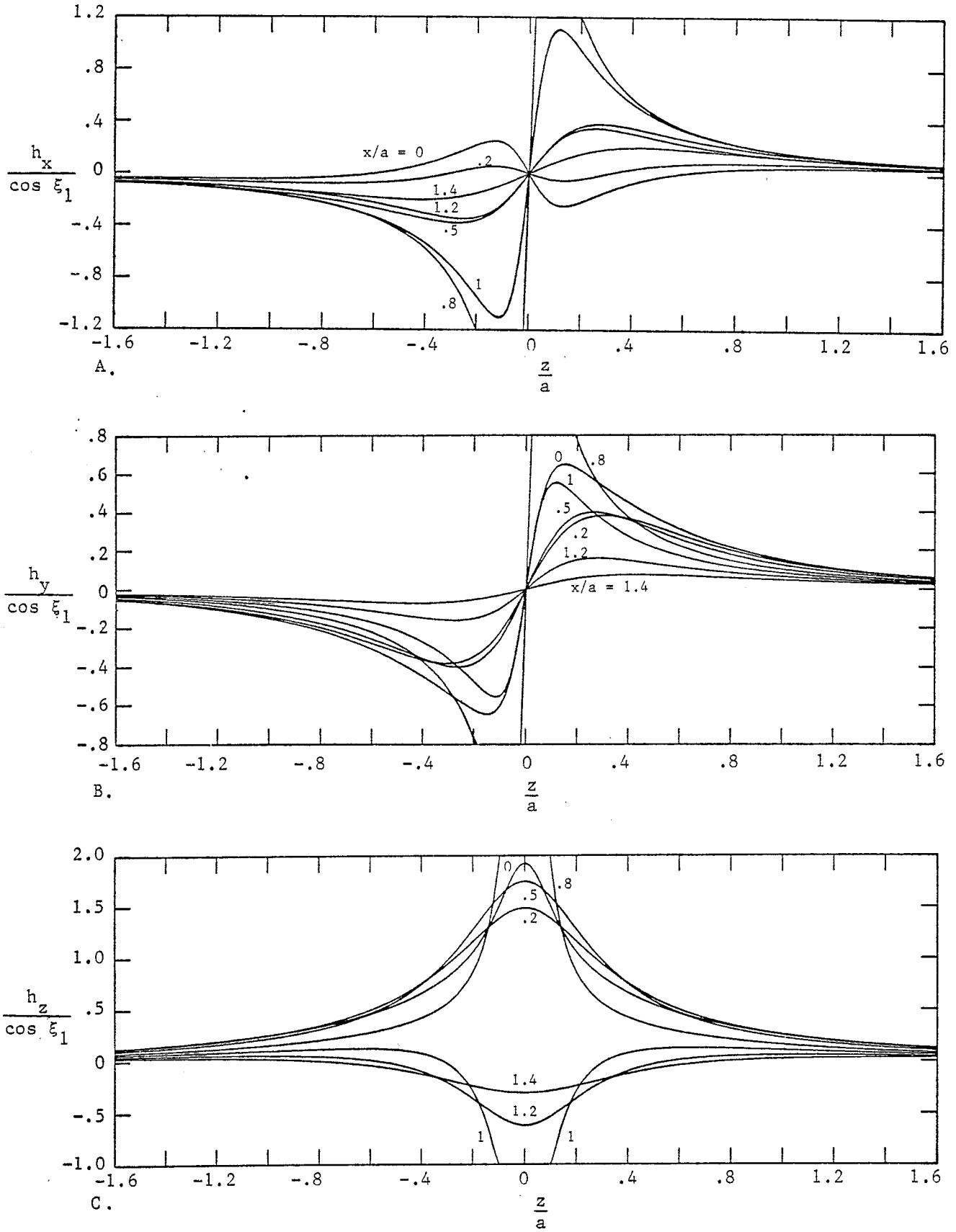

Figure 7. Magnetic Field Components as a Function of z; $\frac{2\xi_1}{\pi} = 0$; $\frac{y}{a} = .5$.

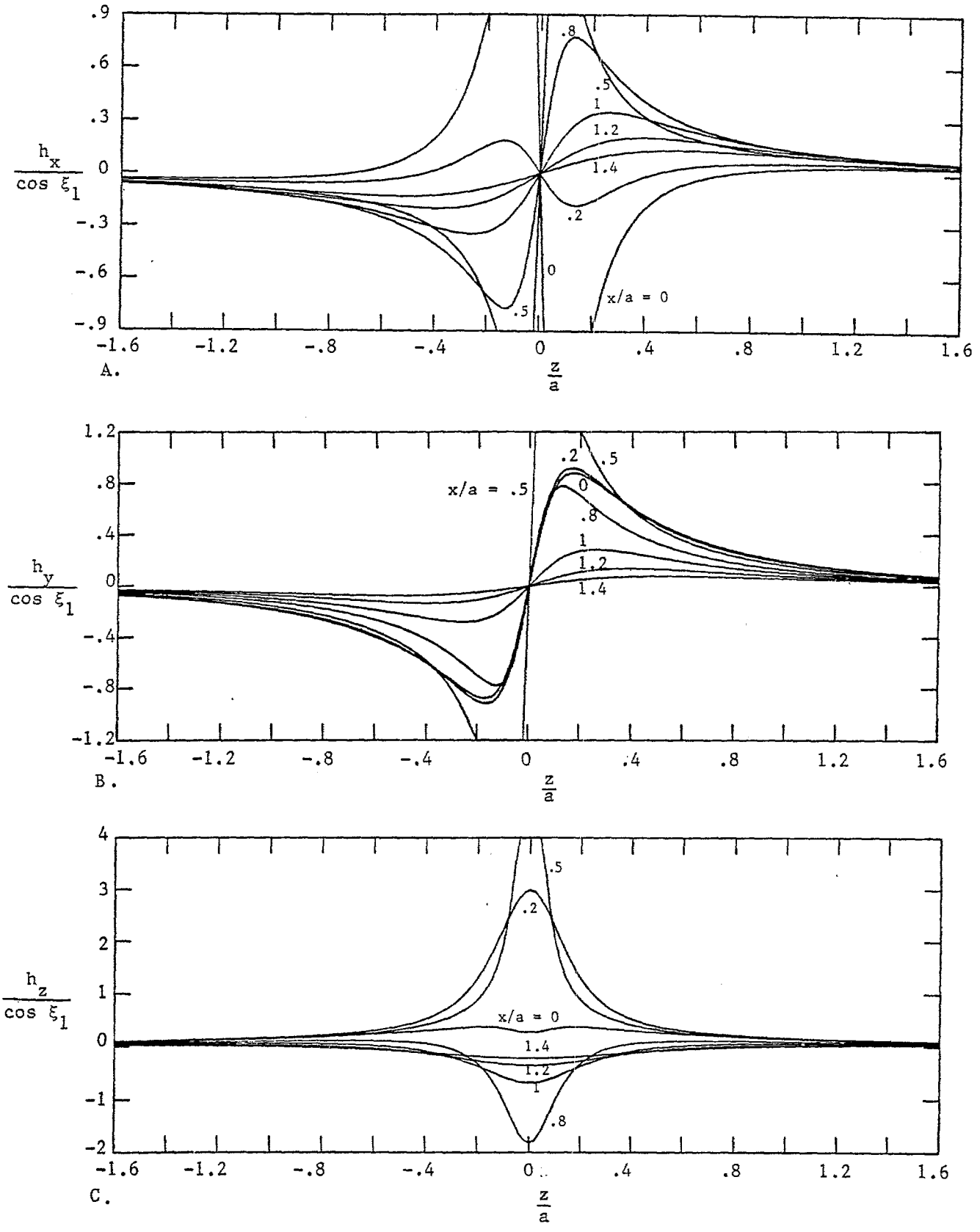

Figure 8. Magnetic Field Components as a Function of z: $\frac{2\xi_1}{\pi} = 0; \frac{y}{a} = .8.$

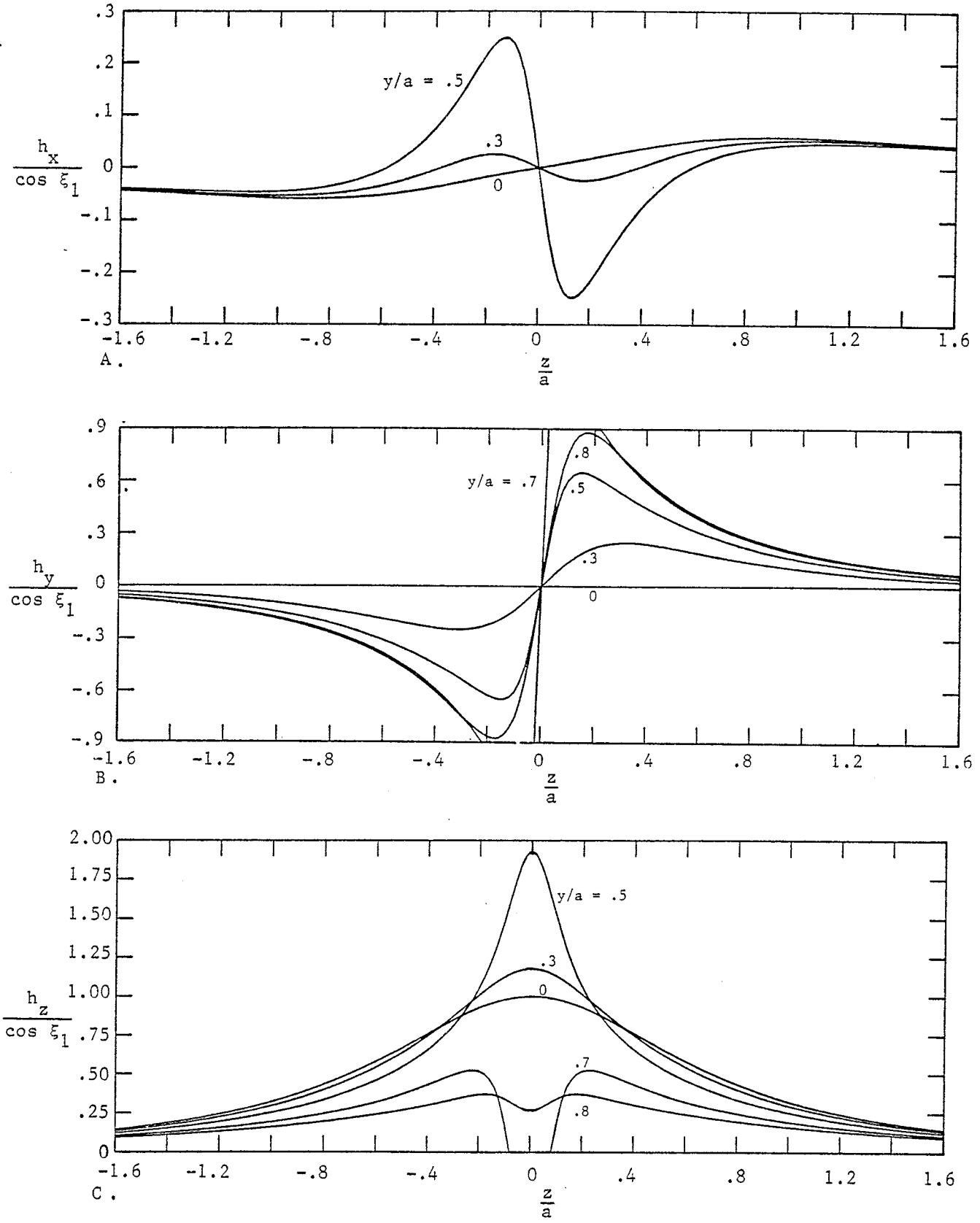

Figure 9. Magnetic Field Components as a Function of z: $\frac{2\xi_1}{\pi} = 0$; $\frac{x}{a} = 0$.

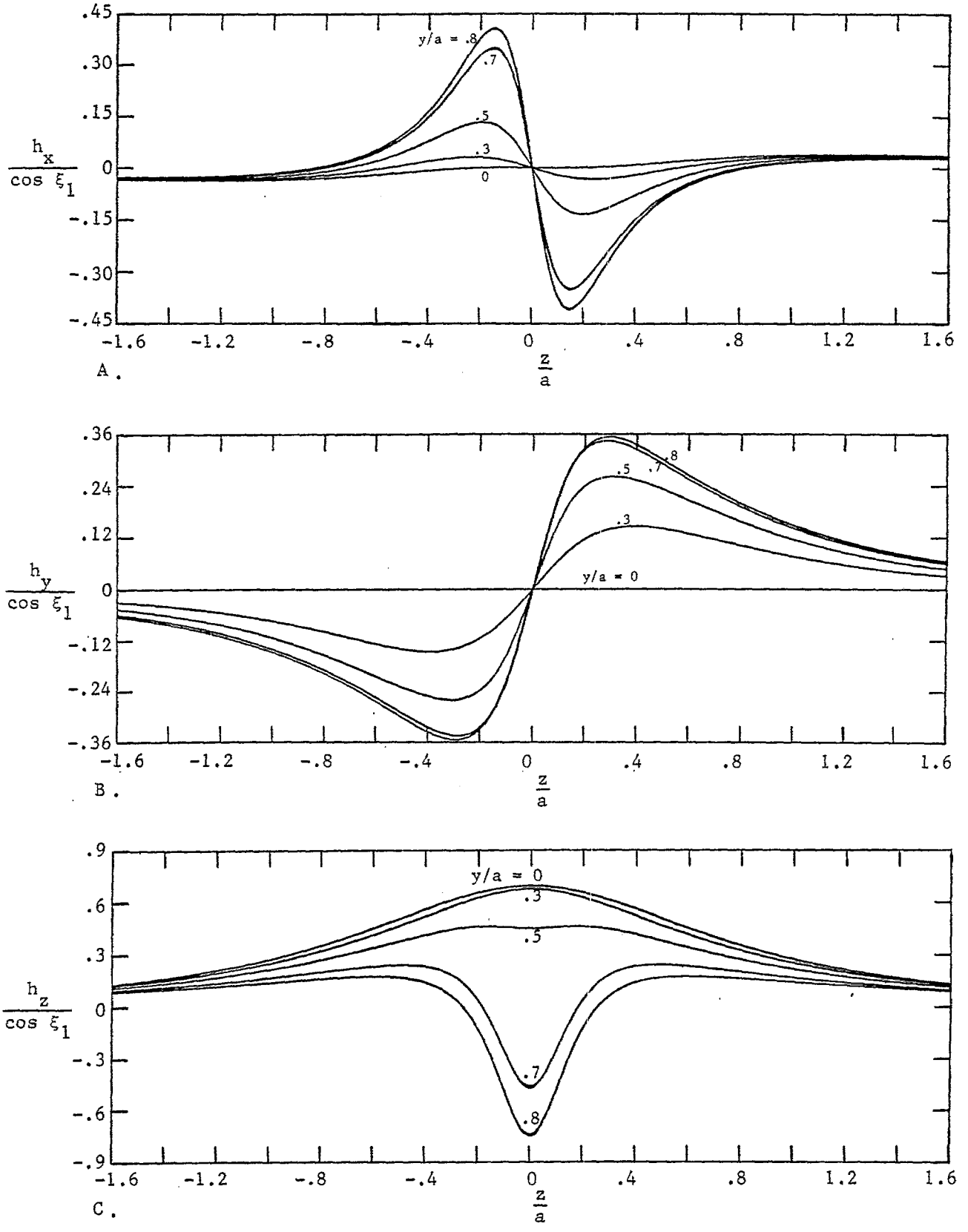

Figure 10. Magnetic Field Components as a Function of z; $\frac{2\xi_1}{\pi} = 0$; $\frac{x}{a} = -.2$.

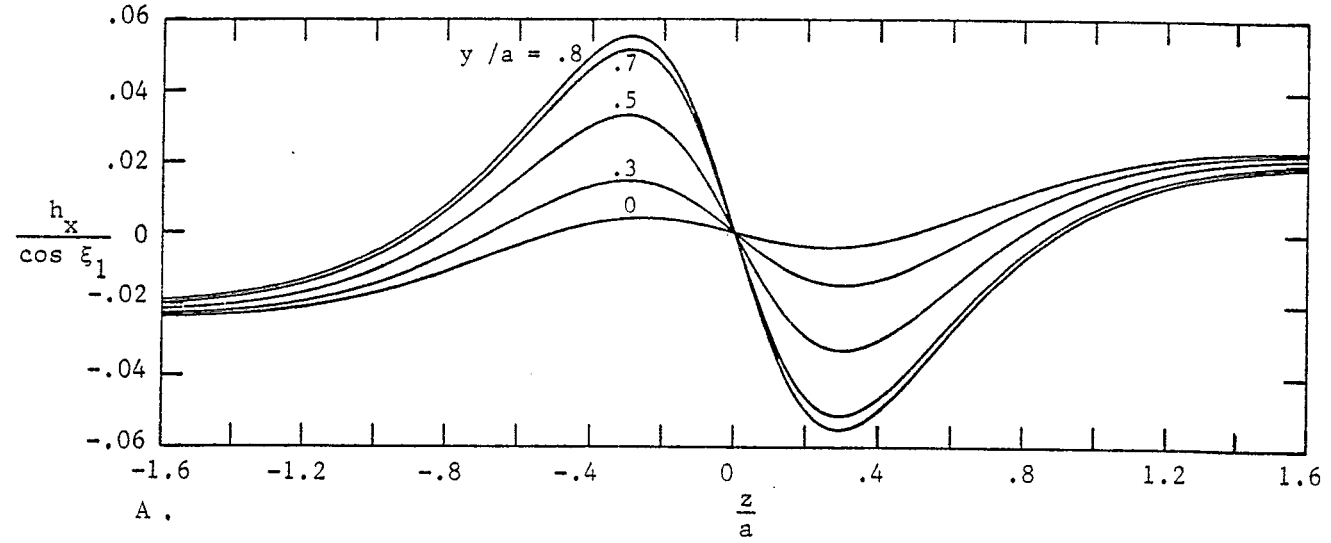

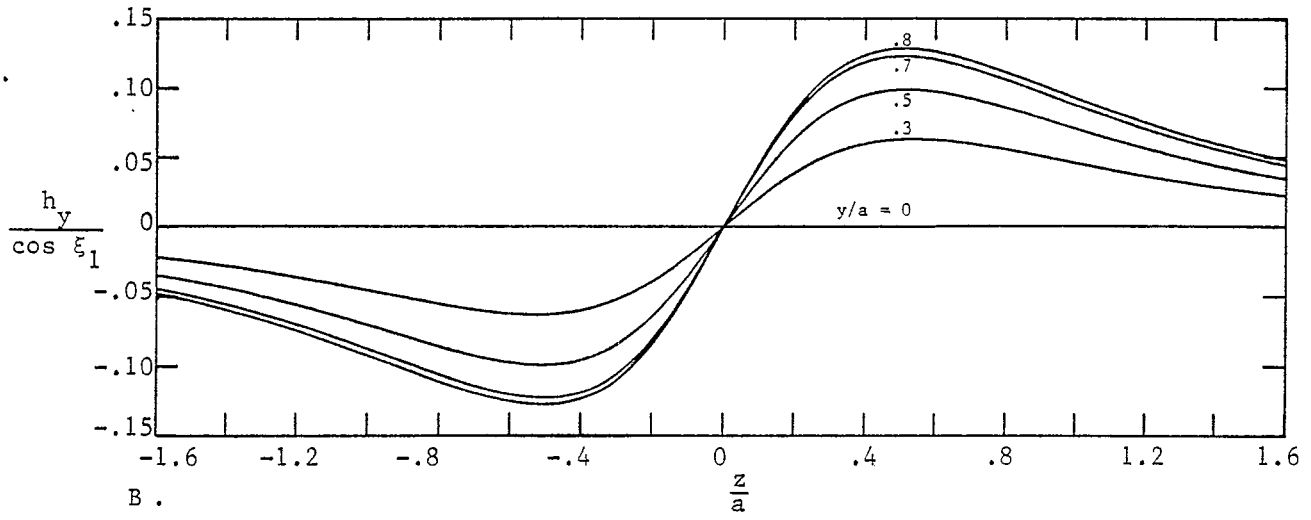

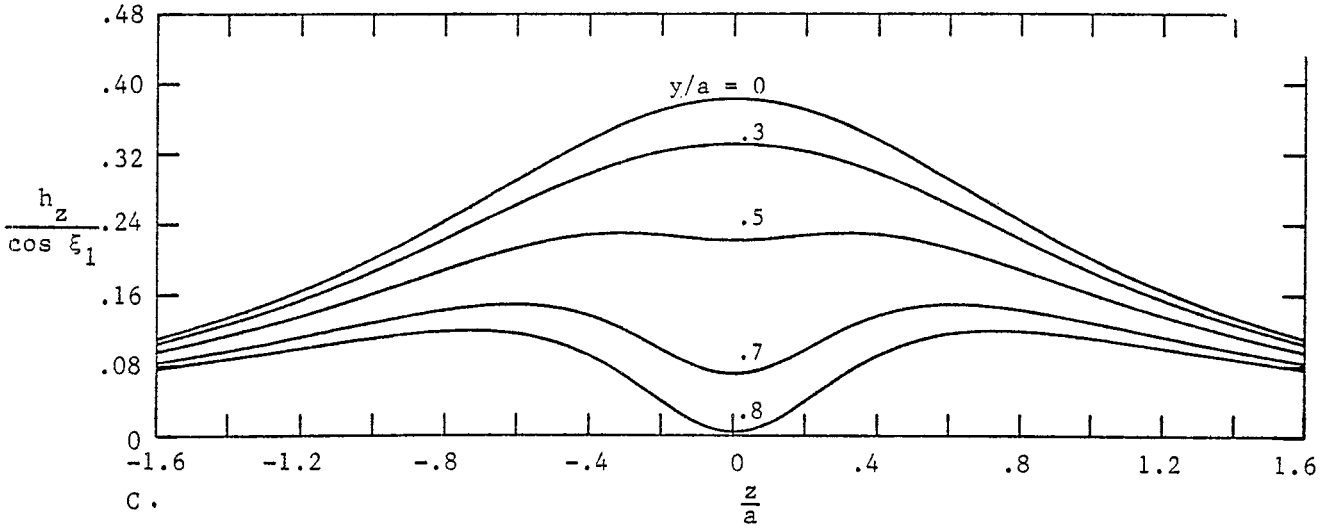

Figure 11. Magnetic Field Components as a Function of z: $\frac{2\xi_1}{\pi} = 0$; $\frac{x}{a} = -.5$.

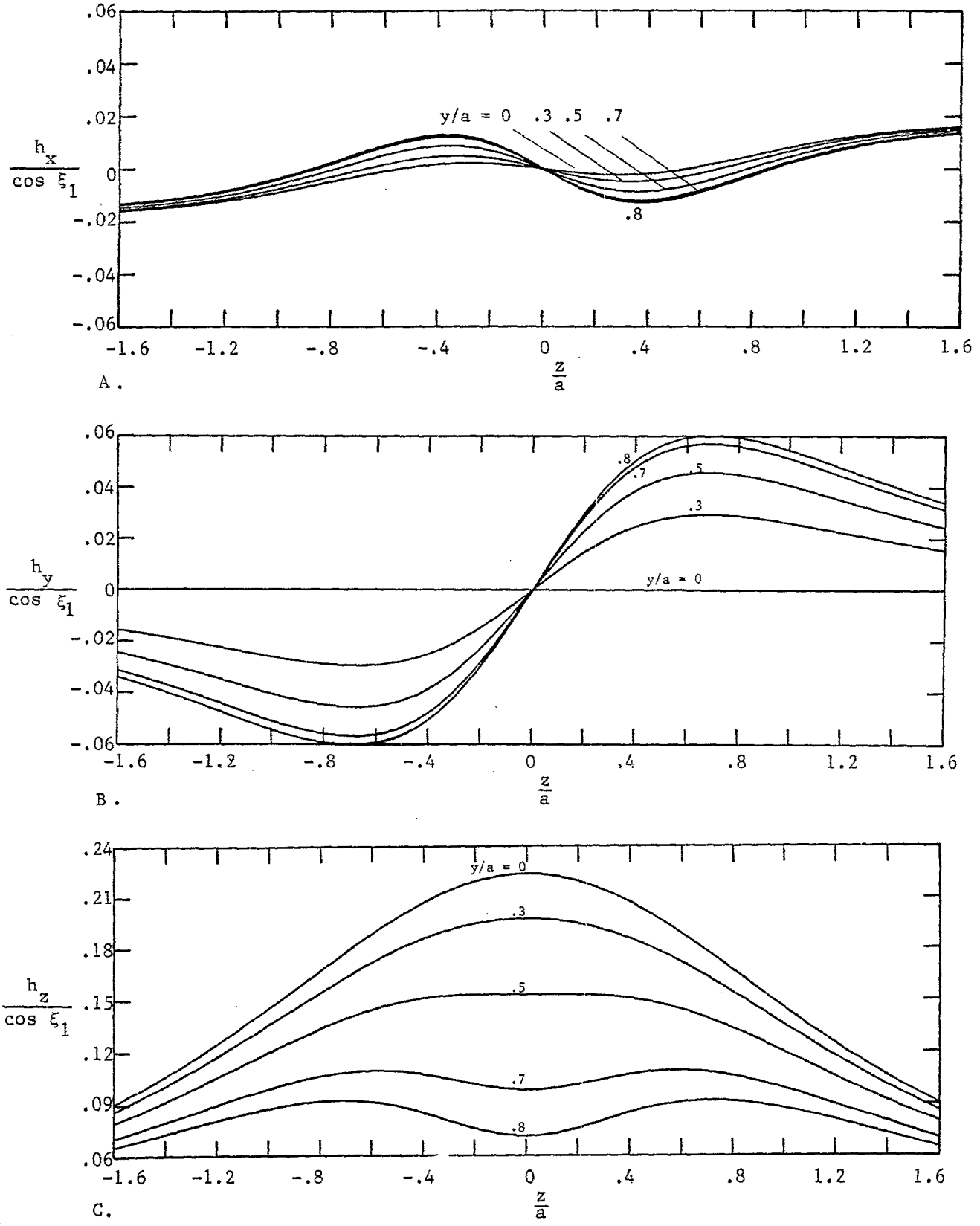

Figure 12. Magnetic Field Components as a Function of z: $\frac{2\xi_1}{\pi} = 0$; $\frac{x}{a} = -.8$.

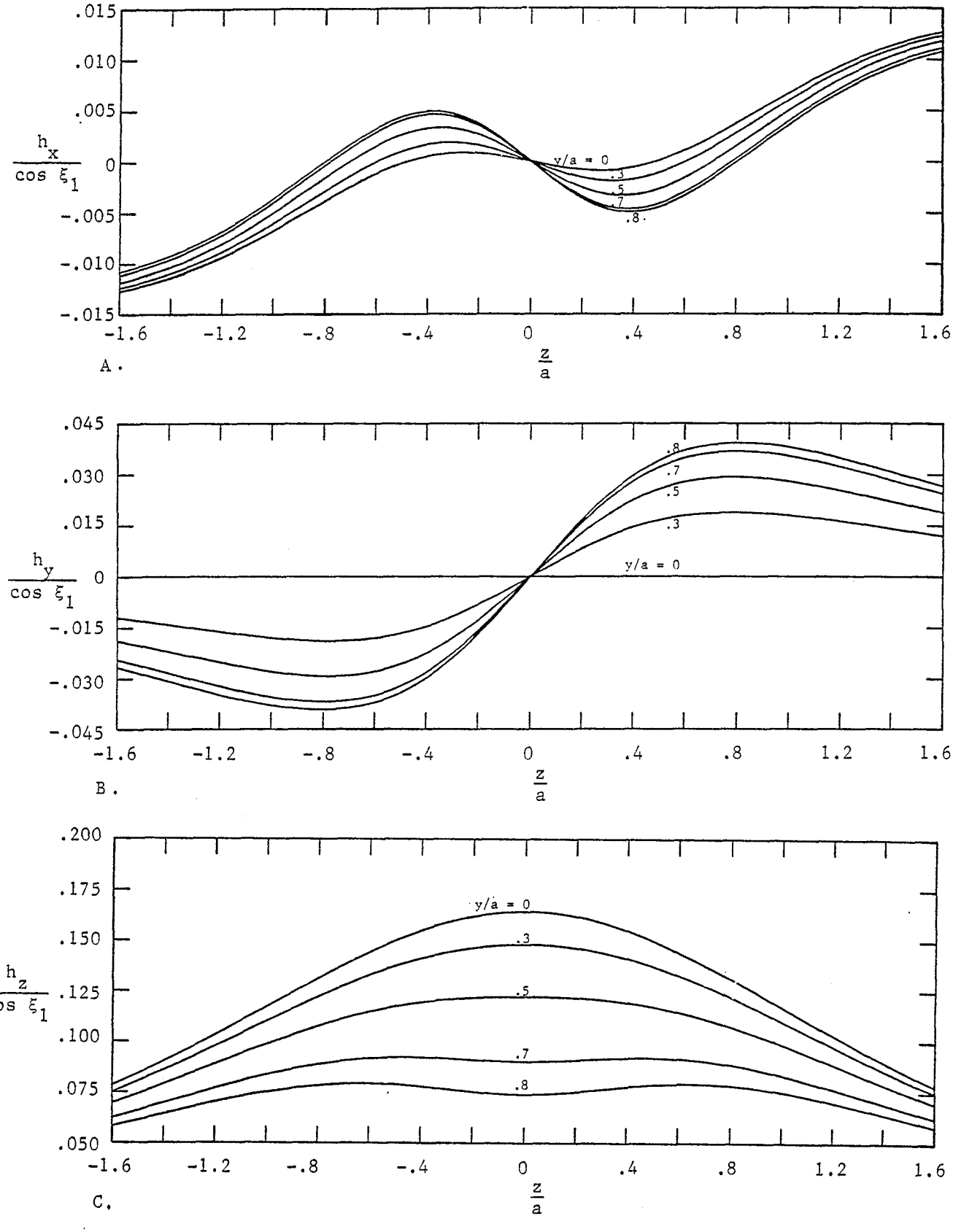

Figure 13. Magnetic Field Components as a Function of z: $\frac{2\xi_1}{\pi} = 0$; $\frac{x}{a} = -1$.

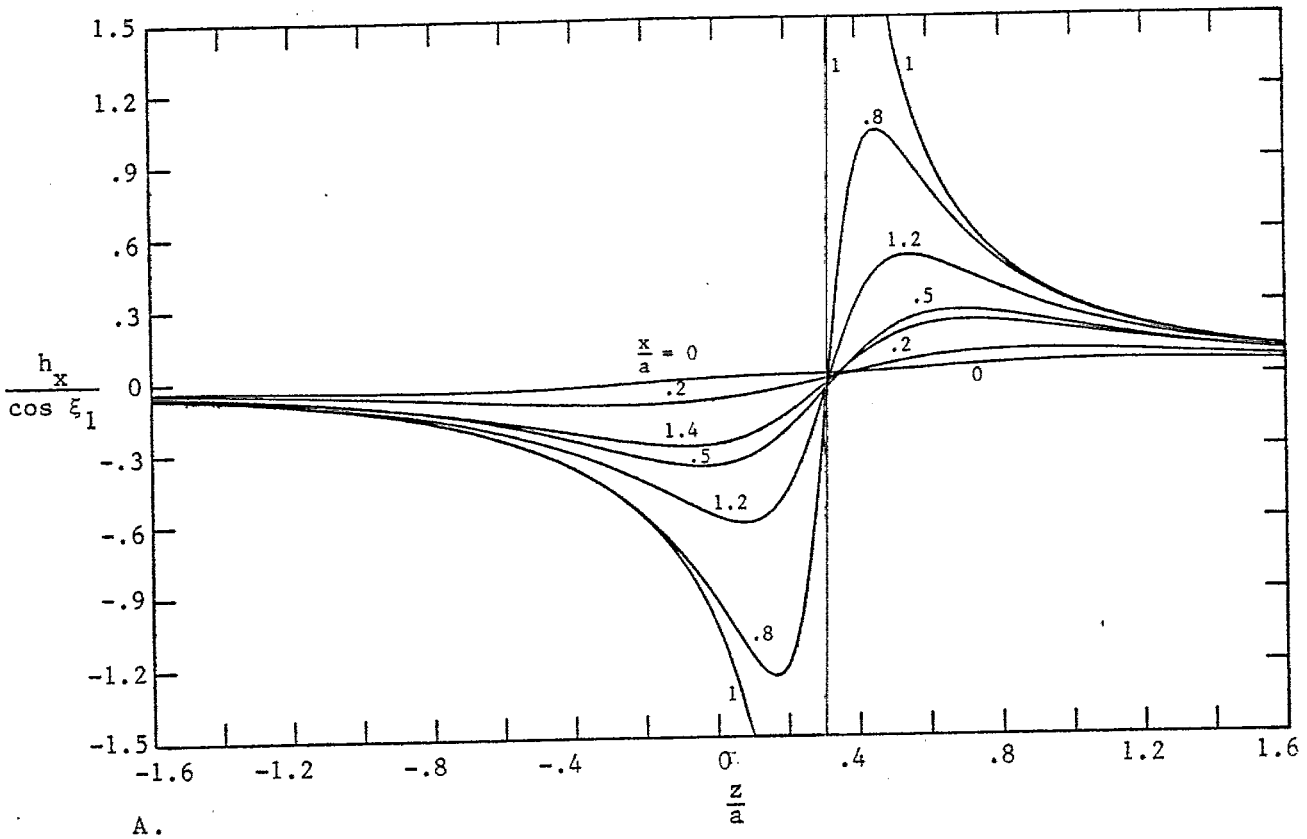

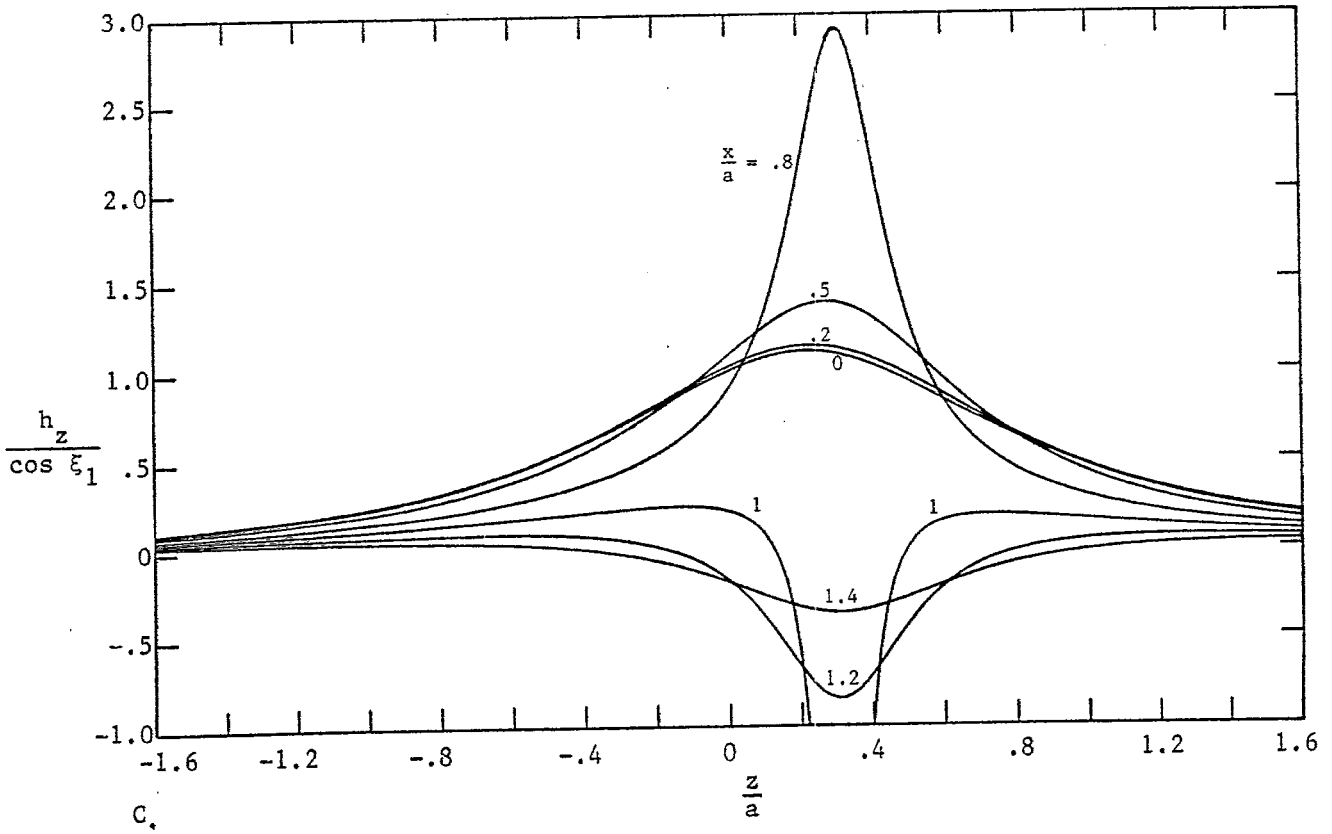

Figure 14. Magnetic Field Components as a Function of z: $\frac{2\xi_1}{\pi} = .2$; $\frac{y}{a} = 0$.

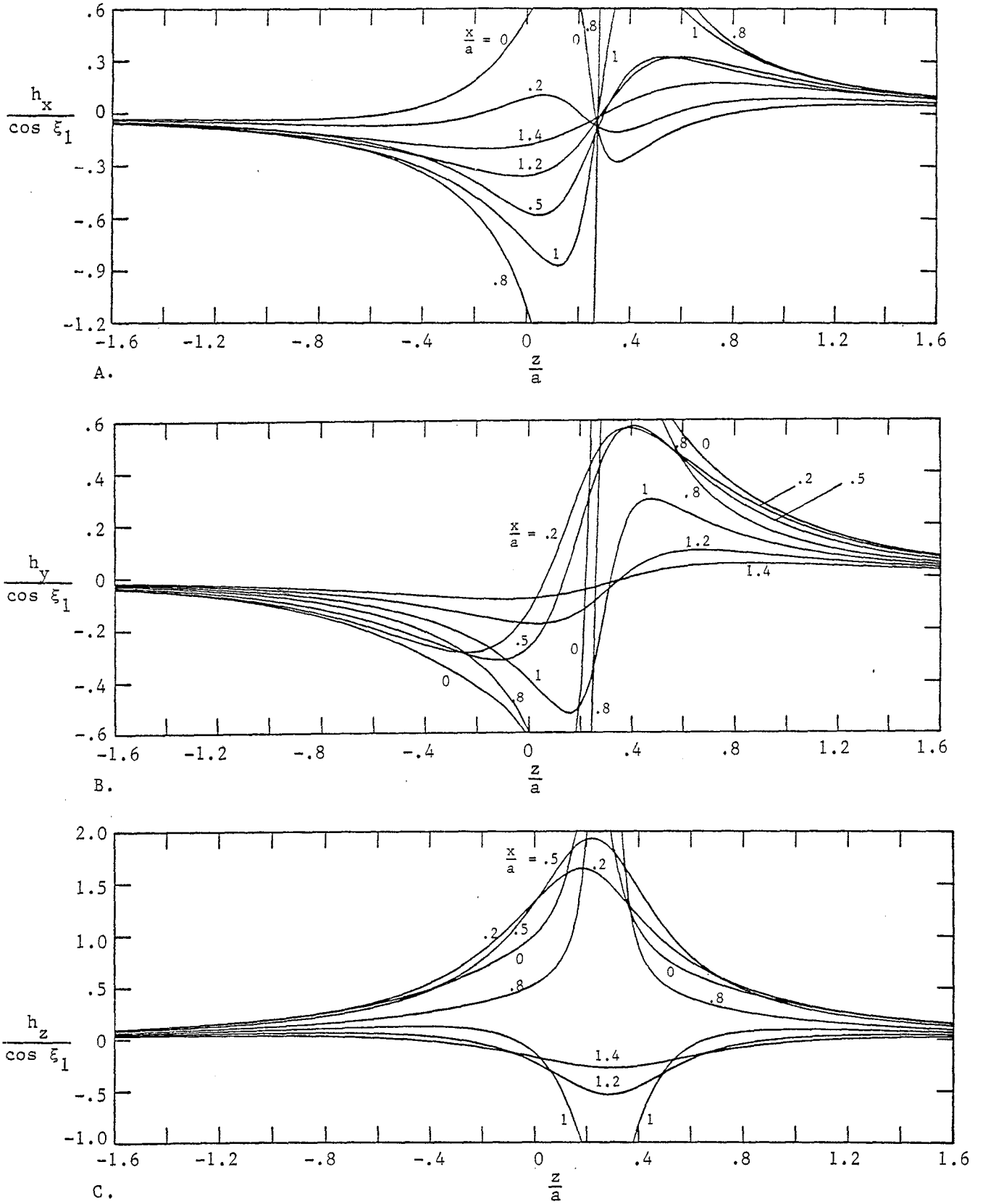

Figure 15. Magnetic Field Components as a Function of z; $\frac{2\xi_1}{\pi} = .2$; $\frac{y}{a} = .5$.

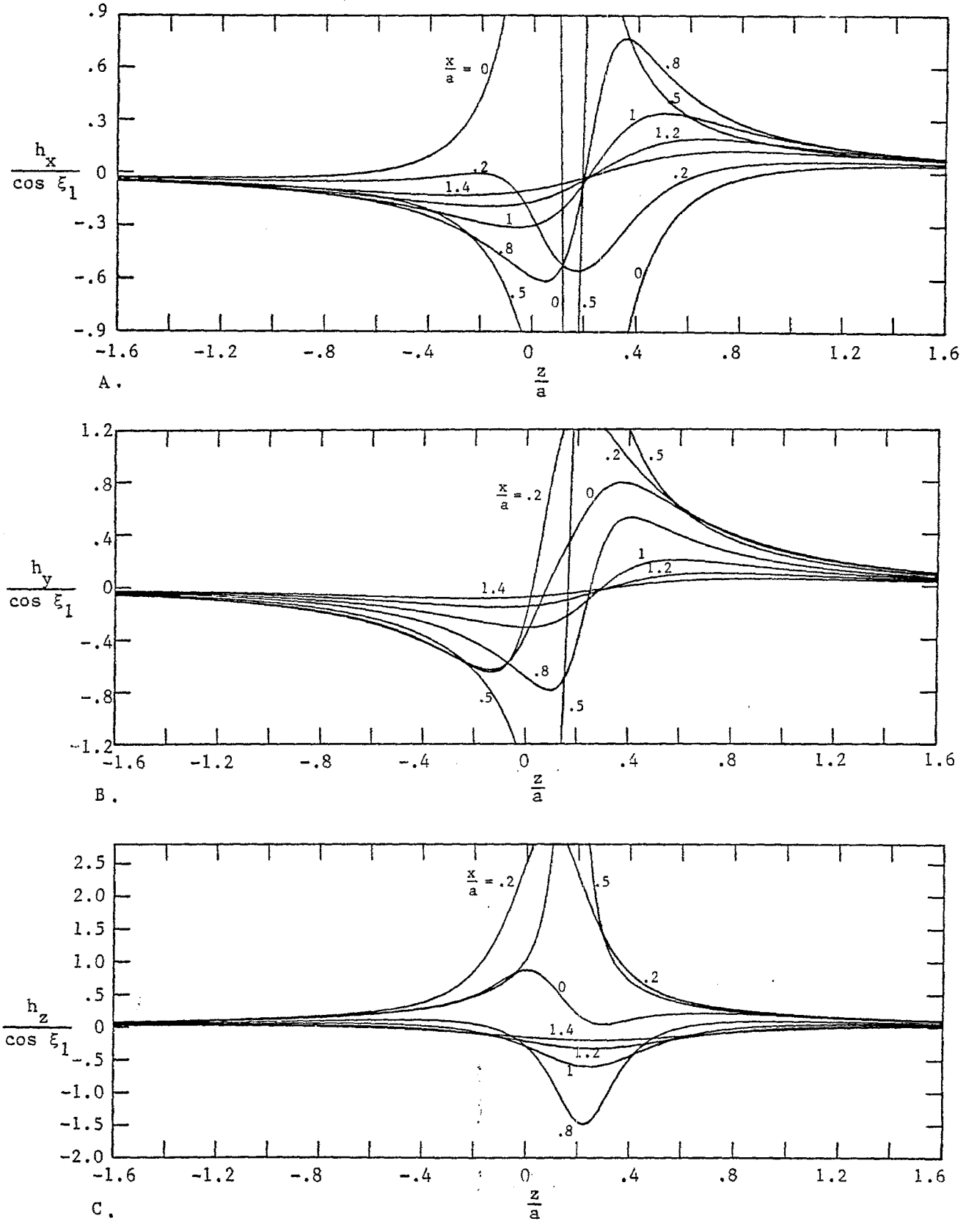

Figure 16. Magnetic Field Components as a Function of z; $\frac{2\xi_1}{\pi} = .2$; $\frac{y}{a} = .8$.

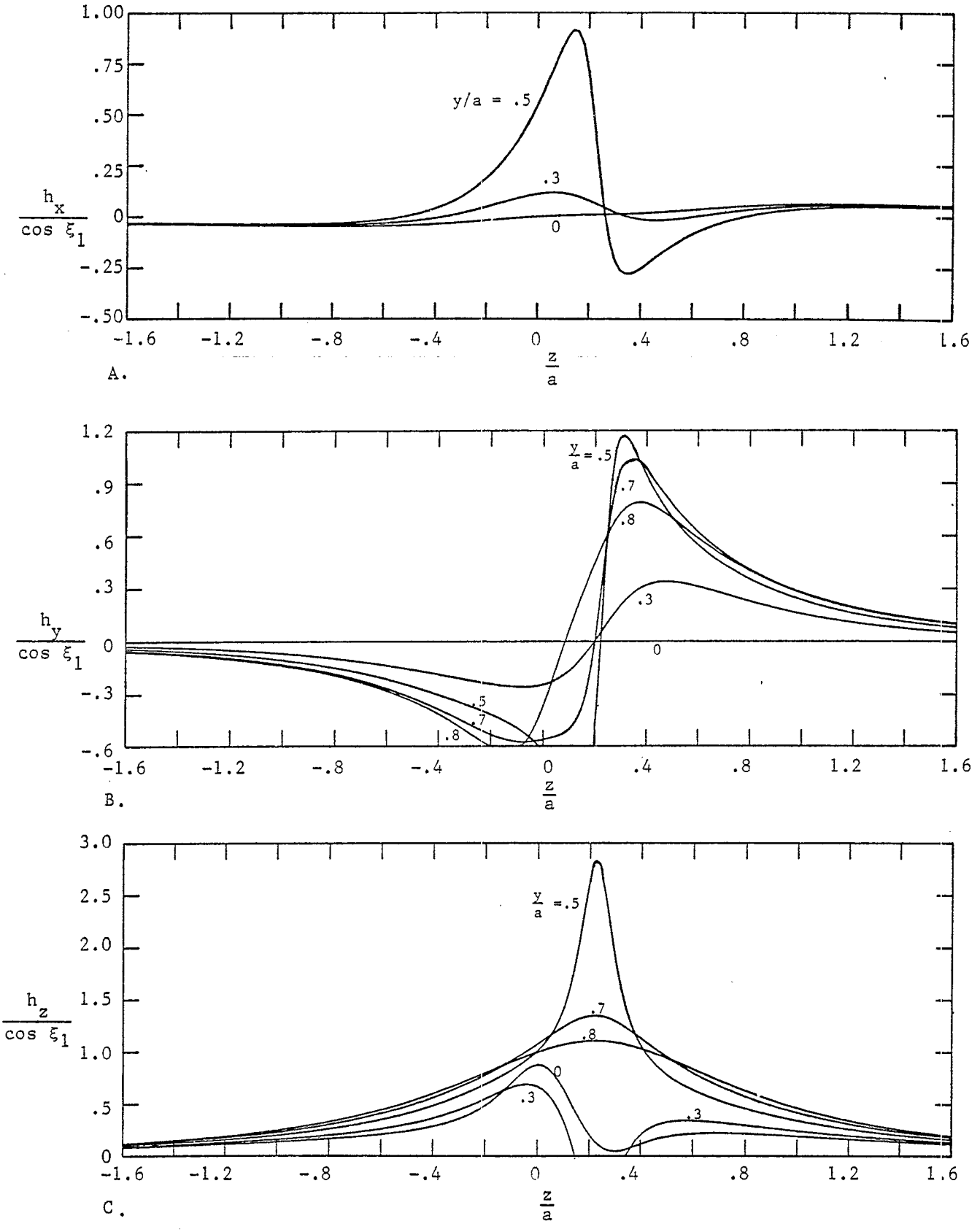

Figure 17. Magnetic Field Components as a Function of z: $\frac{2\xi_1}{\pi} = .2$; $\frac{x}{a} = 0$.

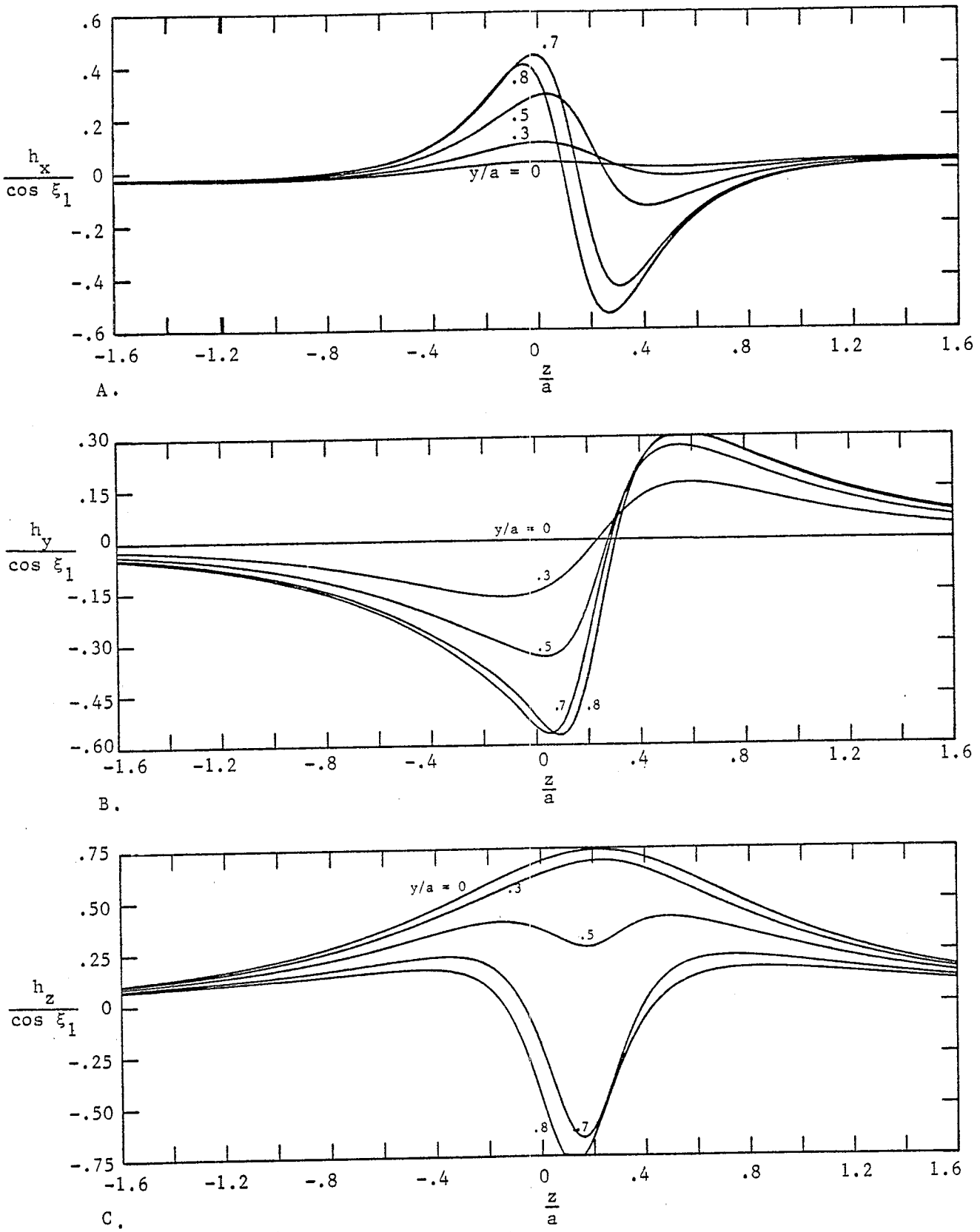

Figure 18. Magnetic Field Components as a Function of z: $\frac{2\xi_1}{\pi} = .2$; $\frac{x}{a} = -.2$.

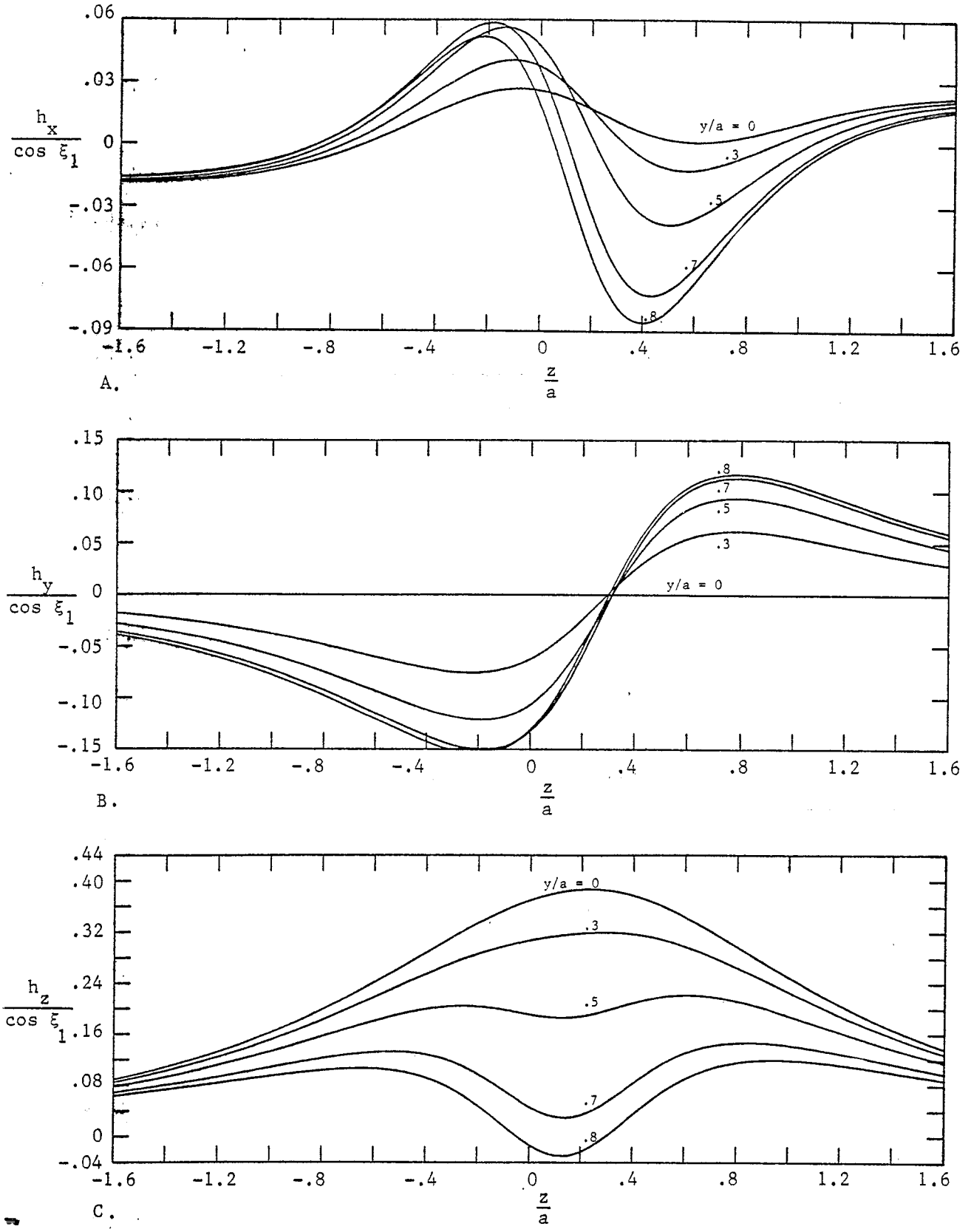

Figure 19. Magnetic Field Components as a Function of z: $\frac{2\xi_1}{\pi} = .2$; $\frac{x}{a} = -.5$.

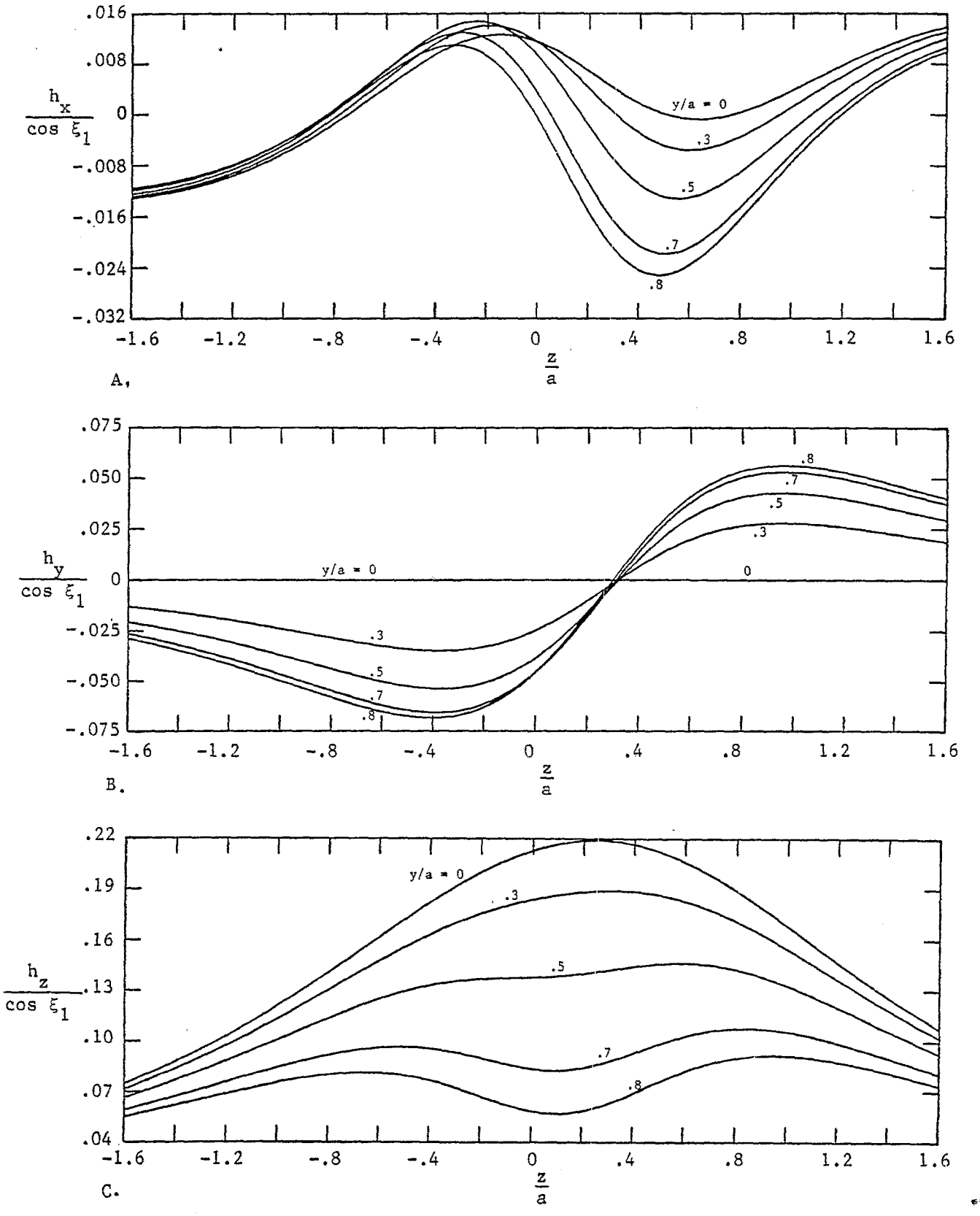

Figure 20. Magnetic Field Components as a Function of z: $\frac{2\xi_1}{\pi} = .2$; $\frac{x}{a} = -.8$.

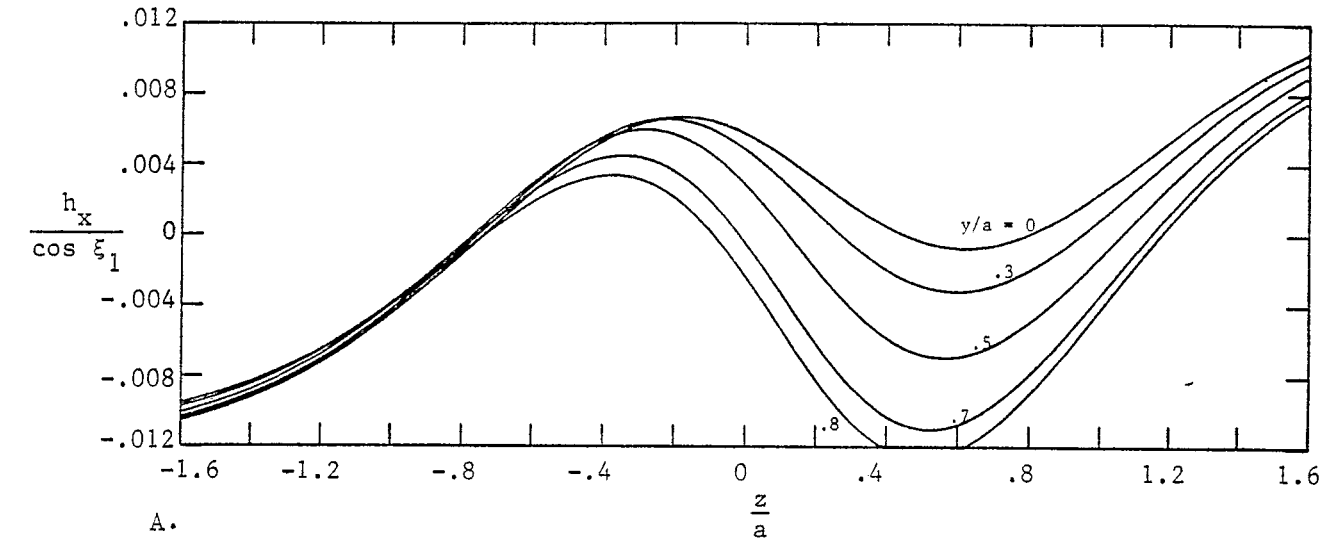

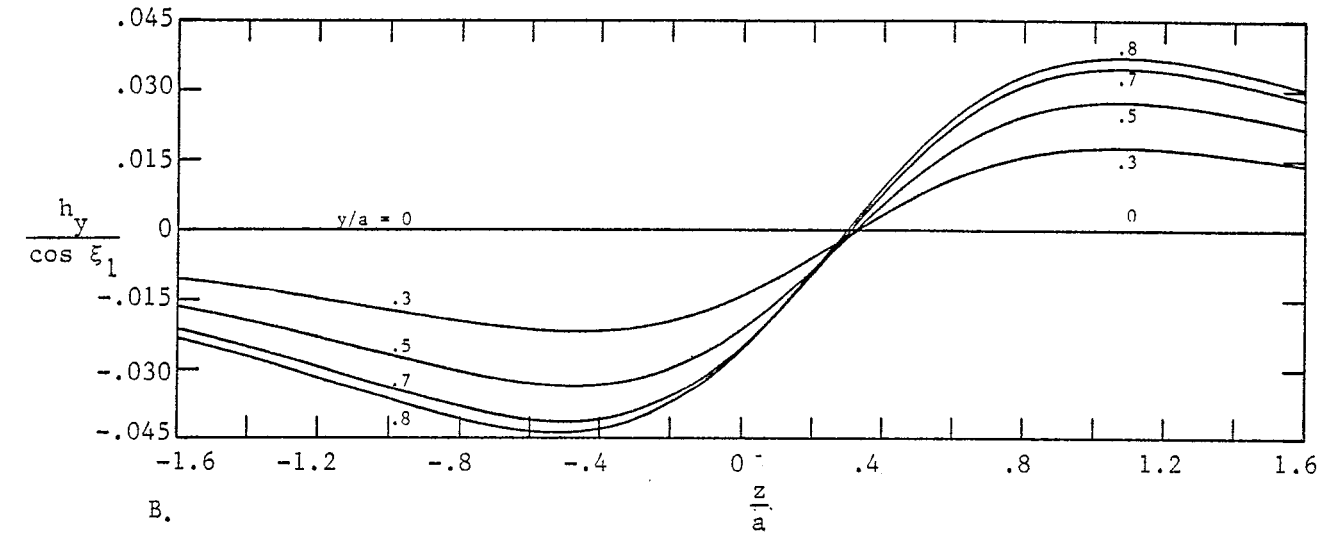

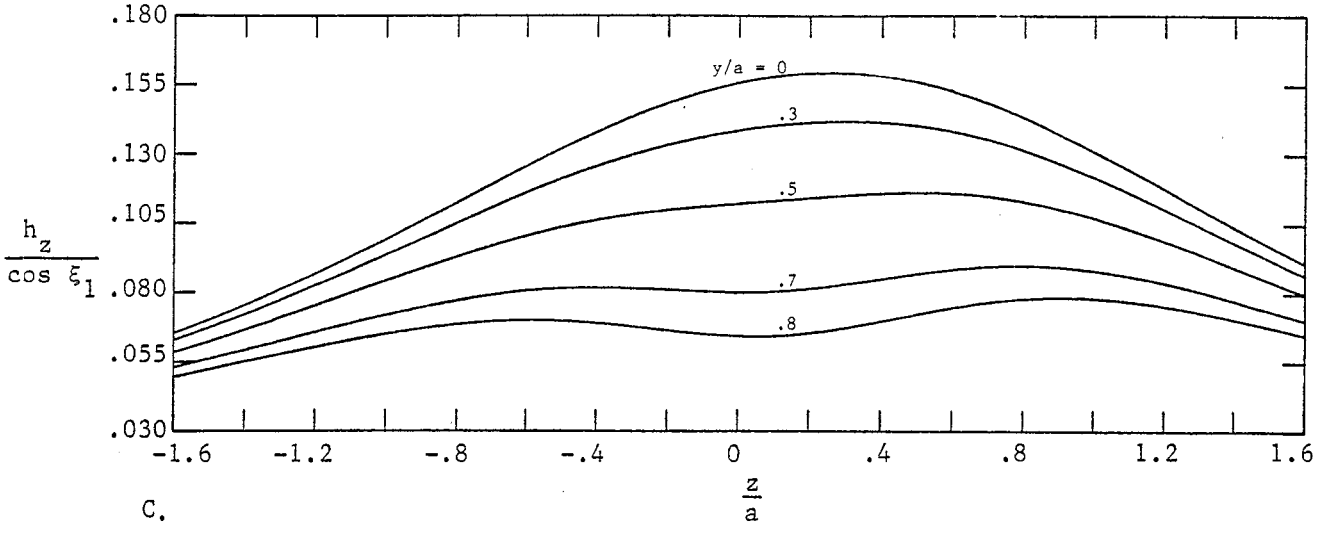

Figure 21. Magnetic Field Components as a Function of z: $\frac{2\xi_1}{\pi} = .2$; $\frac{x}{a} = -1.$

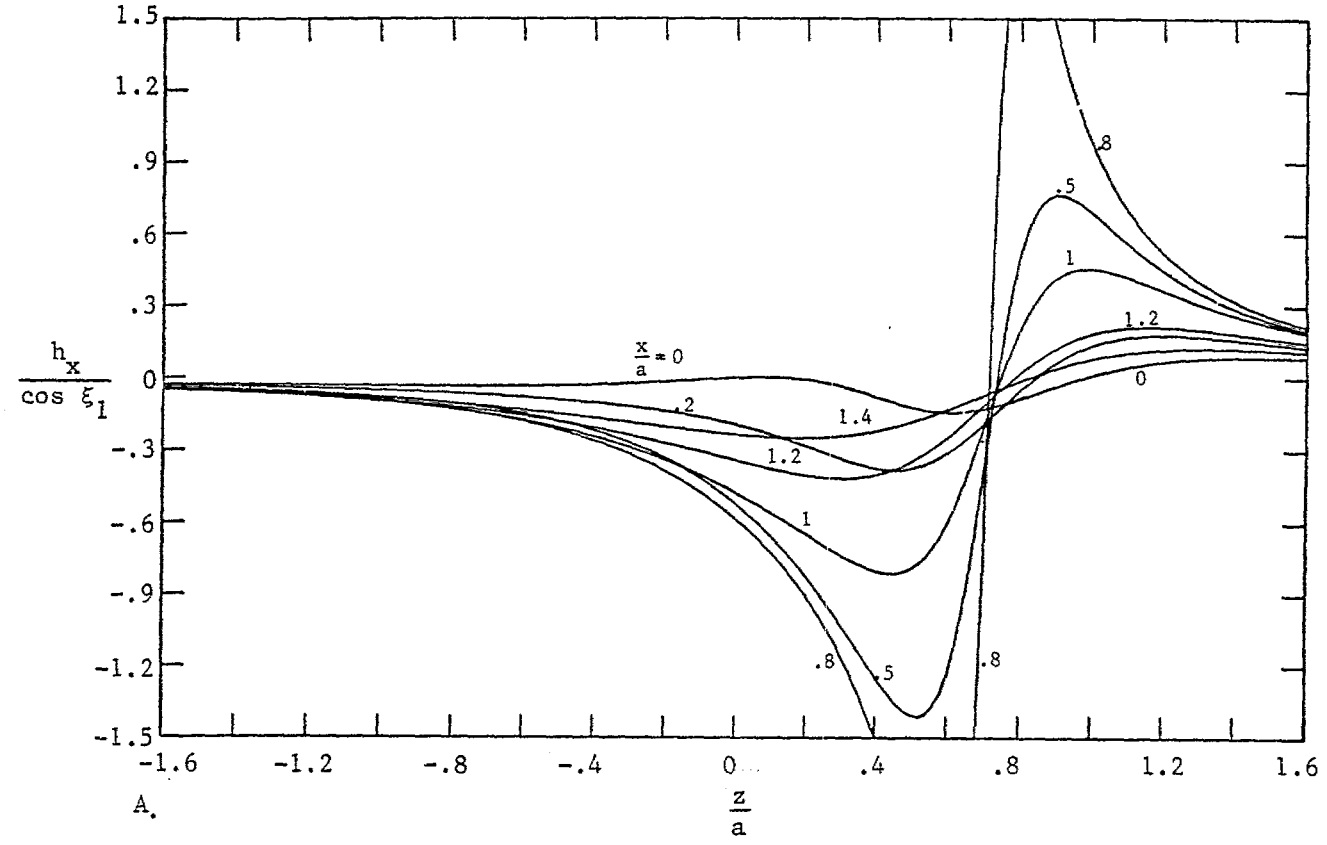

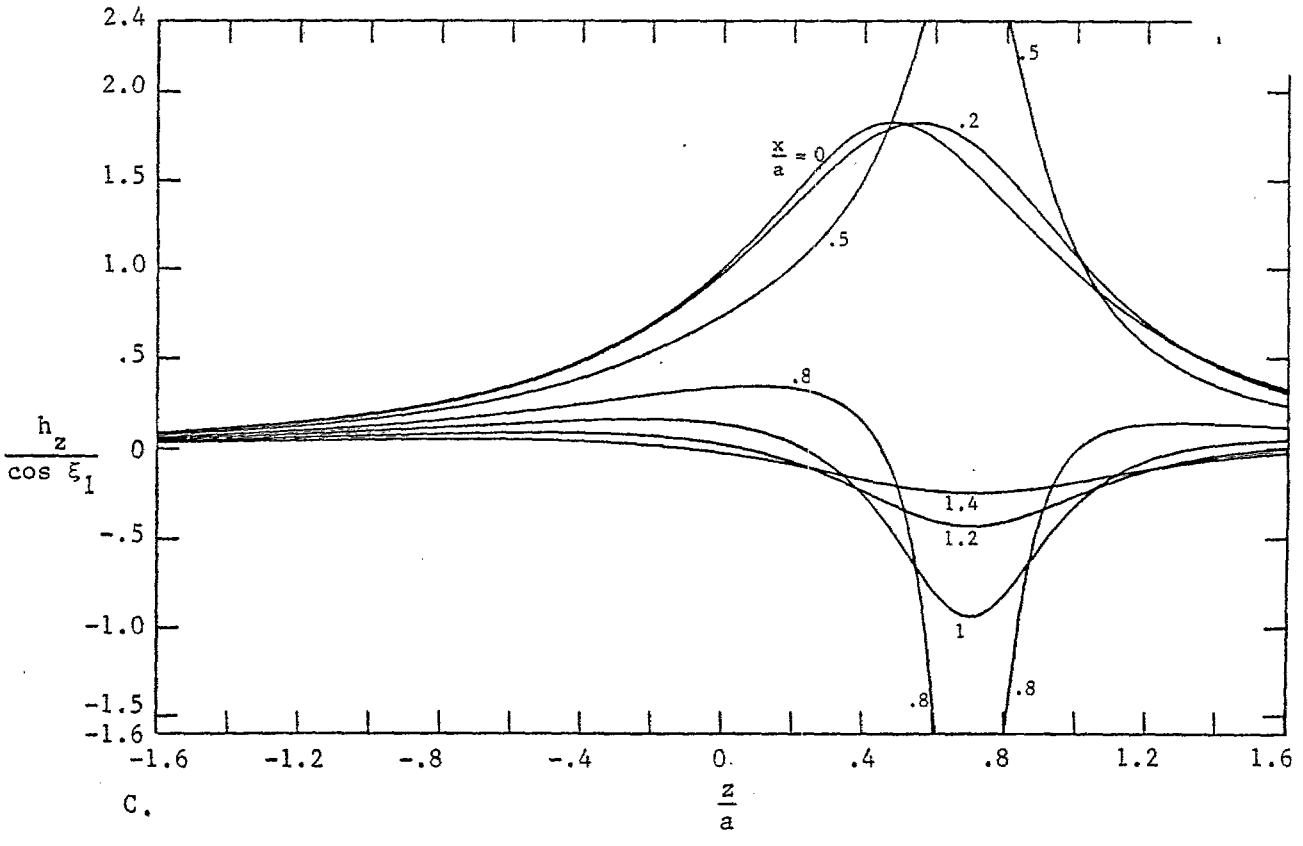

Figure 22. Magnetic Field Components as a Function of z: $\frac{2\xi_1}{\pi} = .5$; $\frac{Y}{a} = 0$.

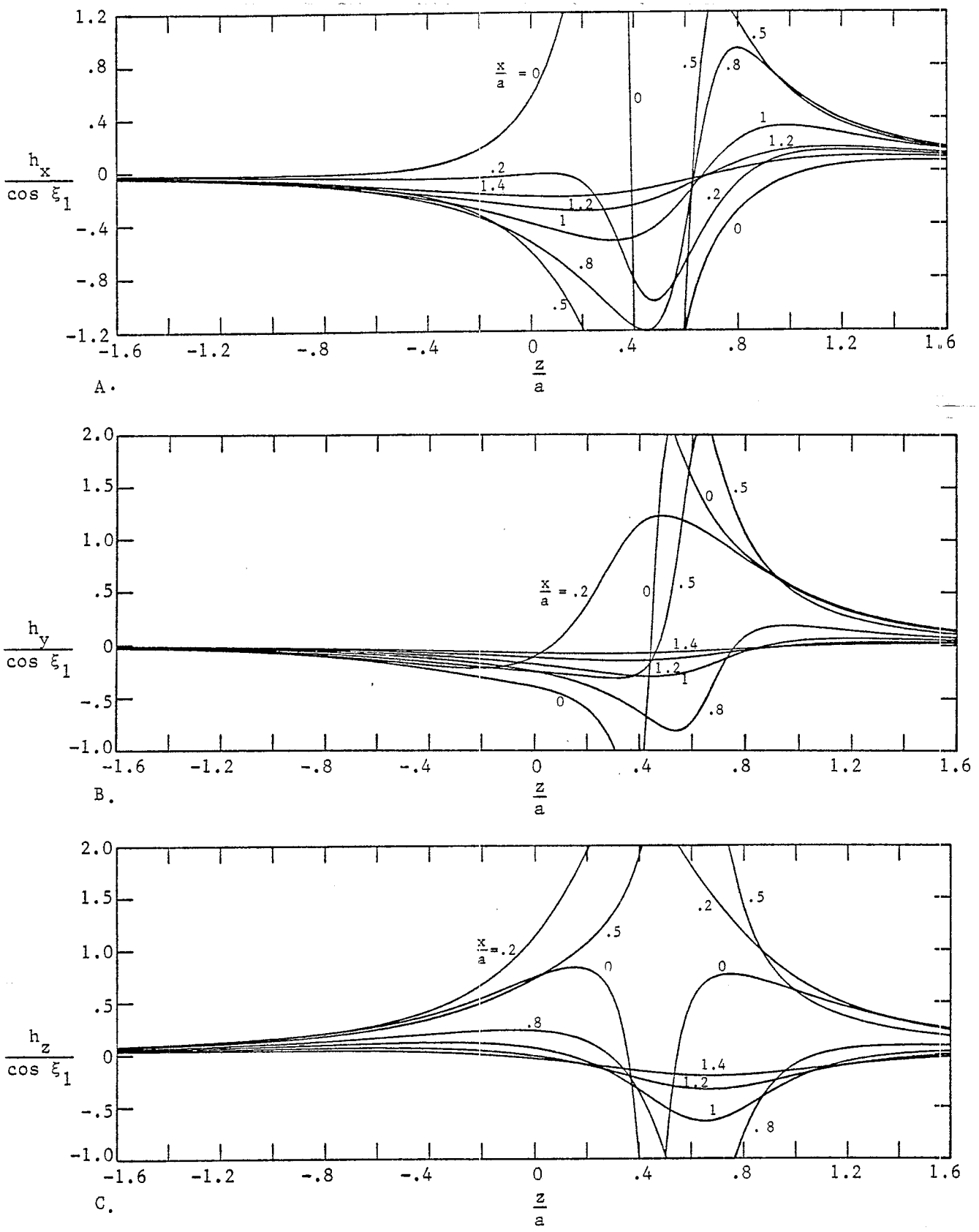

Figure 23. Magnetic Field Components as a Function of z: $\frac{2\xi_1}{\pi} = .5$; $\frac{y}{a} = .5$.

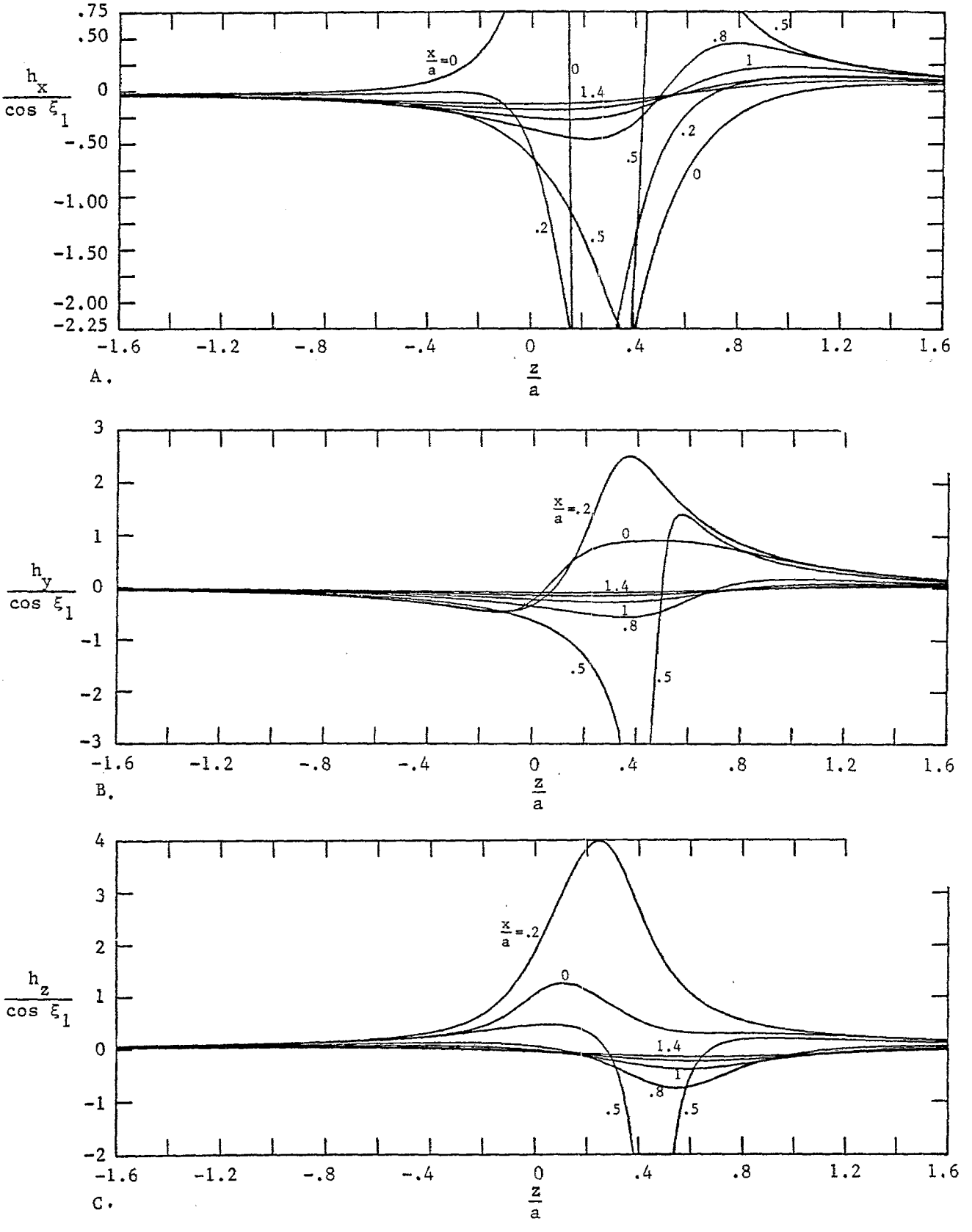

Figure 24. Magnetic Field Components as a Function of z: $\frac{2\xi_1}{\pi} = .5$; $\frac{y}{a} = .8$.

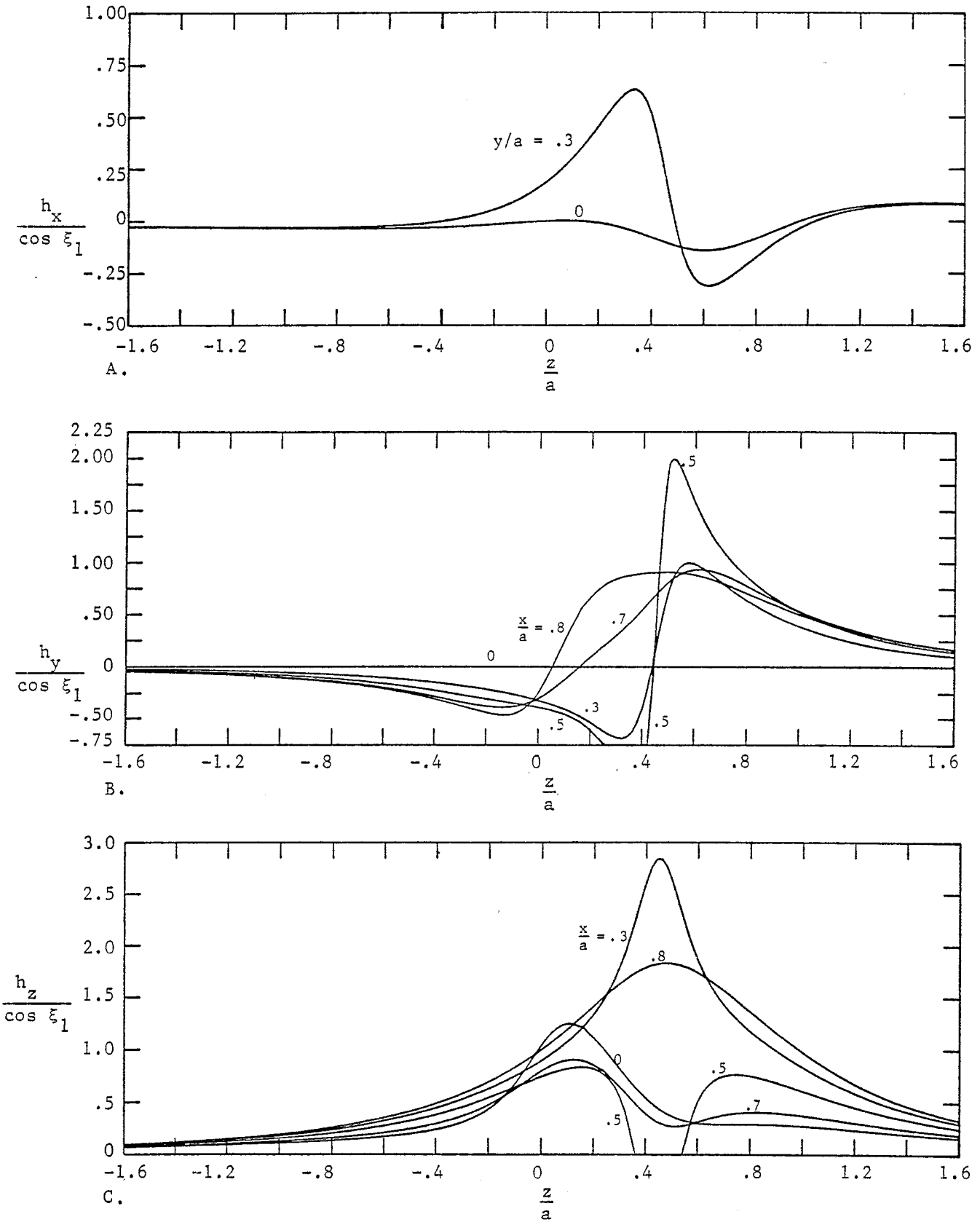

Figure 25. Magnetic Field Components as a Function of z: $\frac{2\xi_1}{\pi} = .5$; $\frac{x}{a} = 0$.

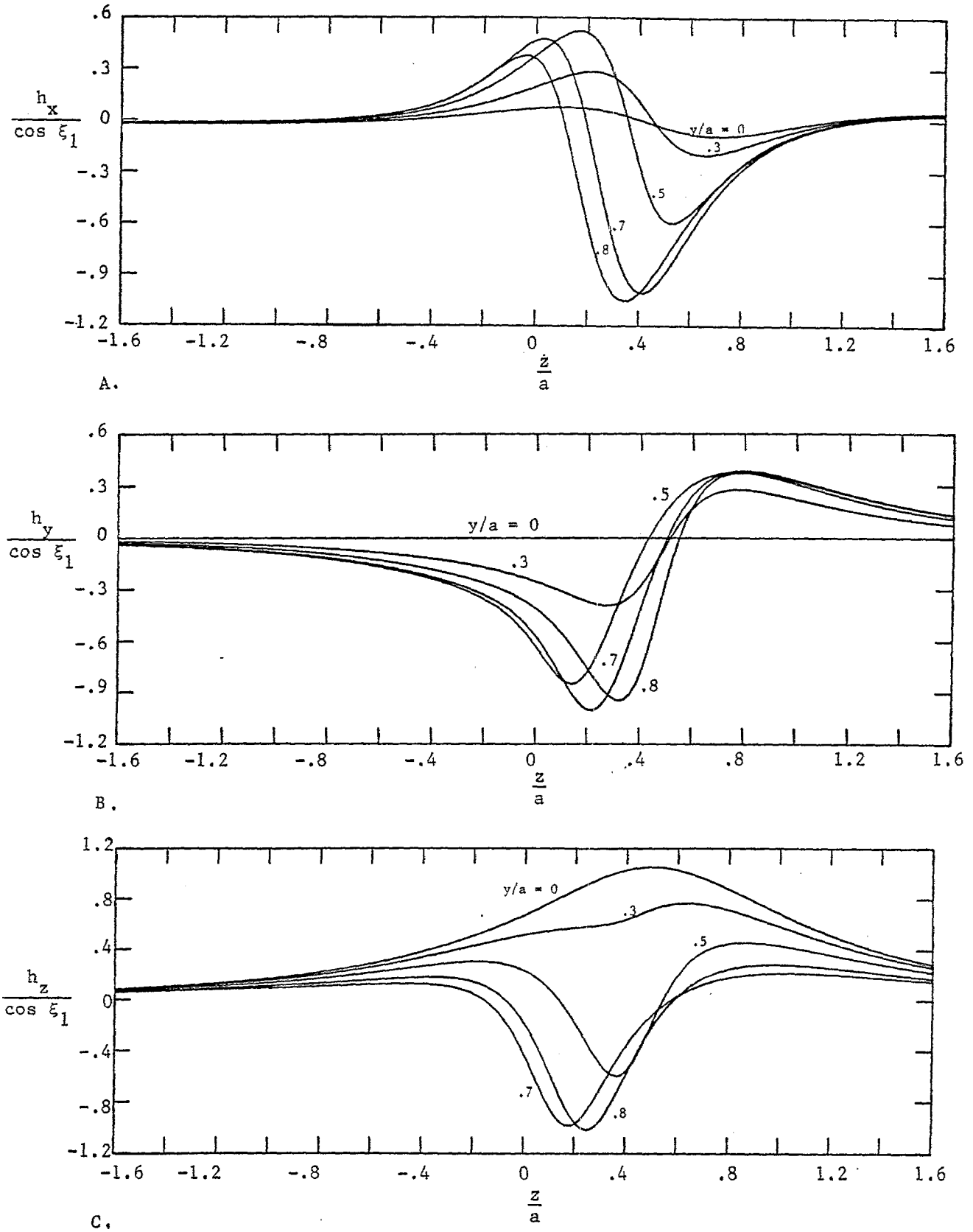

Figure 26. Magnetic Field Components as a Function of z: $\frac{2\xi_1}{\pi} = .5$; $\frac{x}{a} = -.2$.

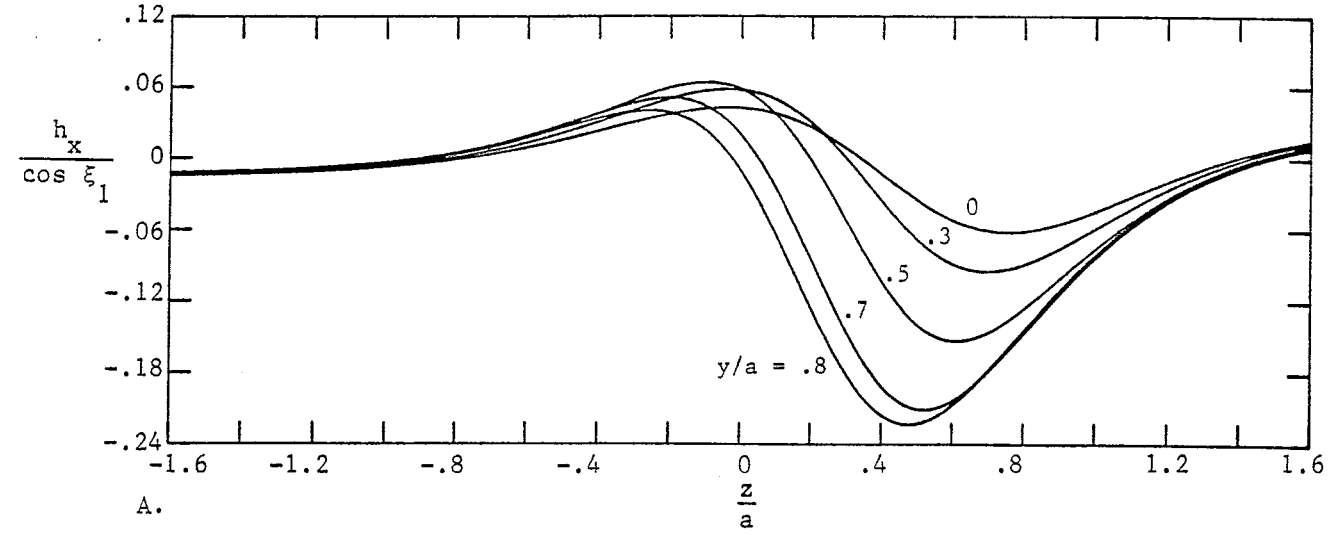

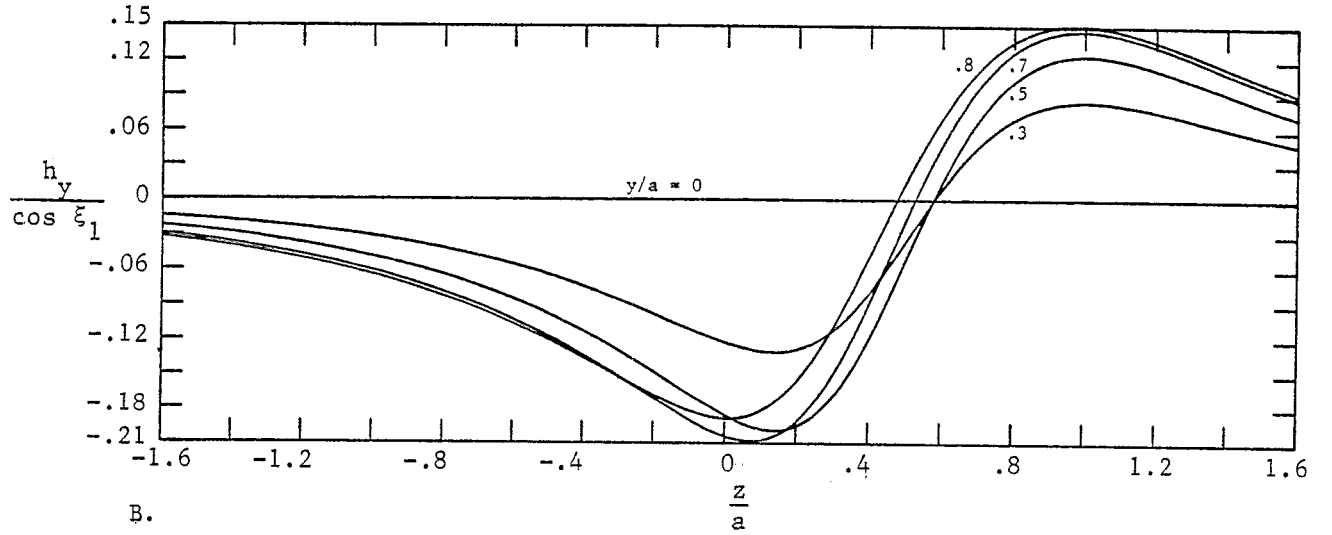

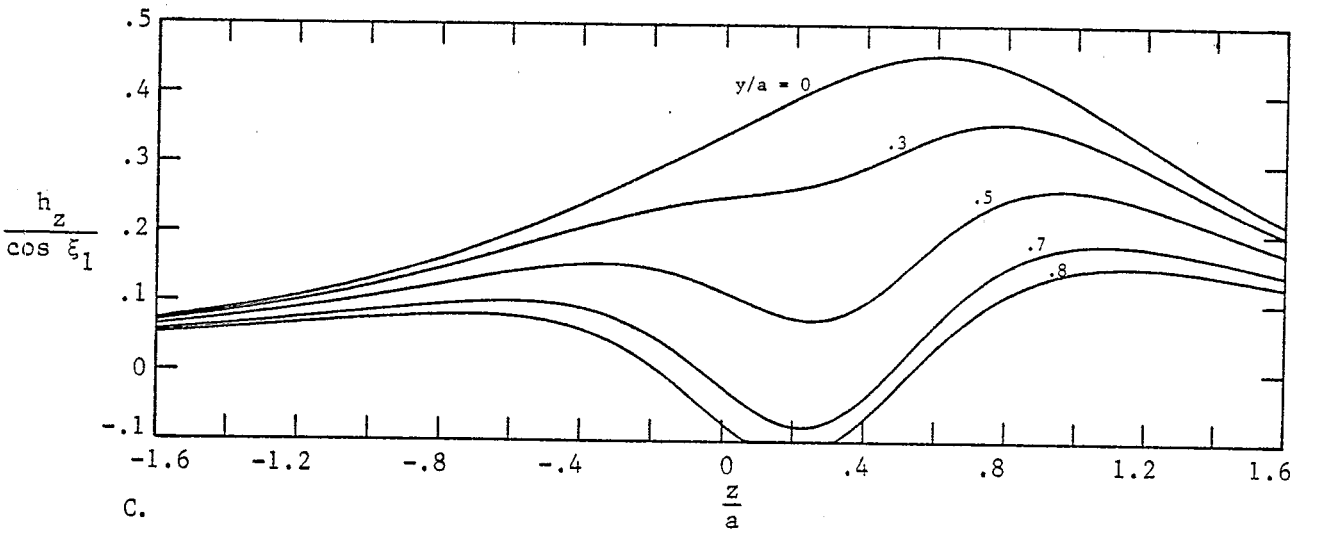

Figure 27. Magnetic Field Components as a Function of z: $\frac{2\xi_1}{\pi} = .5$; $\frac{x}{a} = -.5$.

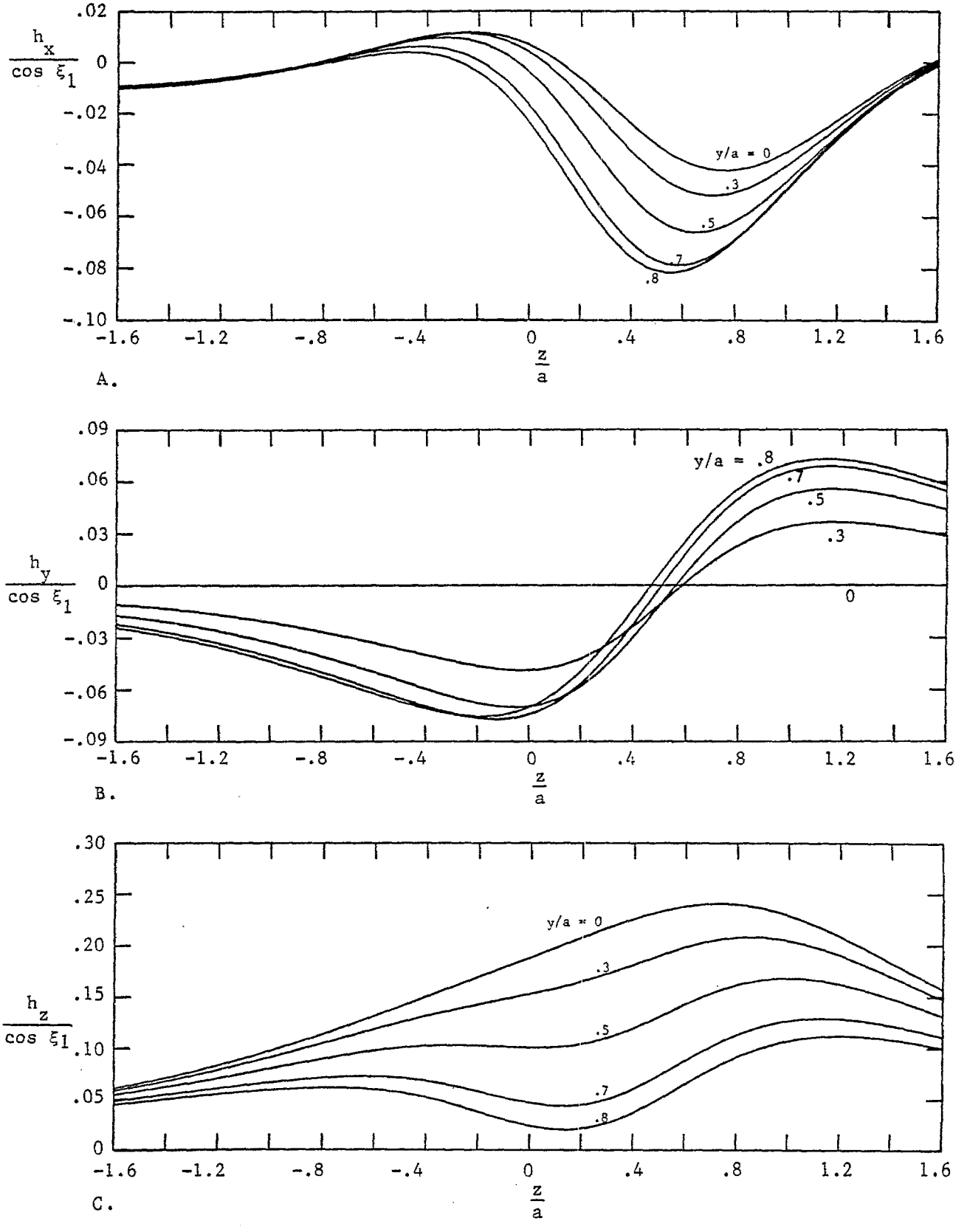

Figure 28. Magnetic Field Components as a Function of z: $\frac{2\xi_1}{\pi} = .5$; $\frac{x}{a} = -.8$,

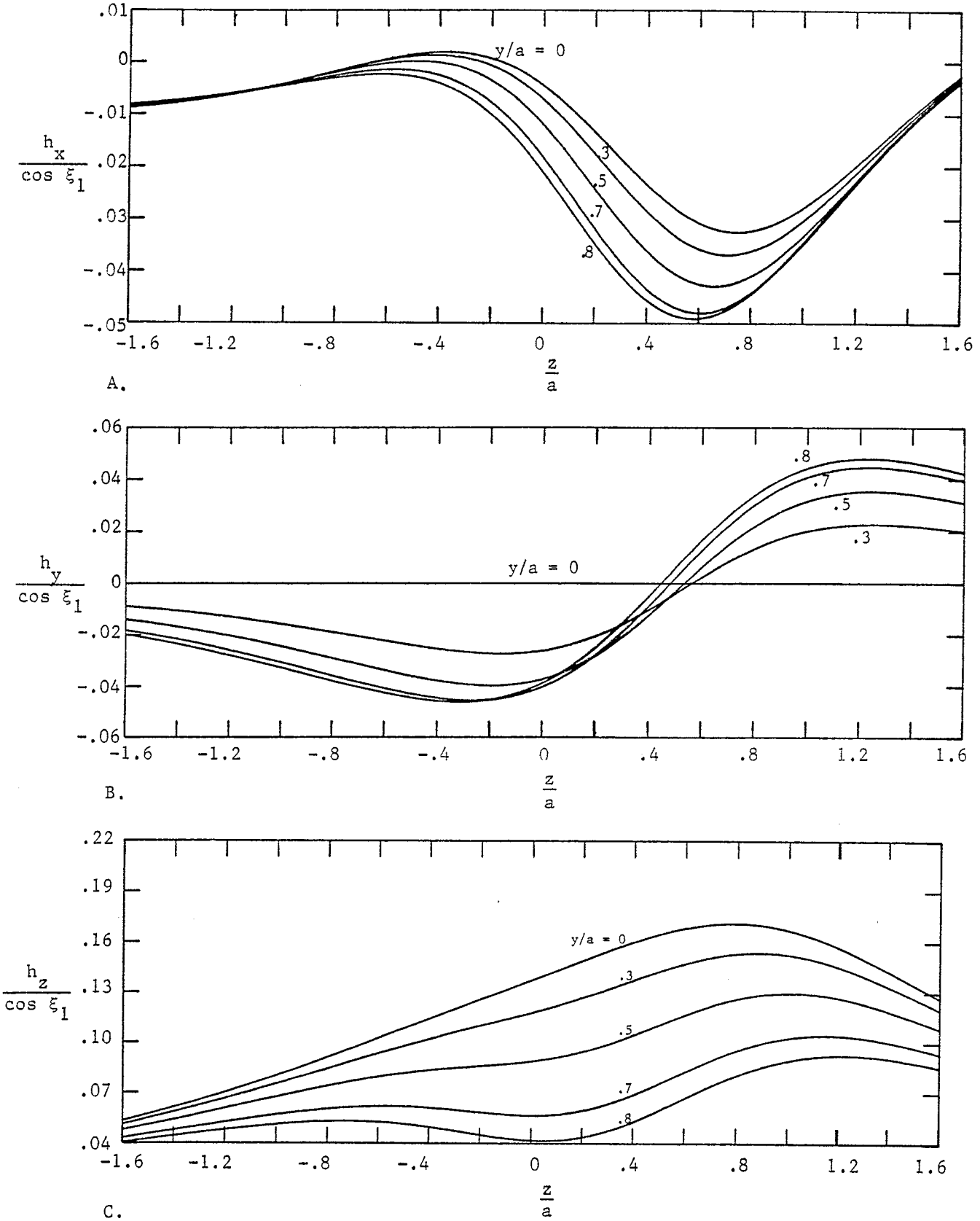

Figure 29. Magnetic Field Components as a Function of z; $\frac{2\xi_1}{\pi} = .5$; $\frac{x}{a} = -1$.

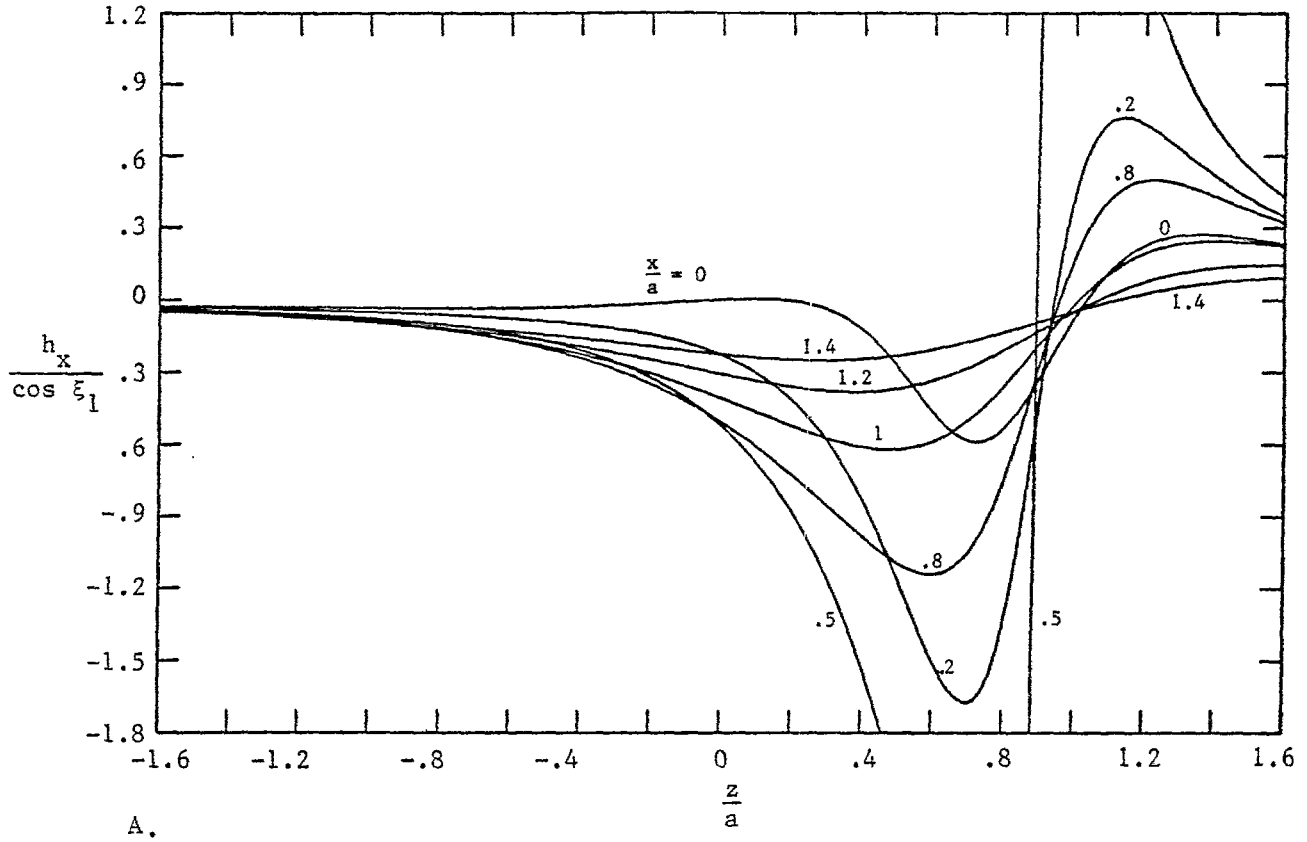

A.

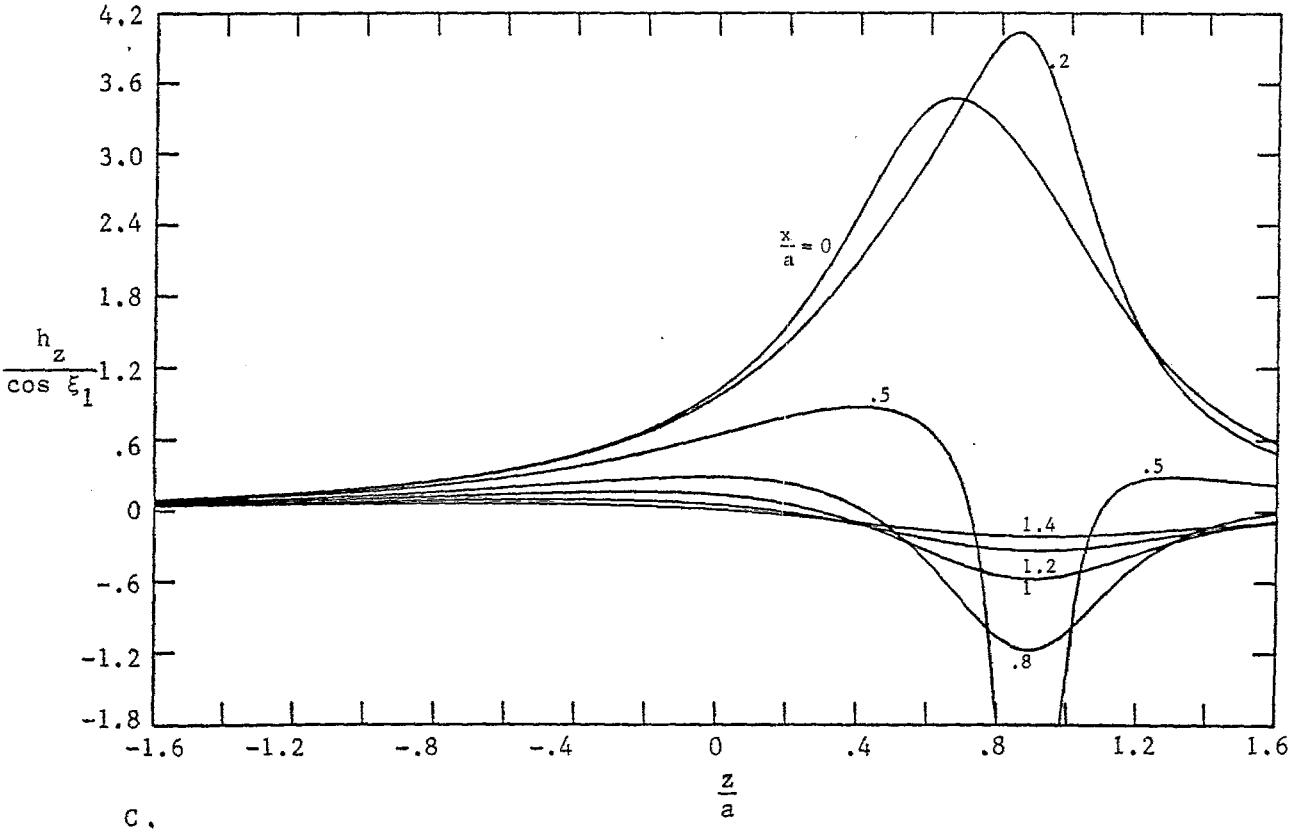

C.

Figure 30. Magnetic Field Components as a Function of z: $\frac{2\xi_1}{\pi} = .7$; $\frac{y}{a} = 0$.

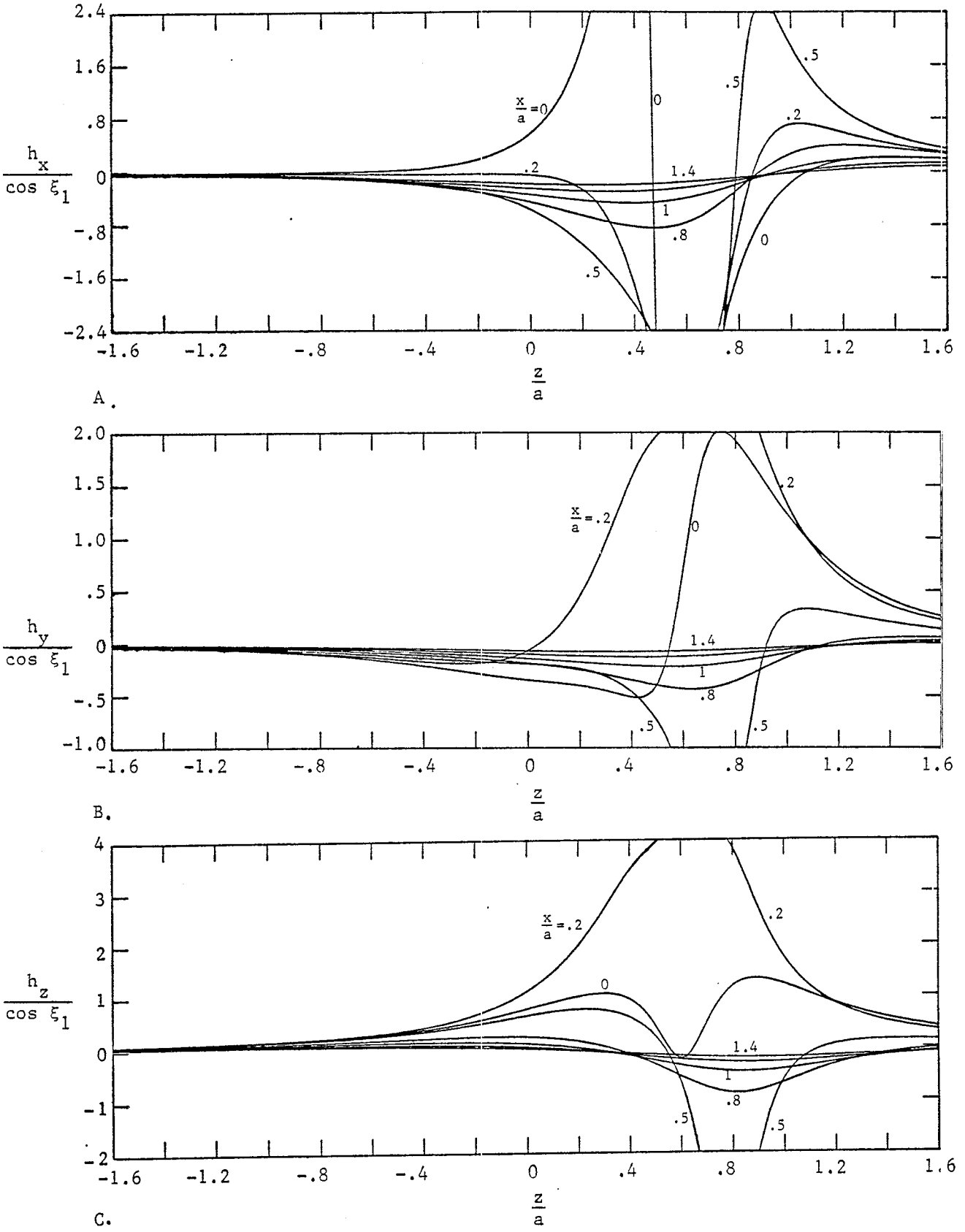

Figure 31. Magnetic Field Components as a Function of z: $\frac{2\xi_1}{\pi} = .7$; $\frac{y}{a} = .5$.

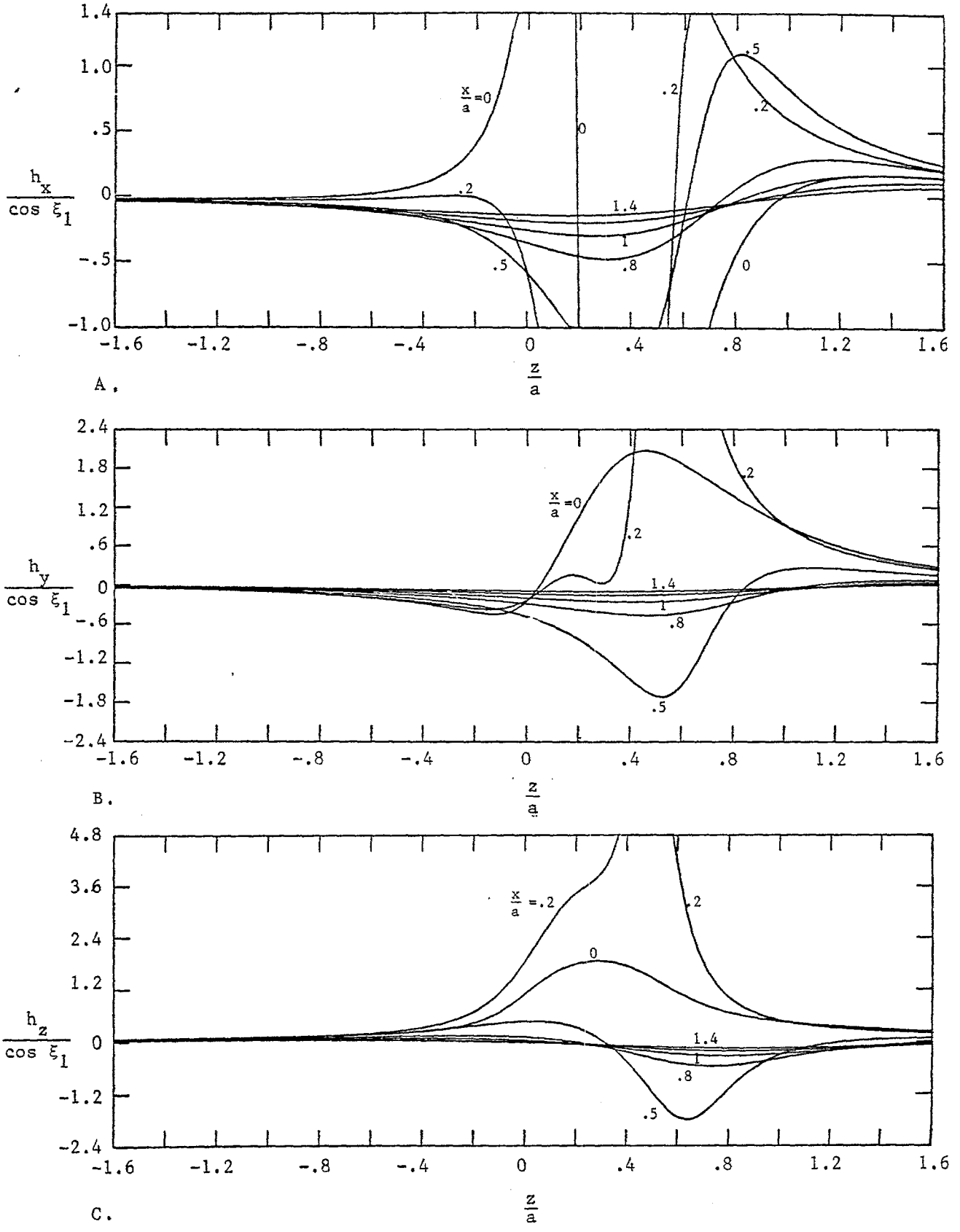

Figure 32. Magnetic Field Components as a Function of z: $\frac{2\xi_1}{\pi} = .7$; $\frac{y}{a} = .8$.

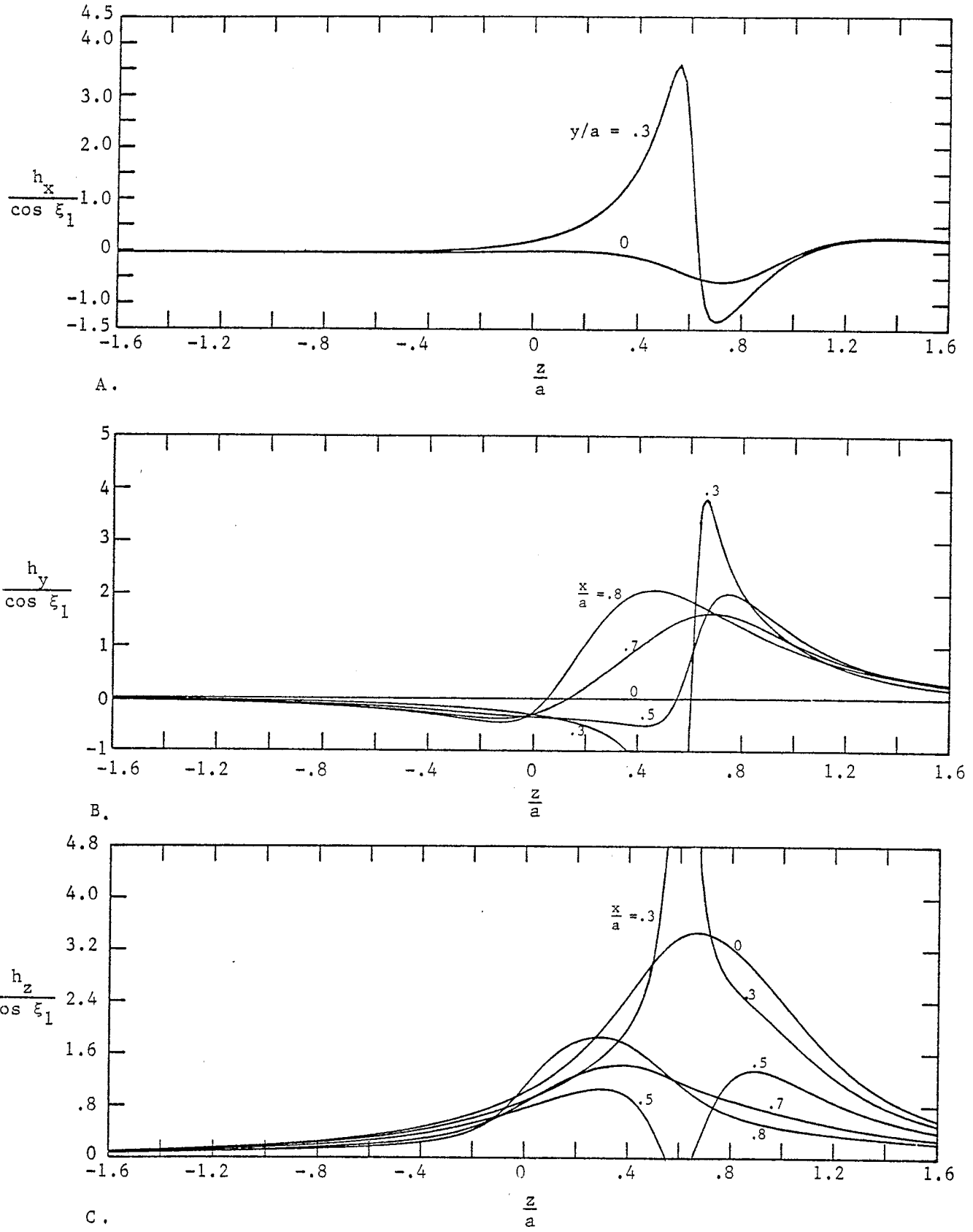

Figure 33. Magnetic Field Components as a Function of z: $\frac{2\xi_1}{\pi} = .7$; $\frac{x}{a} = 0$.

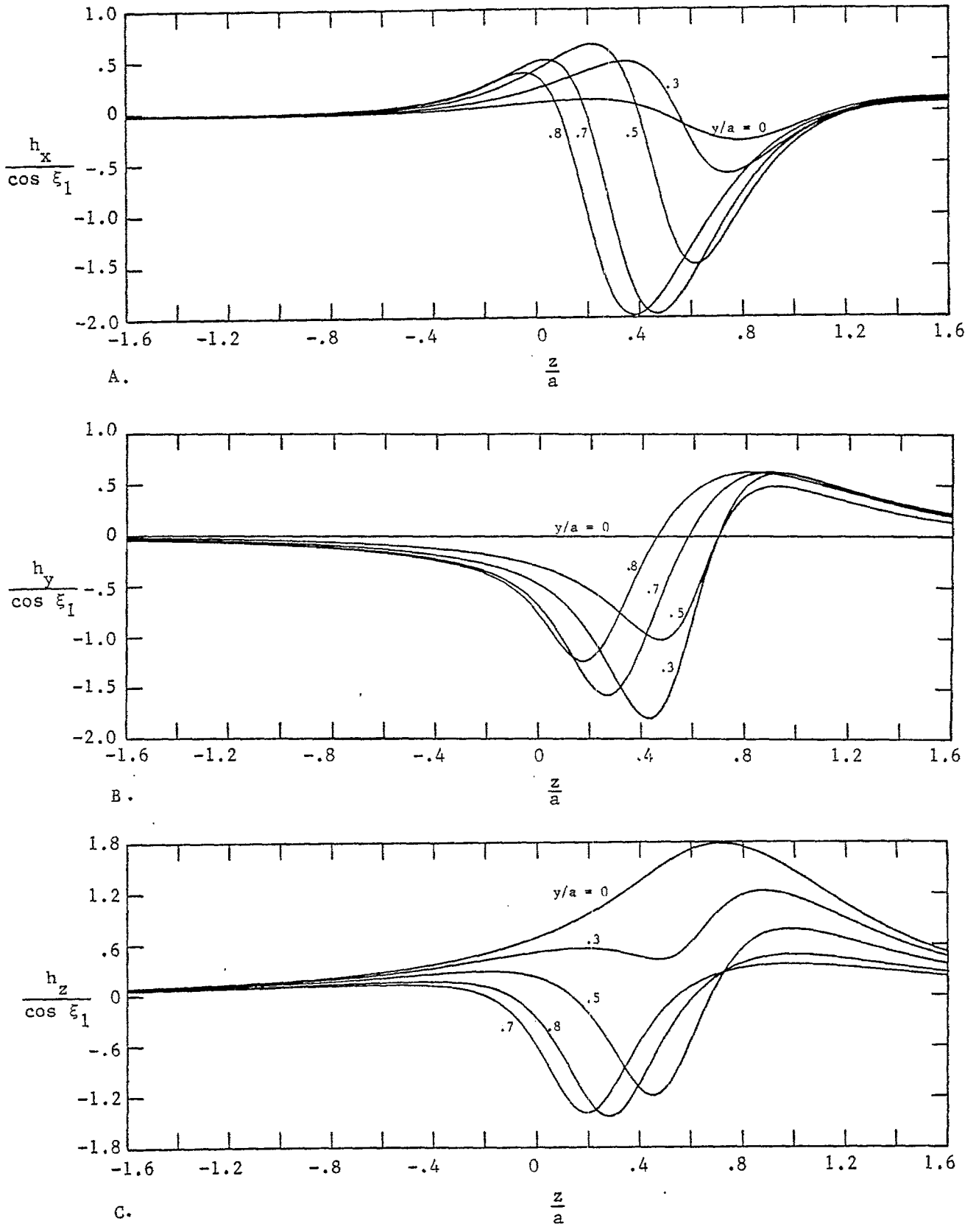

Figure 34. Magnetic Field Components as a Function of z: $\frac{2\xi_1}{\pi} = .7$; $\frac{x}{a} = -.2$.

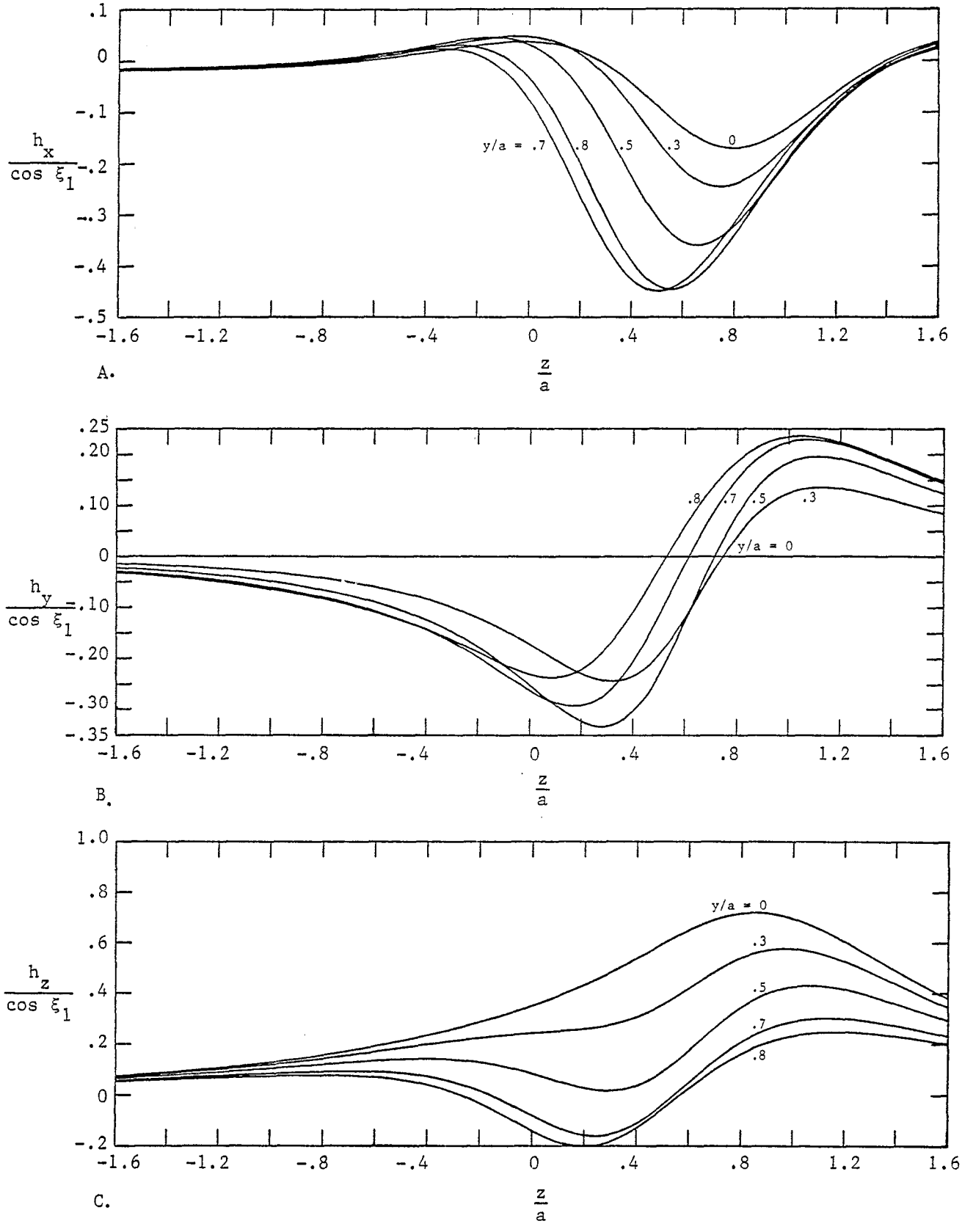

Figure 35. Magnetic Field Components as a Function of z; $\frac{2\xi_1}{\pi} = .7$; $\frac{x}{a} = -.5$.

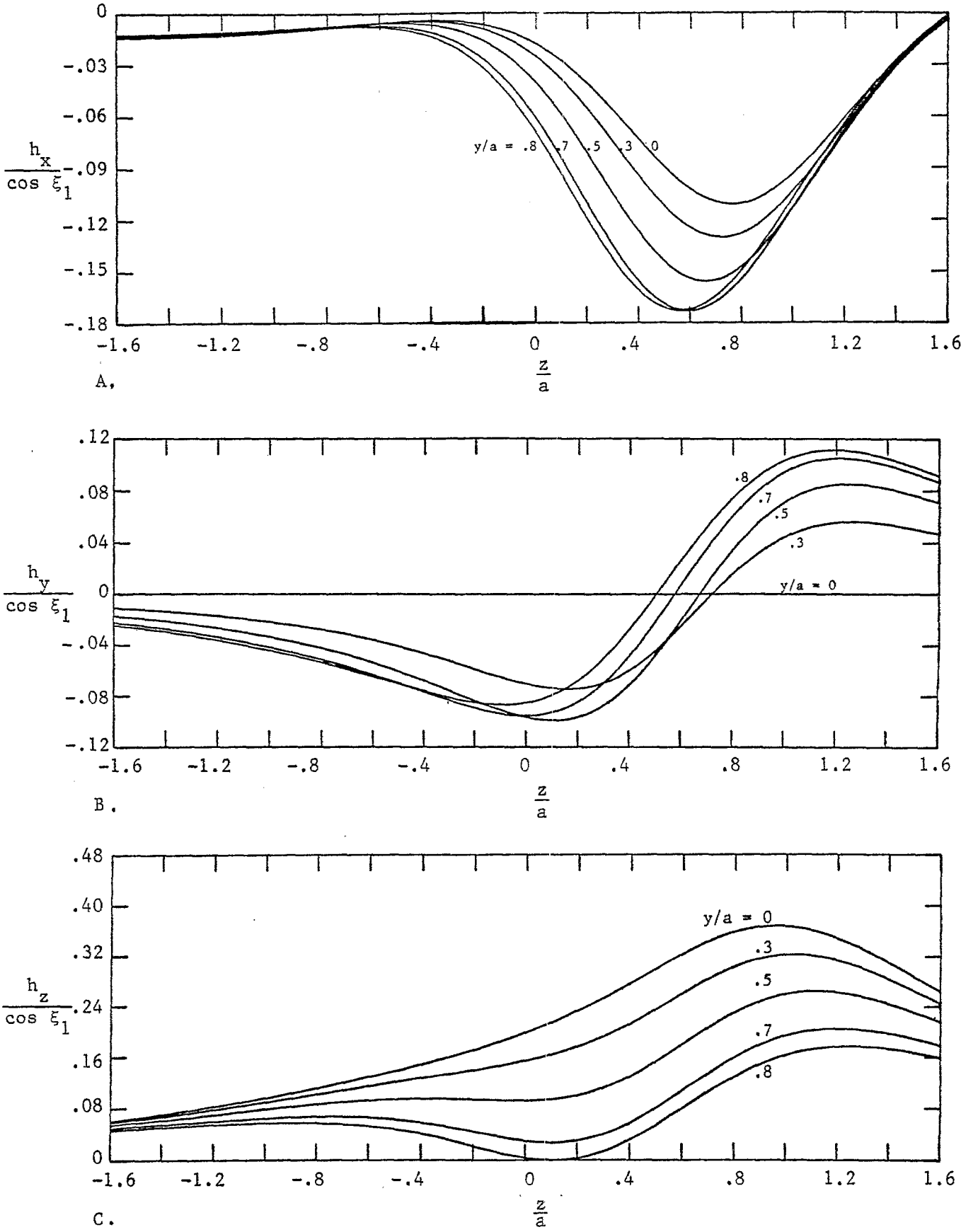

Figure 36. Magnetic Field Components as a Function of z: $\frac{2\xi_1}{\pi} = .7$; $\frac{x}{a} = -.8$.

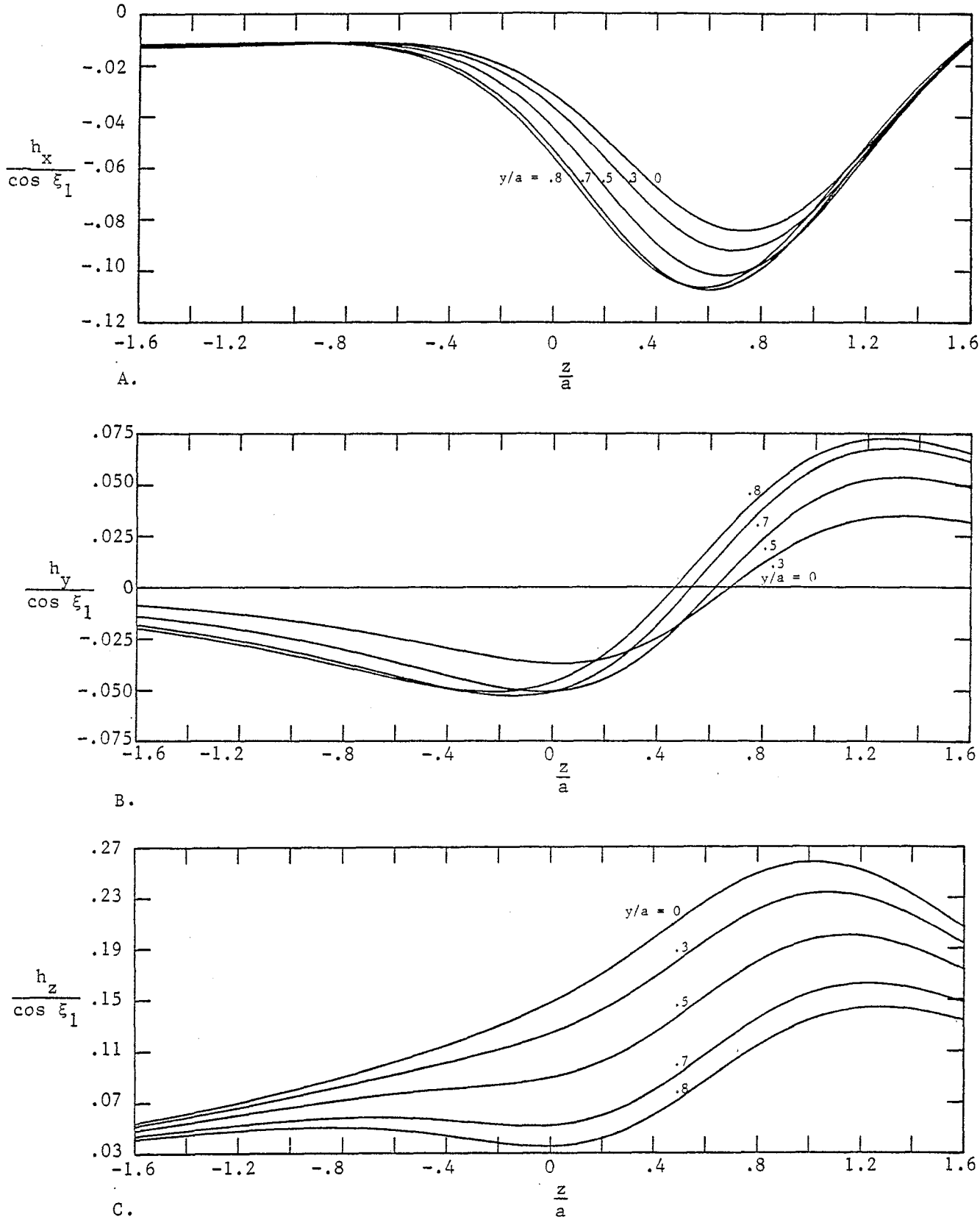

Figure 37. Magnetic Field Components as a Function of z: $\frac{2\xi_1}{\pi} = .7$; $\frac{x}{a} = -1.$

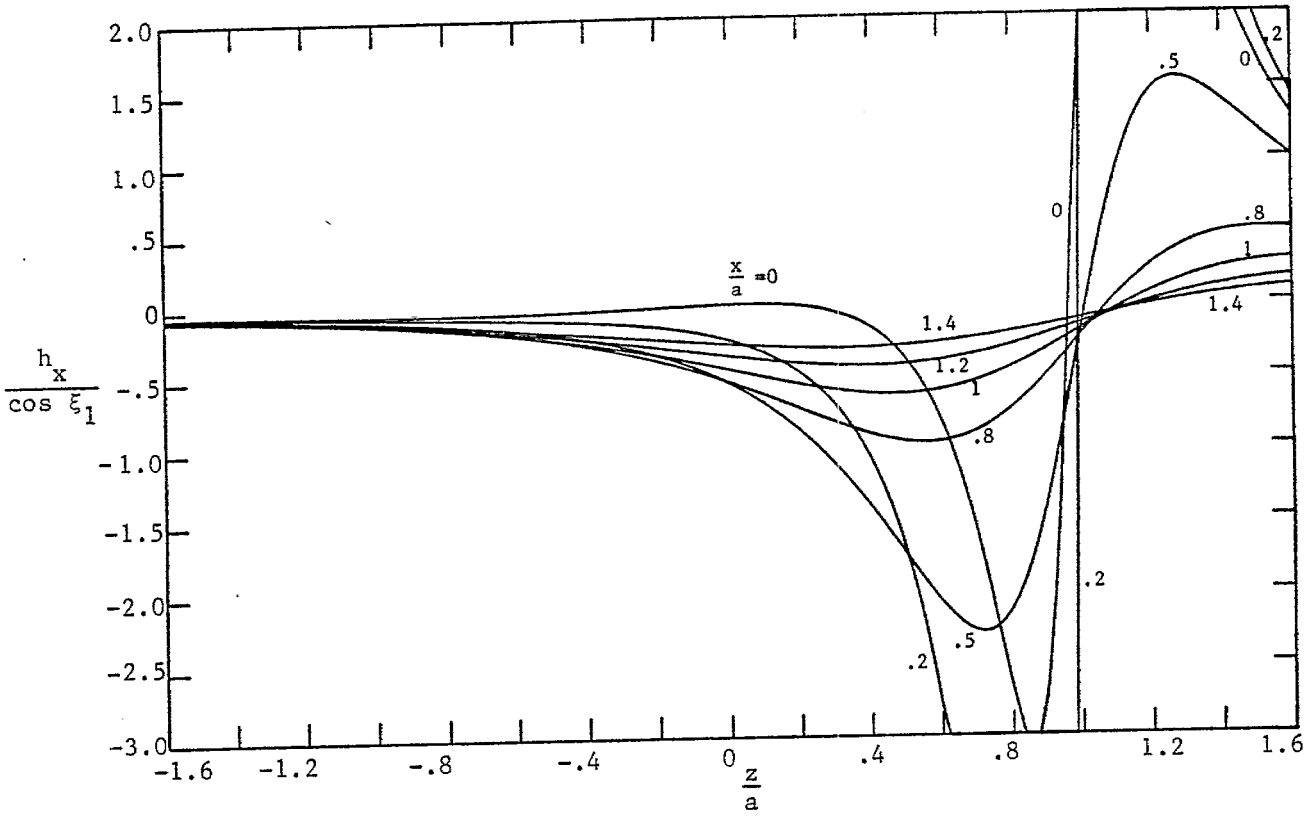

A.

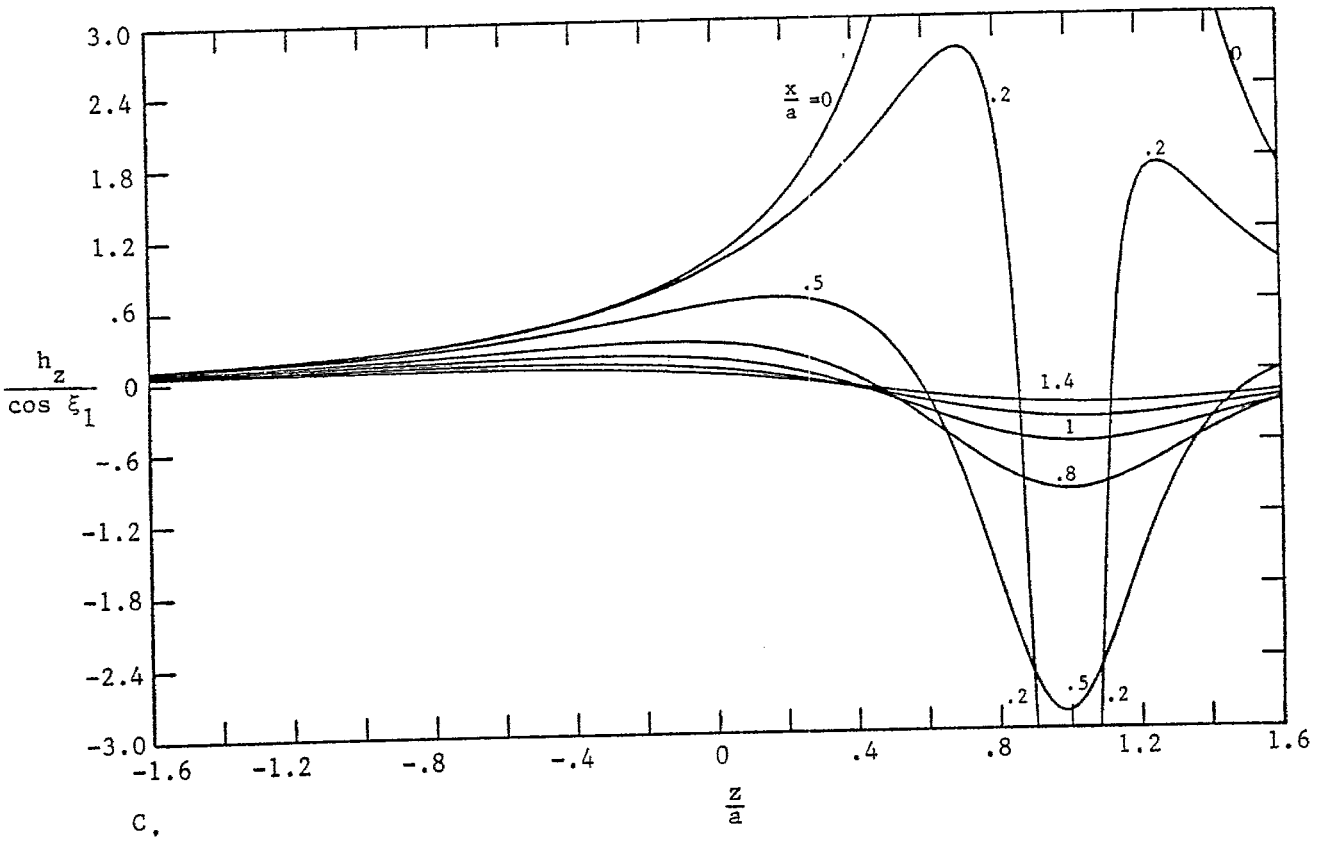

C.

Figure 38. Magnetic Field Components as a Function of z: $\frac{2\xi_1}{\pi} = .9$; $\frac{y}{a} = 0$.

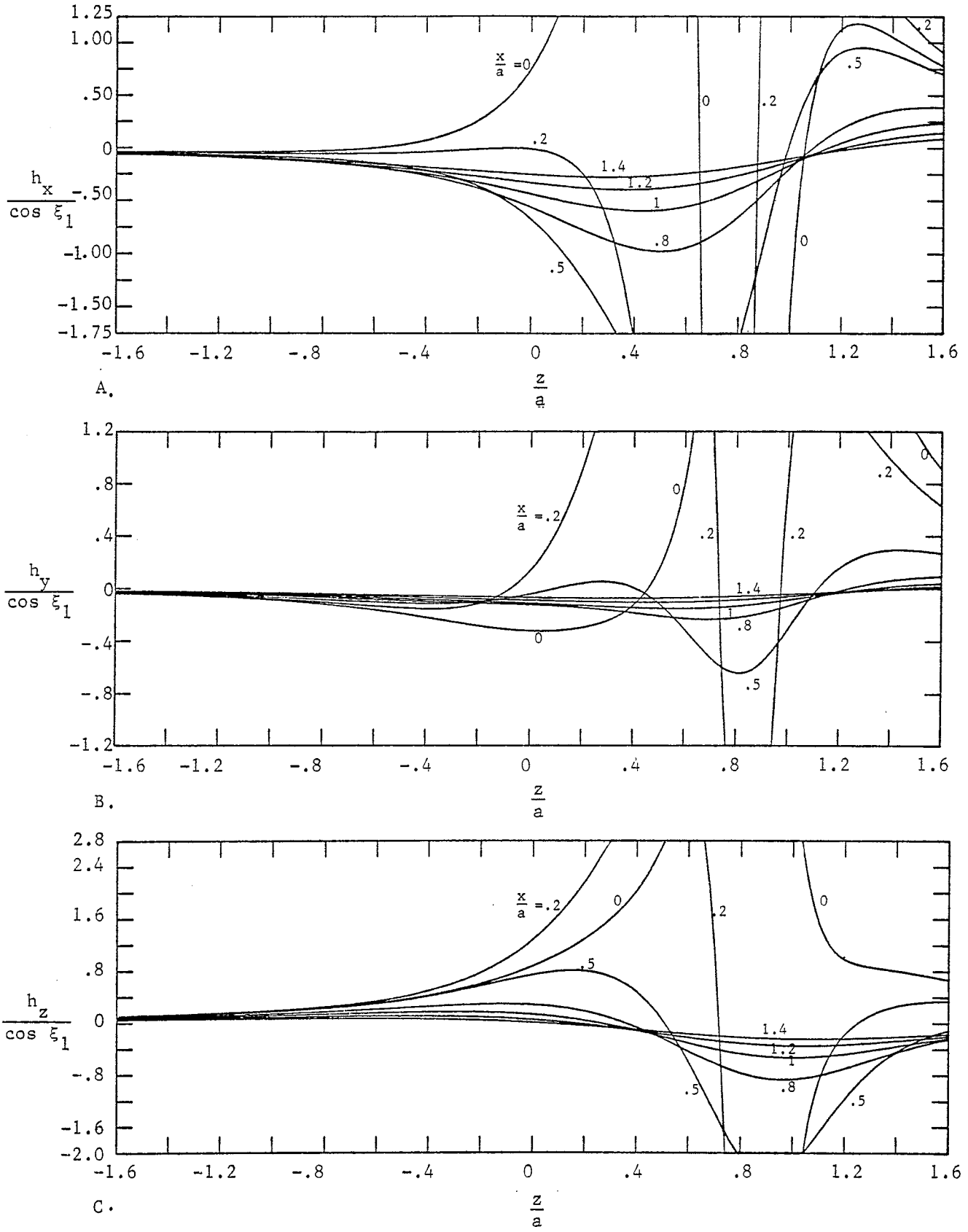

Figure 39. Magnetic Field Components as a Function of z: $\frac{2\xi_1}{\pi} = .9$; $\frac{y}{a} = .5$.

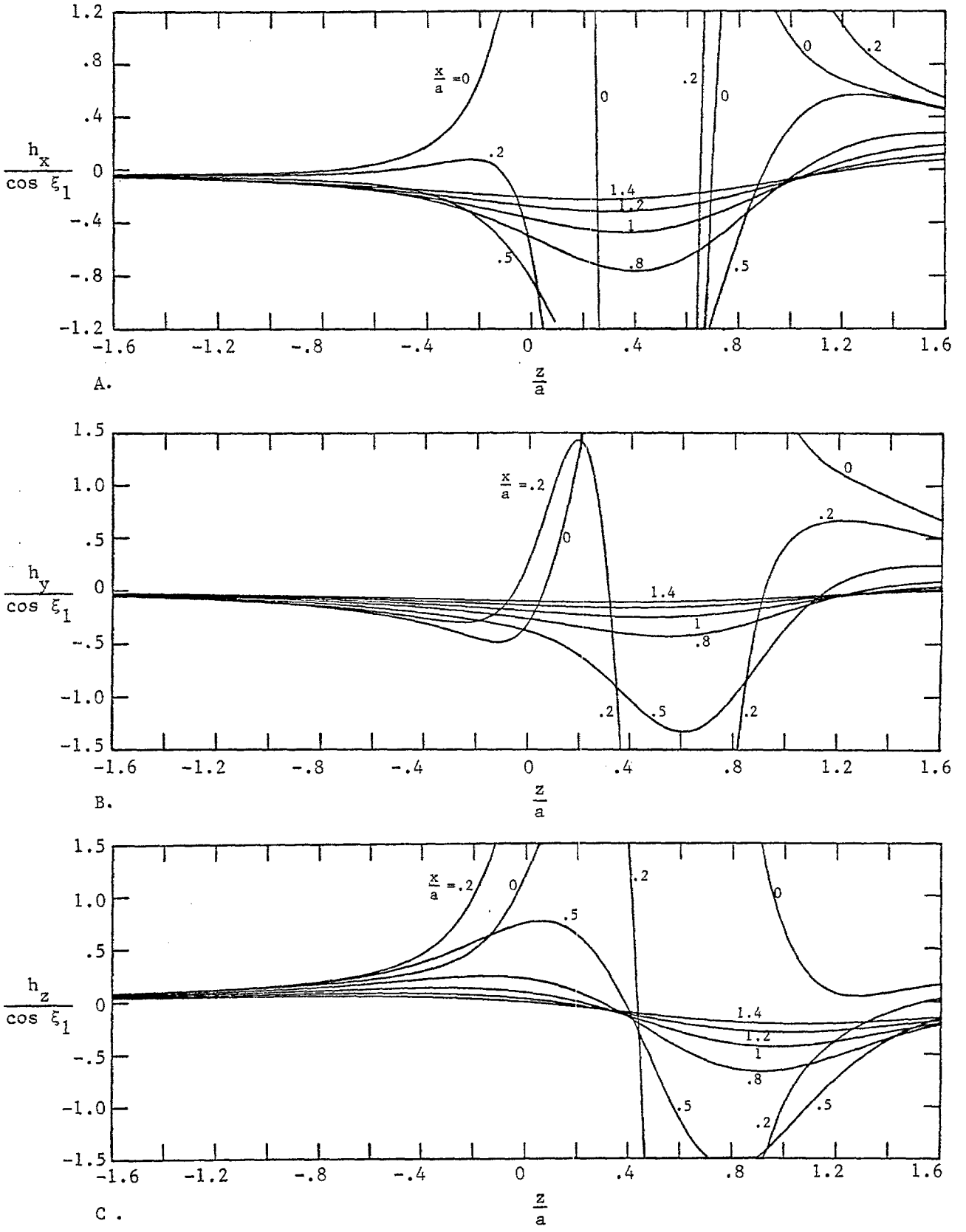

Figure 40. Magnetic Field Components as a Function of z: $\frac{2\xi_1}{\pi}$ = .9; $\frac{y}{a}$ = .8.

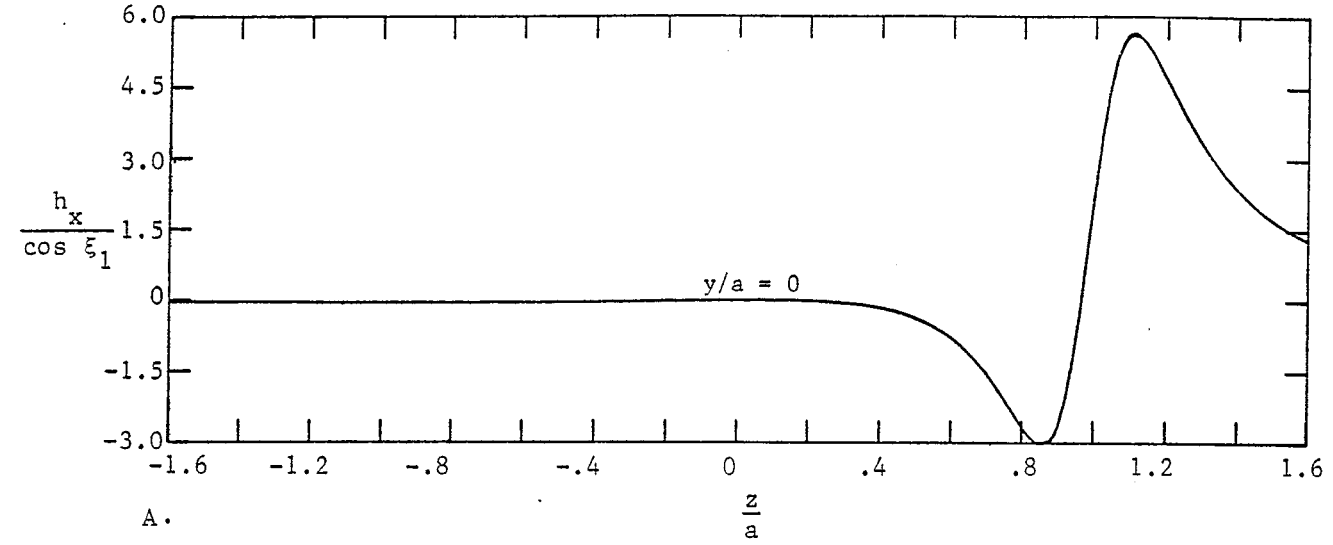

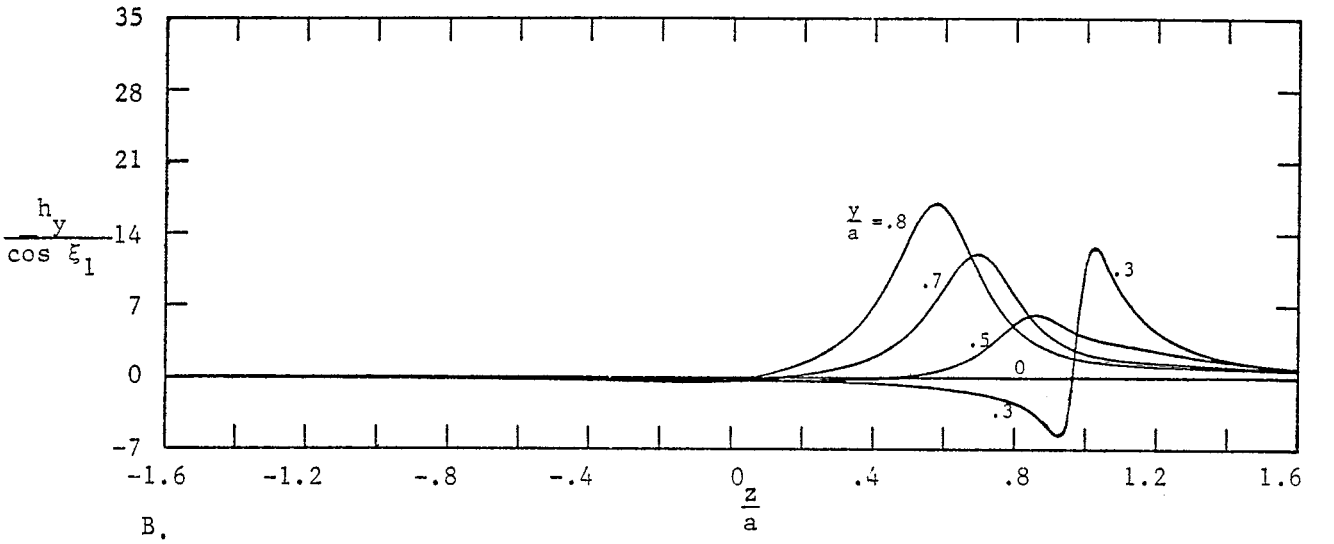

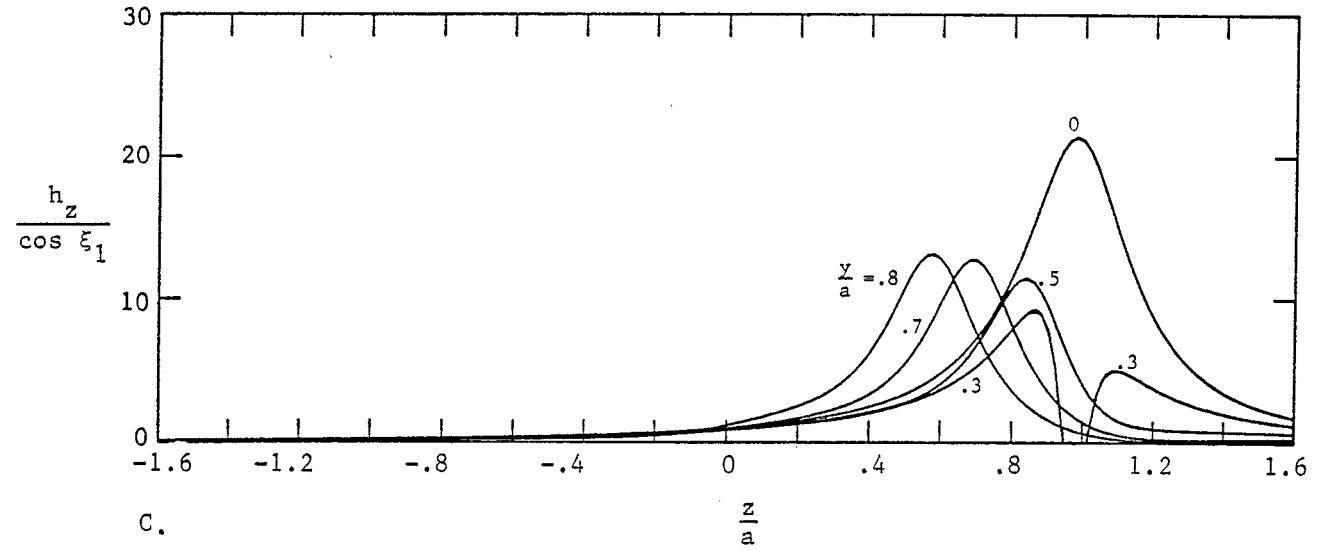

Figure 41. Magnetic Field Components as a Function of z: $\frac{2\xi_1}{\pi} = .9$; $\frac{x}{a} = 0$.

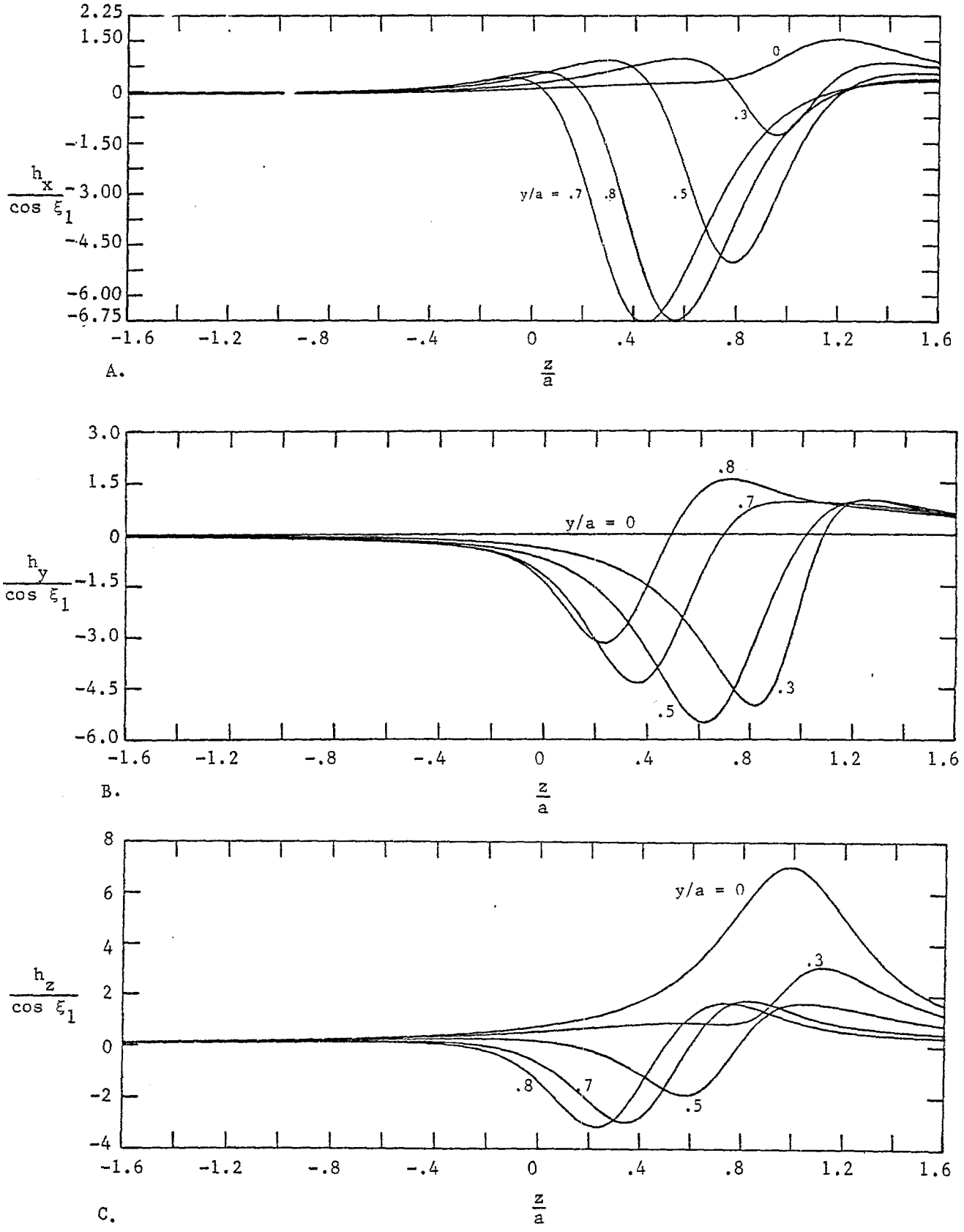

Figure 42. Magnetic Field Components as a Function of z: $\frac{2\xi_1}{\pi} = .9$; $\frac{x}{a} = -.2$.

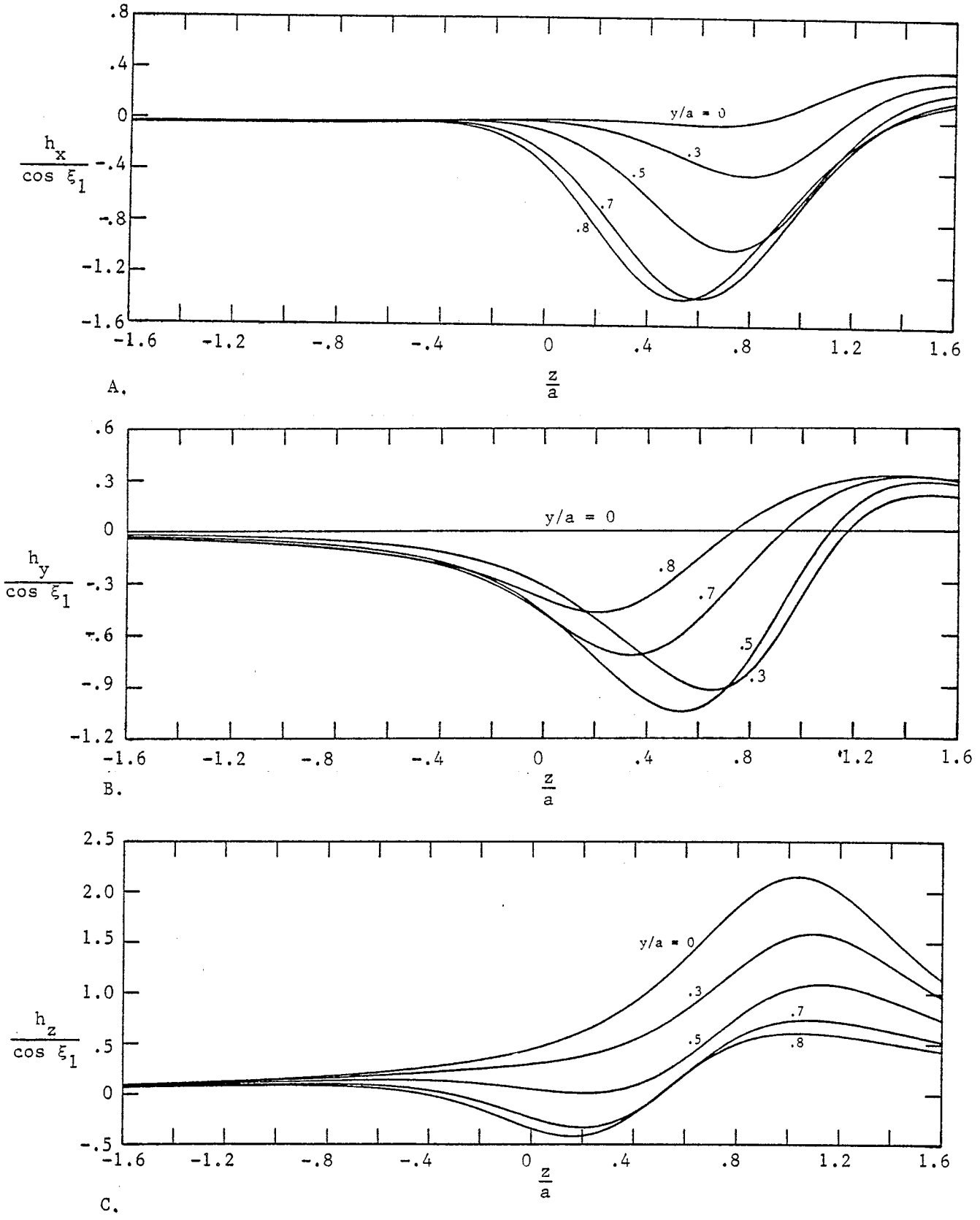

Figure 43. Magnetic Field Components as a Function of z: $\frac{2\xi_1}{\pi} = .9$; $\frac{x}{a} = -.5$.

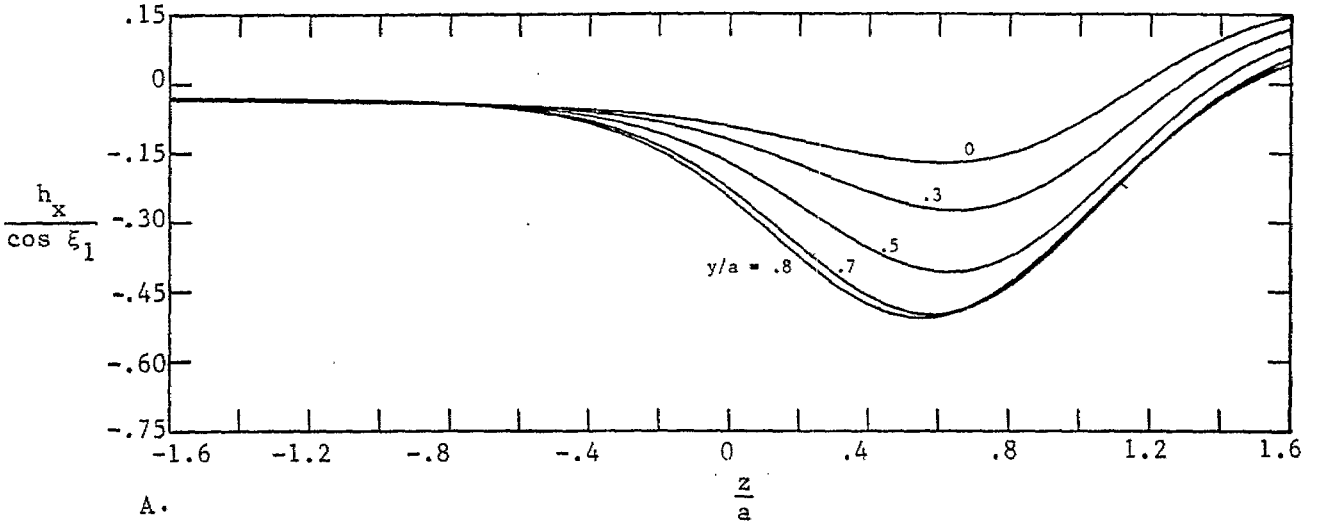

A.

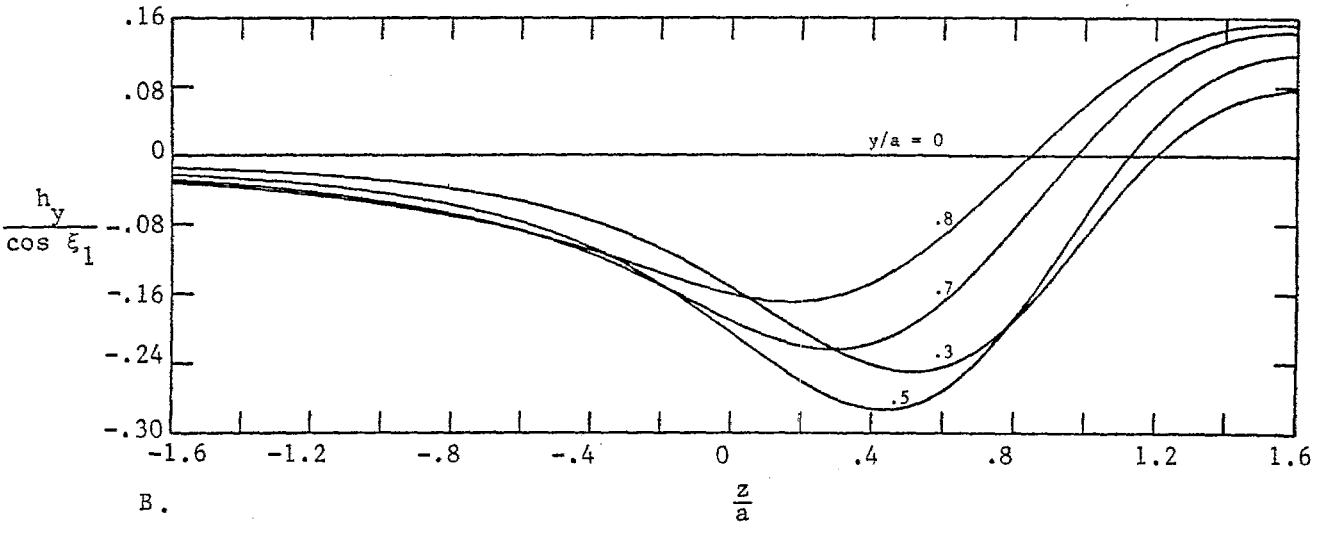

B.

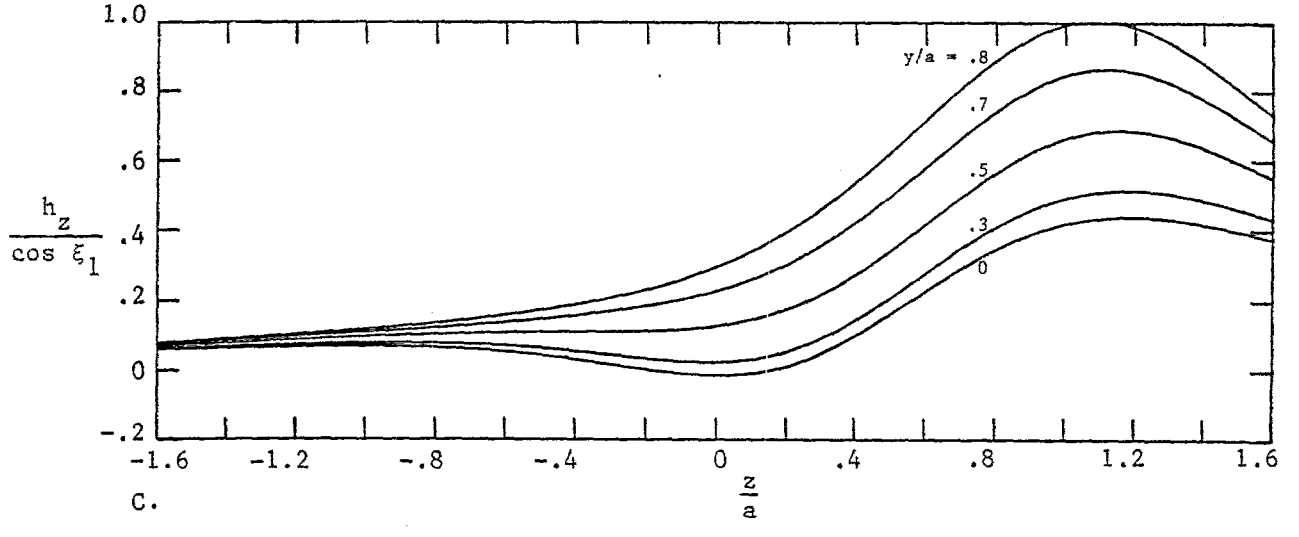

C.

Figure 44. Magnetic Field Components as a Function of z: $\frac{2\xi_1}{\pi} = .9$; $\frac{x}{a} = -.8$.

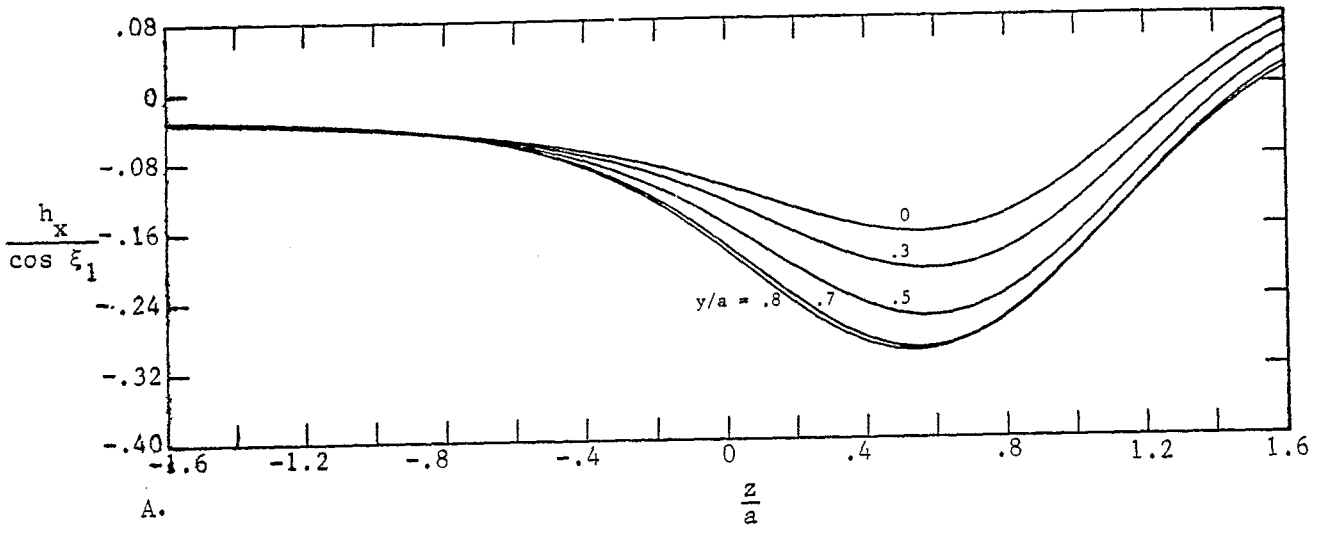

A.

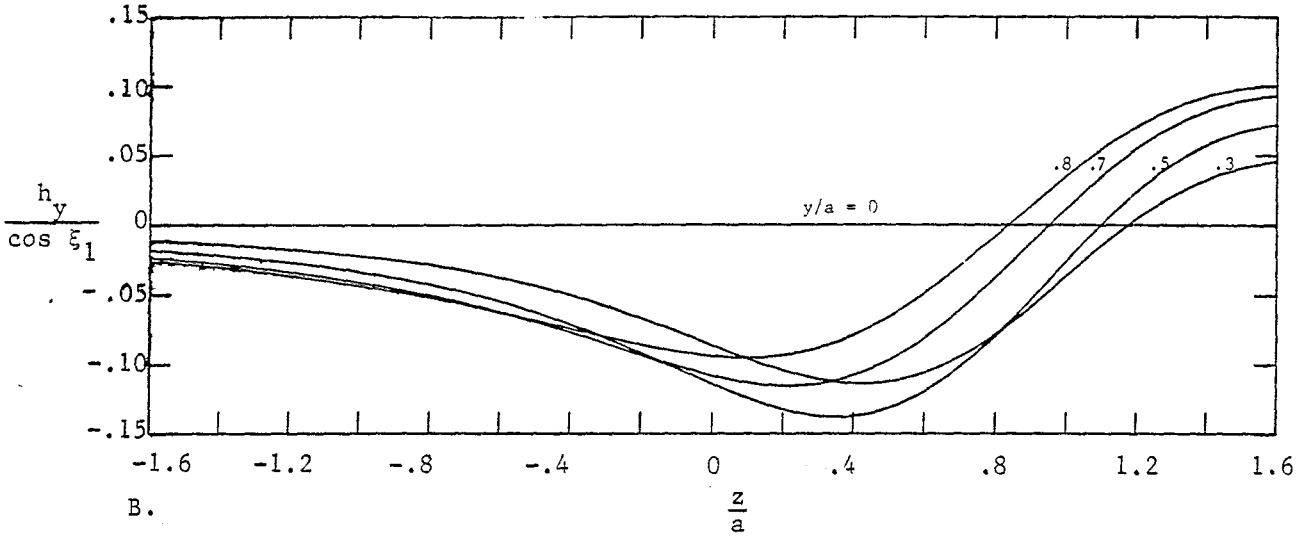

B.

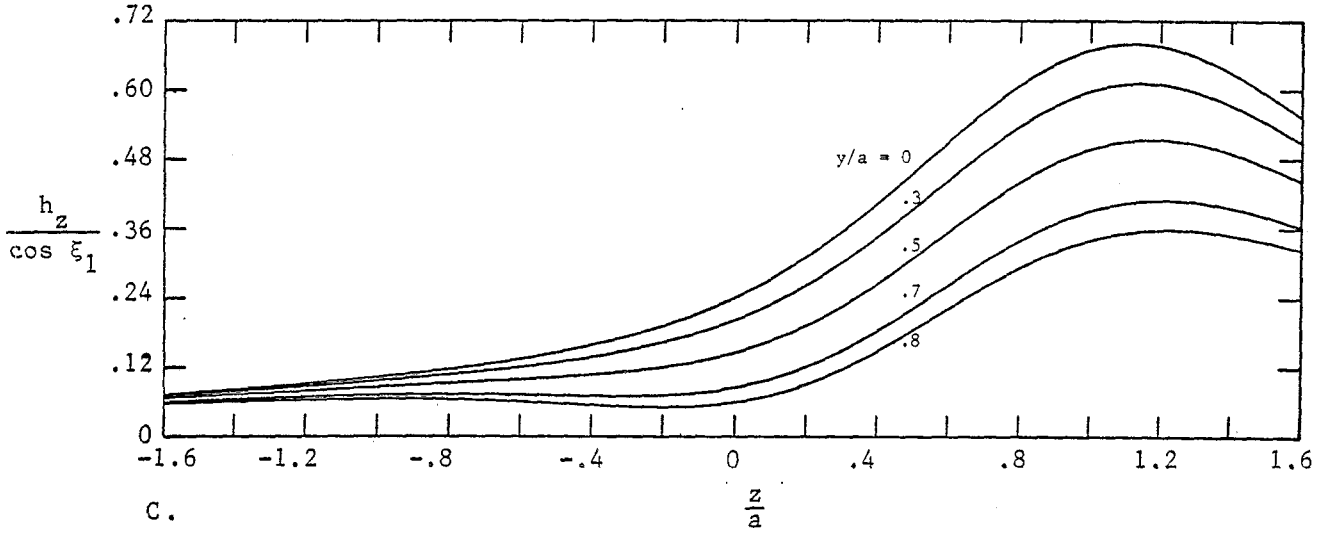

C.

Figure 45. Magnetic Field Components as a Function of z: $\frac{2\xi_1}{\pi} = .9$; $\frac{x}{a} = -1$.

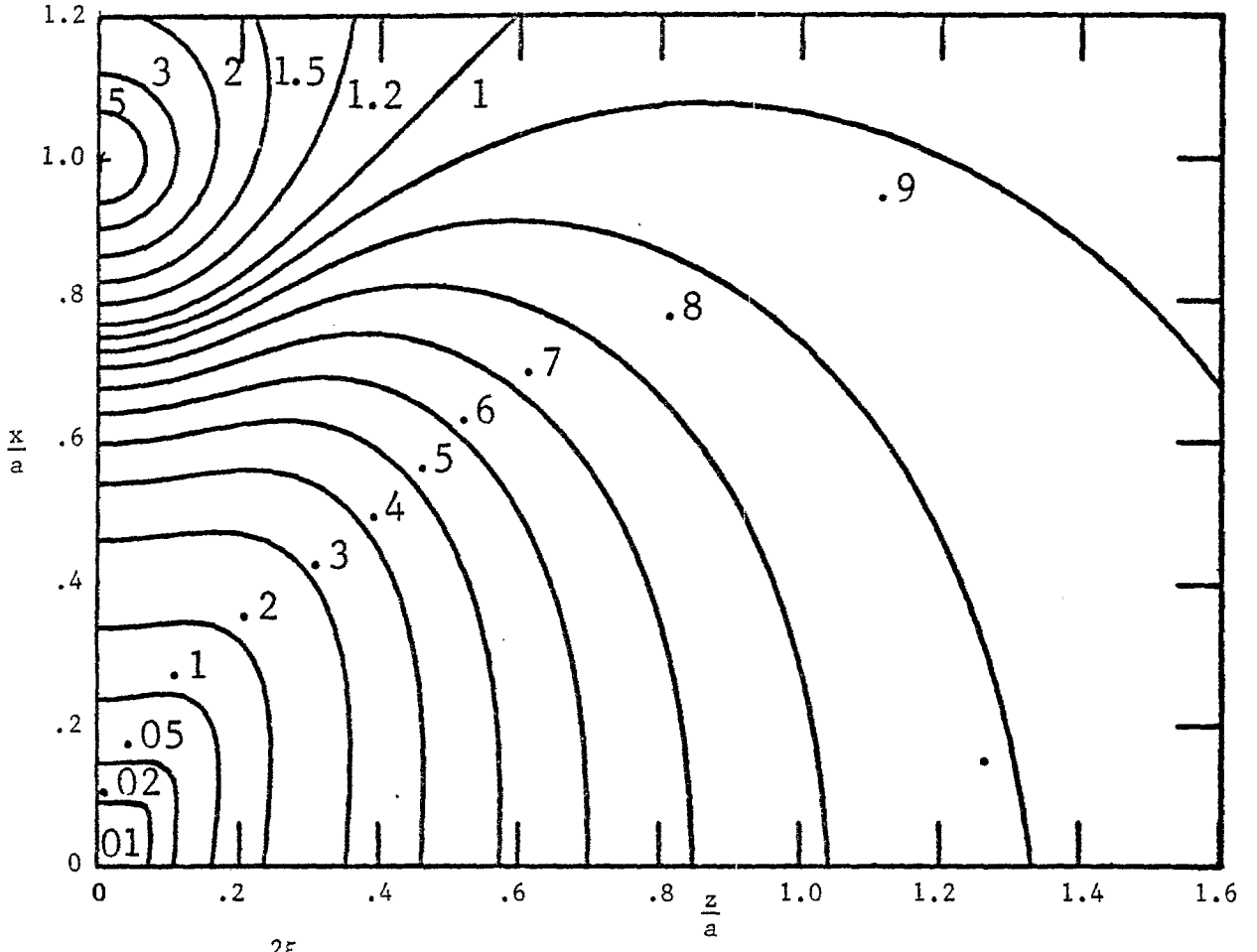

Figure 46. $\frac{2\xi_1}{\pi} = 0$

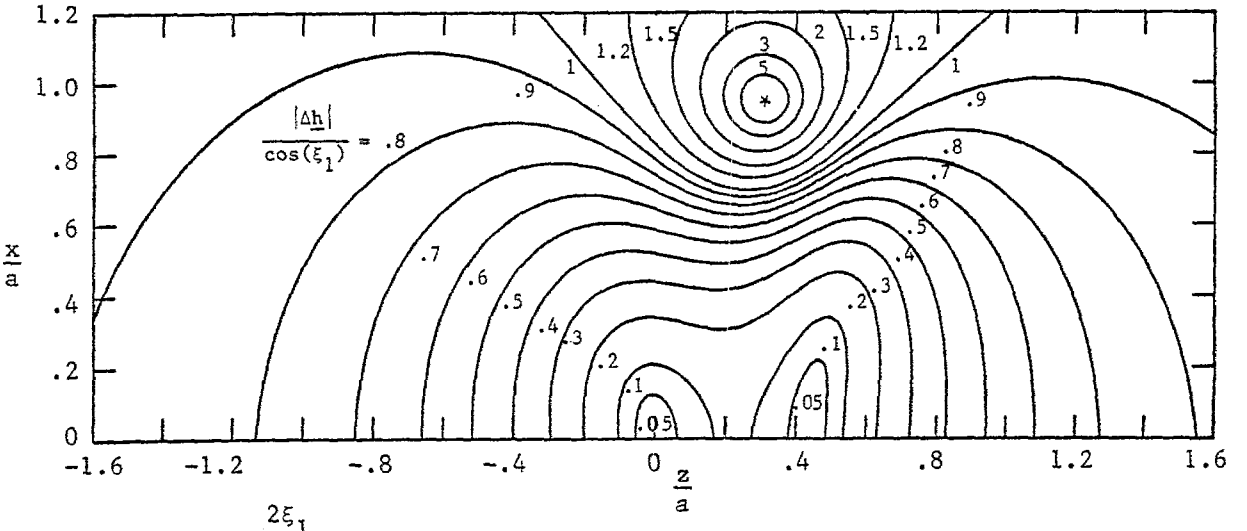

Figure 47. $\frac{2\xi_1}{\pi} = .2$

Contour Plots of $\frac{|\Delta h|}{\cos \xi_1}$ for $\frac{Y}{a} = 0$.

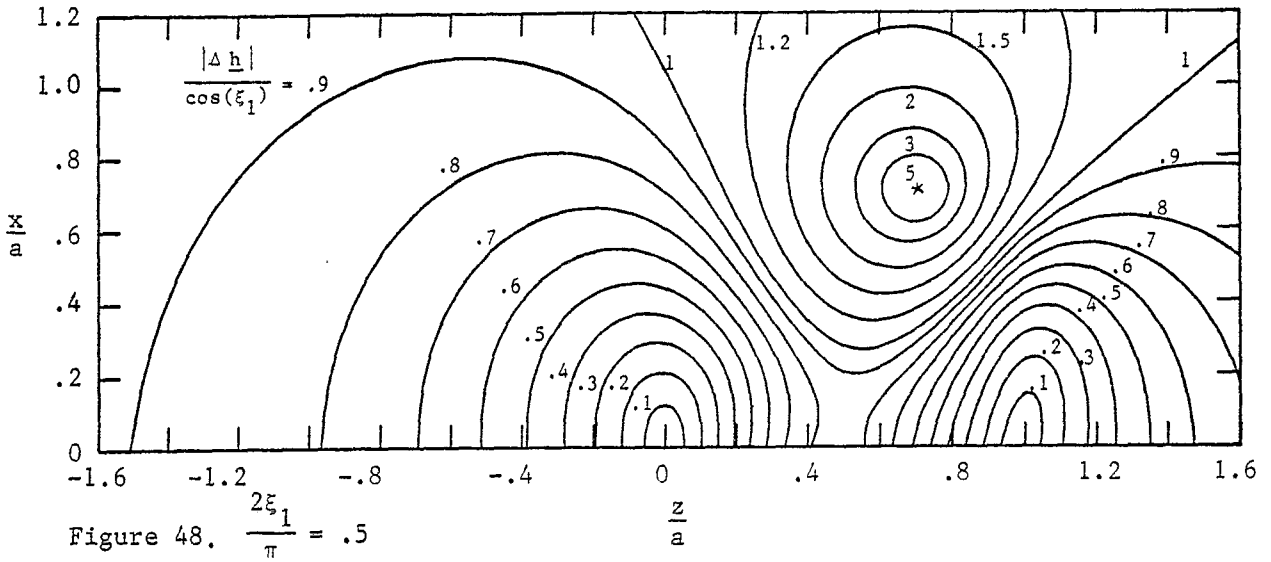

Figure 48. $\frac{2\xi_1}{\pi} = .5$

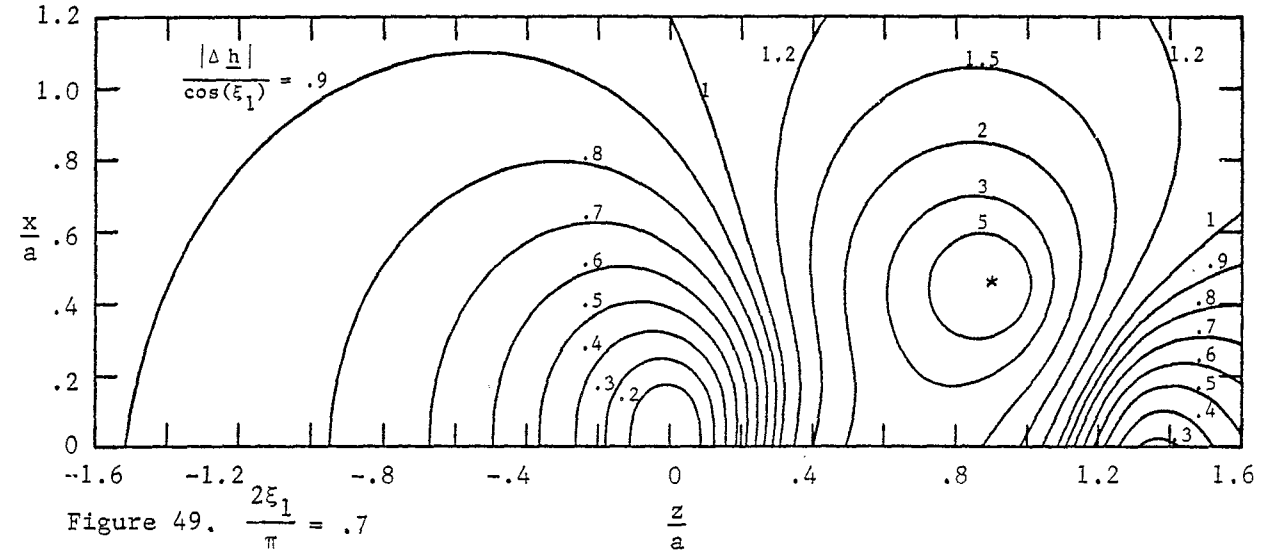

Figure 49. $\frac{2\xi_1}{\pi} = .7$

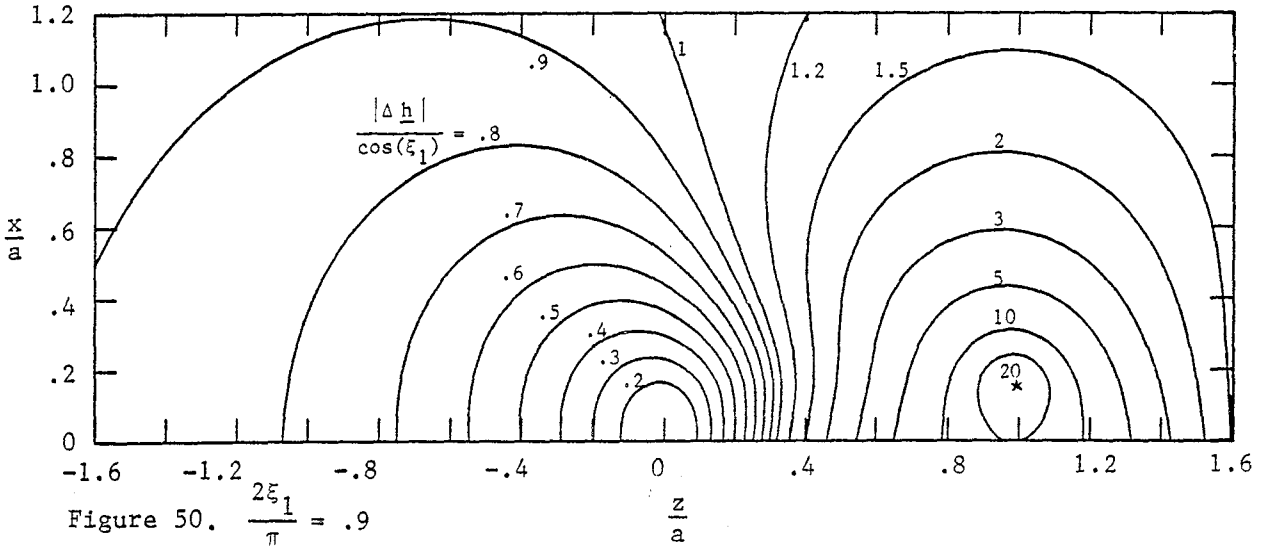

Figure 50. $\frac{2\xi_1}{\pi} = .9$

Contour Plots of $\frac{|\Delta h|}{\cos \xi_1}$ for $\frac{y}{a} = 0$.

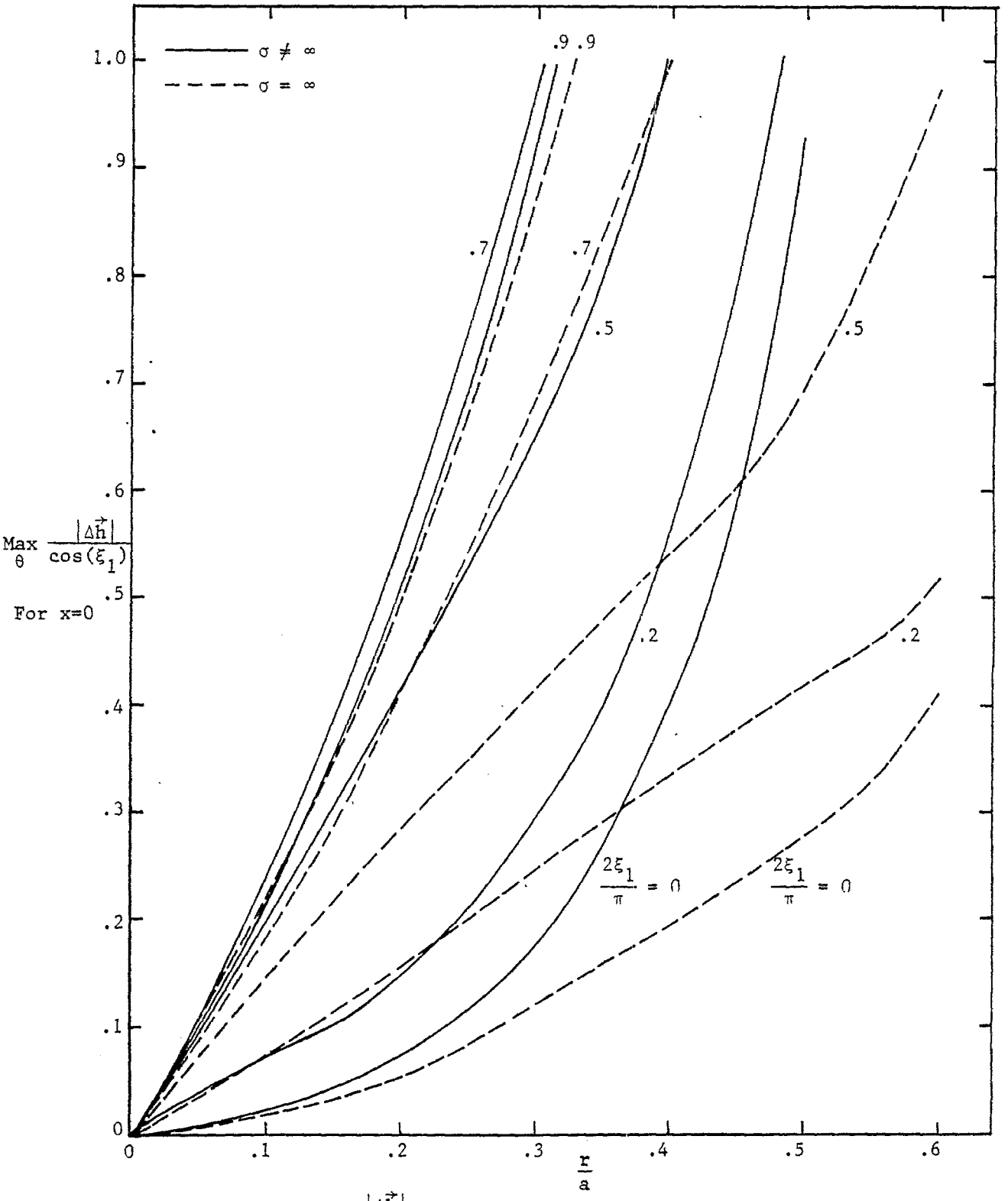

Figure 51. Maximum $\frac{|\vec{\Delta h}|}{\cos(\xi_1)}$ on the perimeter of a circle on the ground surface of radius r centered at the origin: $\frac{x}{a} = 0$.

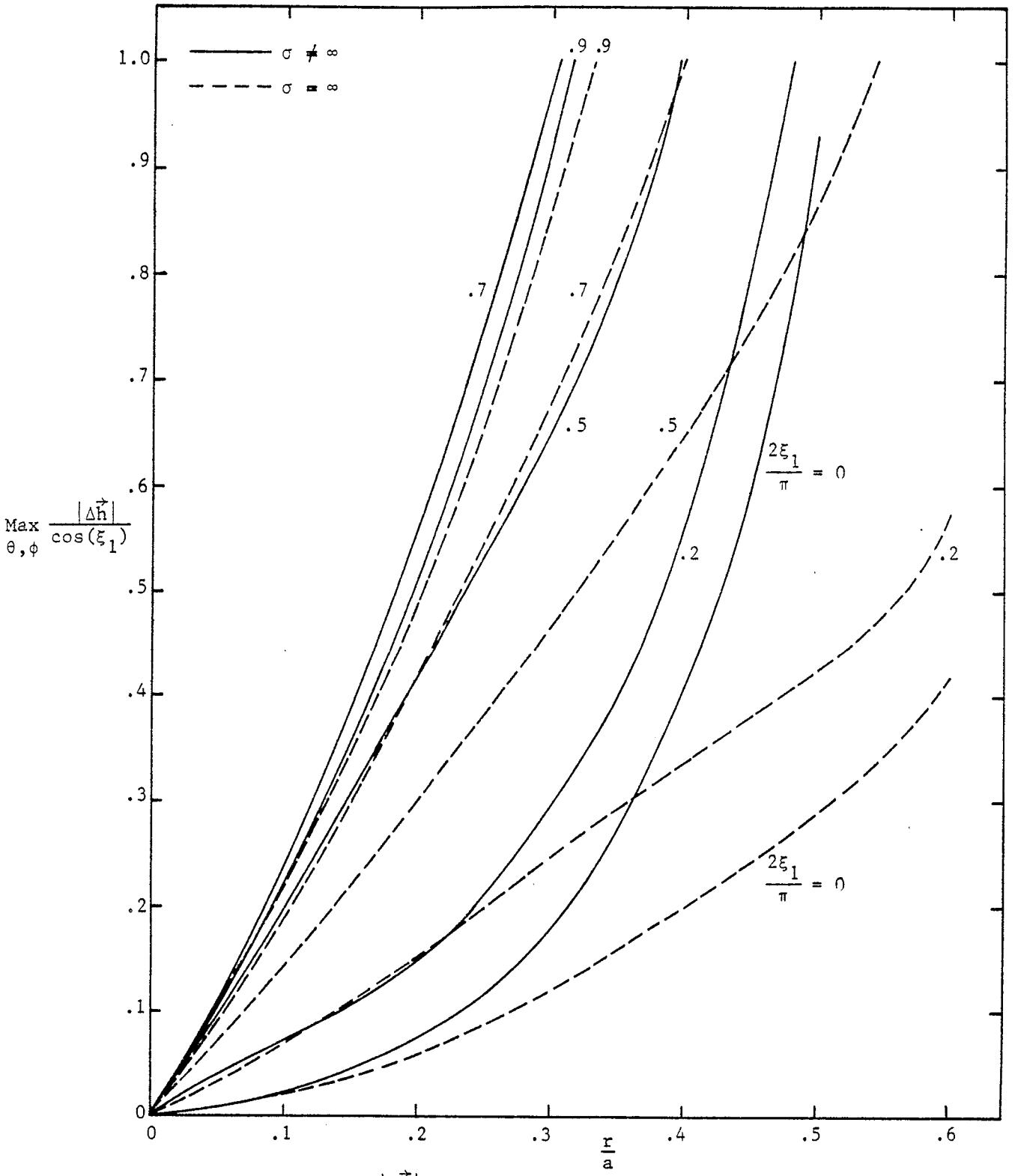

Figure 52. Maximum $\frac{|\Delta\vec{h}|}{\cos(\xi_1)}$ on the surface of a hemisphere of radius r centered at the origin.

Acknowledgement

We thank Mr. R. W. Sassman for his invaluable assistance which enabled the computer plotting of our results. We also thank Dr. C. E. Baum for his helpful comments and Dr. K. S. H. Lee for his continued interest.

References

1. A. D. Varvatsis and M. I. Sancer, "Low-Frequency Magnetic Field Distribution for a Half Toroid Simulator Joined to a Finitely Conducting Ground: Simple Ground Connections," Sensor and Simulation Note 122, February 1971.

2. Capt. Carl E. Baum, "Some Considerations Concerning a Simulator with the Geometry of a Half Toroid Joined to a Ground or Water Surface," Sensor and Simulation Note 94, 17 November 1969.

3. Capt. Carl E. Baum, "Low-Frequency Magnetic Field Distribution for a Simulator with the Geometry of a Half Toroid Joined to the Surface of a Medium with Infinite Conductivity," Sensor and Simulation Note 112, 1 July 1970.